RDECOM TR 10-D-110

**U.S. ARMY RESEARCH,
DEVELOPMENT AND
ENGINEERING COMMAND**

TITLE: The S411, S412, and S413 Airfoils

AUTHOR: **Dan M. Somers**

COMPANY NAME: **Airfoils, Incorporated**

COMPANY ADDRESS: **122 Rose Drive
Port Matilda PA 16870-7535**

DATE: **August 2010**

FINAL REPORT: **Contract Number W911W6-07-C-0047, SBIR Phase II,
Topic Number A06-006, Proposal Number A2-2972**

Prepared for:

U.S. ARMY RESEARCH, DEVELOPMENT AND ENGINEERING COMMAND, AVIATION APPLIED TECHNOLOGY DIRECTORATE, FORT EUSTIS, VA 23604-5577

AIRFOILS, INCORPORATED
122 ROSE DRIVE
PORT MATILDA, PA 16870-7535 USA
WEBSITE WWW.AIRFOILS.COM
TELEPHONE (814) 357-0500
FACSIMILE (814) 357-0357

THE S411, S412, AND S413 AIRFOILS

DAN M. SOMERS

AUGUST 2010

ABSTRACT

A family of airfoils, the S411, S412, and S413, intended for rotorcraft applications has been designed and analyzed theoretically. The two primary objectives of high maximum lift, relatively insensitive to roughness, and low profile drag have been achieved. The constraint on the pitching moment of the primary airfoil, the S411, has been exceeded; those of the outboard and tip airfoils, the S412 and S413, respectively, have been satisfied. The constraints on the airfoil thicknesses have been satisfied. The primary airfoil incorporates a 5-percent-chord tab.

INTRODUCTION

Almost all airfoils in use on rotorcraft today were developed under the assumption that extensive laminar flow is not likely on a rotor. (See ref. 1, for example.) Because the airfoil family designed under the present effort is intended for a small helicopter with its attendant low Reynolds numbers and because of the precision blade manufacturing technique being employed, however, the achievement of laminar flow warrants exploration. To complement the design effort, the primary airfoil of this family was investigated in The Pennsylvania State University Low-Speed, Low-Turbulence Wind Tunnel (ref. 2). This family is part of an effort sponsored by the U.S. Army to design theoretically and verify experimentally several airfoils for rotorcraft applications.

SYMBOLS

C_p	pressure coefficient
c	airfoil chord, mm
c_d	section profile-drag coefficient
c_l	section lift coefficient
c_m	section pitching-moment coefficient about quarter-chord point
M	free-stream Mach number
R	Reynolds number based on free-stream conditions and airfoil chord
t	airfoil thickness, mm
x	airfoil abscissa, mm
α	angle of attack relative to x-axis, deg

Subscripts:

ll	lower limit of low-drag range
max	maximum
min	minimum
S	separation
T	transition
ul	upper limit of low-drag range
0	zero lift

Abbreviations:

L.	lower surface
S.	boundary-layer separation location, x_S/c
T.	boundary-layer transition location, x_T/c
U.	upper surface

AIRFOIL DESIGN

OBJECTIVES AND CONSTRAINTS

The design specifications for the airfoil family are contained in table I. The family consists of three airfoils: primary, outboard, and tip.

Two primary objectives are evident from the specifications. The first objective is to achieve a high maximum lift coefficient. A requirement related to this objective is that the maximum lift coefficient not decrease significantly with transition fixed near the leading edge on both surfaces. In addition, the airfoils should exhibit docile stall characteristics. The second objective is to obtain low profile-drag coefficients over the specified ranges of lift coefficients.

Three major constraints were placed on the design of the airfoil family. First, the zero-lift pitching-moment coefficient must be nearly 0. Second, the primary airfoil must incorporate a tab having a length of 5-percent chord and a thickness of 0.352-percent chord; for geometric compatibility, the outboard and tip airfoils must have a trailing-edge thickness equal to that of the tab on the primary airfoil. Third, the airfoil thicknesses must equal those specified.

PHILOSOPHY

Given the above objectives and constraints, certain characteristics of the designs are apparent. The following sketch illustrates a drag polar that meets the goals for the primary airfoil. (The polars for the outboard and tip airfoils should be qualitatively similar.)

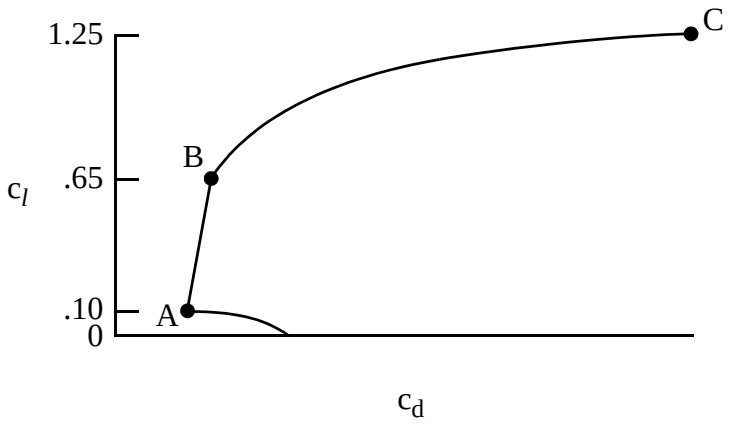

Sketch 1

The desired airfoil shape can be traced to the pressure distributions that occur at the various points in sketch 1. Point A is the lower limit of the low-drag range of lift coefficients; point B, the upper limit. The profile-drag coefficient at point B is not as low as at point A, unlike the polars of many laminar-flow airfoils where the drag coefficient within the laminar bucket is nearly constant. (See, for example, ref. 3.) This characteristic is related to the elimination of significant (i.e., drag-producing) laminar separation bubbles on the upper surface for the design range of Reynolds numbers. (See ref. 4.) The drag coefficient increases rapidly outside the low-drag, lift-coefficient range because boundary-layer transition moves quickly toward the leading edge with increasing (or decreasing) lift coefficient. This feature results in a leading edge that produces a suction peak at higher lift coefficients, which ensures that transition on the upper surface will occur very near the leading edge. Thus, the maximum lift coefficient, point C, occurs with turbulent flow along the entire upper surface and, therefore, should be relatively insensitive to roughness at the leading edge.

An unusual design approach was taken for the primary airfoil. Rather than design a thicker airfoil and then add the required tab, the airfoil was designed from the outset for the specified thickness including the tab. Specifically, the airfoil was initially designed with a trailing-edge shape that geometrically and aerodynamically approximated the tab. This shape was then modified to the required tab geometry. Accordingly, the performance of the final, tabbed airfoil is likely better than that of an airfoil altered by the addition of a relatively arbitrary tab.

From the preceding discussion, the pressure distributions along the polar can be deduced. The pressure distribution at point A for the primary airfoil shape, with the pseudo tab, should look something like sketch 2.

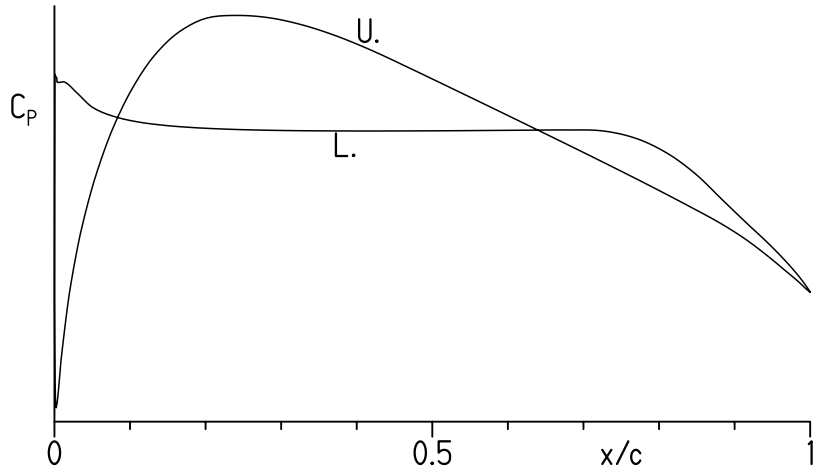

Sketch 2

To achieve low drag, a favorable pressure gradient is desirable along the upper surface to about 25-percent chord. Aft of this point, a short region having a shallow, adverse pressure gradient (i.e., a "transition ramp") promotes the efficient transition from laminar to turbulent flow (ref. 5). The transition ramp is followed by a very slightly convex pressure recovery. The specific pressure recovery employed represents a compromise between maximum lift, drag, pitching moment, stall characteristics, and drag divergence. The steeper, adverse pressure gradient aft of about 90-percent chord is a "separation ramp," originally proposed by F. X. Wortmann,[1] which confines turbulent separation to a small region near the trailing edge. By constraining the movement of the separation point at high angles of attack, higher lift coefficients can be achieved with little drag penalty. This feature has the added benefit of promoting docile stall characteristics. (See ref. 6.)

Along the lower surface, the pressure gradient is initially adverse, then zero, and then favorable to about 70-percent chord. Thus, transition is imminent over the entire forward portion of the lower surface. (See ref. 7.) This concept allows a wide low-drag range to be achieved and increases the loading in the leading-edge region. The forward loading serves to balance, with respect to the pitching-moment constraint, the aft loading, both of which contribute to the achievement of the specified maximum lift coefficient and low profile-drag coefficients. This region is followed by a transition ramp and then a roughly linear pressure recovery. The pressure recovery must begin farther forward than optimum for low drag and

[1]Director, Institute for Aerodynamics and Gas Dynamics, University of Stuttgart, Germany, 1974–1985.

the constrained pitching moment to alleviate separation at lower lift coefficients, especially with transition fixed near the leading edge.

The amounts of pressure recovery on the upper and lower surfaces are determined by the airfoil-thickness and pitching-moment constraints.

At point B, the pressure distribution should look like sketch 3.

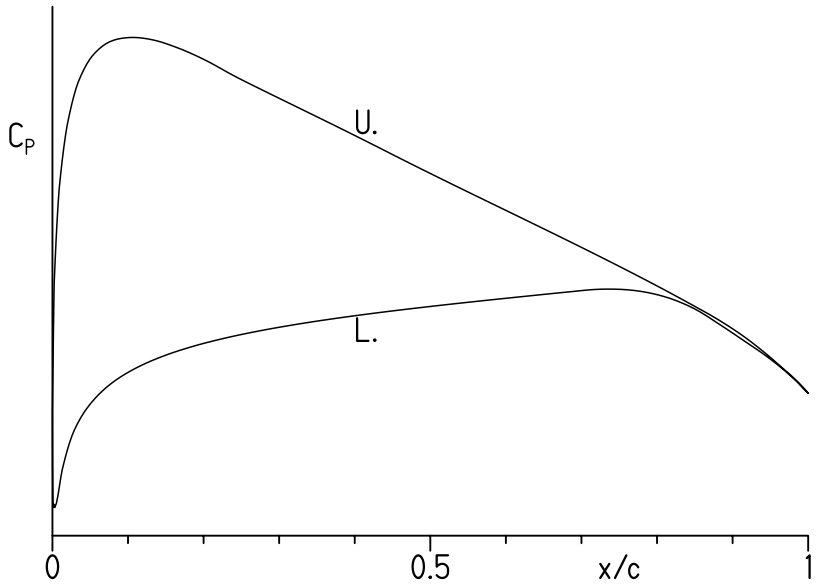

Sketch 3

No suction peak exists at the leading edge. Instead, a rounded peak occurs aft of the leading edge, which allows some laminar flow, although not to the extent of point A.

EXECUTION

Given the pressure distributions previously discussed, the design of the airfoils is reduced to the inverse problem of transforming the pressure distributions into airfoil shapes. The Eppler Airfoil Design and Analysis Code (refs. 8 and 9) was used because of its unique capability for multipoint design and because of confidence gained during the design, analysis, and experimental verification of many other airfoils. (See ref. 10, for example.) The code also offers useful options for the modification of the airfoil geometry with respect to the tab.

The primary airfoil is designated the S411. The airfoil shape incorporates a tab that is 5-percent-chord long and 0.352-percent-chord thick, which satisfies the design constraint.

The outboard and tip airfoils, the S412 and S413, respectively, were derived from the S411 airfoil to increase the aerodynamic and geometric compatibilities of the three airfoils. It should be noted that, because of the design requirements, the S412 and S413 airfoils are symmetric.

The airfoil shapes and coordinates are available from Airfoils, Incorporated. The S411 airfoil thickness is 14.00-percent chord; the S412, 12.00-percent chord; and the S413, 9.99-percent chord, which satisfy the design constraints.

THEORETICAL PROCEDURE

The results are predicted using the method of references 8 and 9 (PROFIL07), commonly known as the Eppler code, and the method of reference 11 (MSES 3.0). Critical amplification factors of 11 and 9 were specified for the computations using the method of references 8 and 9 and the method of reference 11, respectively. Because the maximum lift coefficient computed by the method of references 8 and 9 is not always realistic, an empirical criterion has been applied to the computed results. The criterion assumes the maximum lift coefficient has been reached if the drag coefficient of the upper surface reaches a certain value that is a function of the Reynolds number and the wind-tunnel facility. It should also be noted that the compressibility correction (ref. 12) incorporated in the method of references 8 and 9 is invalid if the local flow is supersonic.

Computations were performed over the range of operational conditions in table I with transition free (smooth) and with transition fixed near the leading edge, 2-percent chord on the upper surface and 7-percent chord on the lower surface, to simulate full-chord, turbulent flow. For the primary airfoil, computations were also performed with transition fixed at 10-percent chord on the upper and lower surfaces to simulate a possible manufacturing deficiency. It should be noted that, for the outboard and tip airfoils, the computations were performed for the design trailing edge, which has zero thickness, rather than for the specified finite-thickness trailing edge.

DISCUSSION OF RESULTS

S411 AIRFOIL

Pressure Distributions

The pressure distributions for the S411 airfoil predicted using the method of reference 11 at various angles of attack at a Mach number of 0.30 and a Reynolds number of 0.97×10^6 with transition free are shown in figure 1. At an angle of attack of $-2.00°$ (fig. 1(a)), a short laminar separation bubble is evident on the upper surface around 65-percent chord. At an angle of attack of $-1.00°$ (fig. 1(a)), a short laminar separation bubble is evident on the lower surface around 80-percent chord. As the angle of attack is increased, the bubble on the upper surface moves forward, whereas the bubble on the lower surface remains rela-

tively fixed (figs. 1(a)–1(c)). At an angle of attack of 10.00° (fig. 1(d)), turbulent, trailing-edge separation occurs on the upper surface. The amount of separation increases with increasing angle of attack. The maximum lift coefficient occurs at an angle of attack of about 14° (fig. 1(d)). The flow is subsonic at all angles of attack shown.

The pressure distributions predicted at various angles of attack at a Mach number of 0.45 and a Reynolds number of 1.45×10^6 with transition free are shown in figure 2. At an angle of attack of −2.00° (fig. 2(a)), transition occurs around 60-percent chord on the upper surface and near the leading edge on the lower surface. At an angle of attack of 0.00° (fig. 2(a)), a short laminar separation bubble is evident on the lower surface around 80-percent chord. As the angle of attack is increased, transition moves forward on the upper surface, whereas the bubble on the lower surface remains relatively fixed (figs. 2(a) and 2(b)). The flow is subsonic at all angles of attack shown.

The pressure distributions predicted at various angles of attack at a Mach number of 0.60 and a Reynolds number of 1.94×10^6 with transition free are shown in figure 3. At an angle of attack of −2.00°, transition occurs around 55-percent chord on the upper surface and near the leading edge on the lower surface, where the flow is supersonic. At an angle of attack of 0.00°, a short laminar separation bubble is evident on the lower surface around 80-percent chord. As the angle of attack is increased, transition moves forward on the upper surface, whereas the bubble on the lower surface remains relatively fixed. The flow is subsonic up to an angle of attack of 2°.

The pressure distributions predicted at various angles of attack at a Mach number of 0.70 and a Reynolds number of 2.26×10^6 with transition free are shown in figure 4. At an angle of attack of −2.00° (fig. 4(a)), transition occurs around 50-percent chord on the upper surface and within a short laminar separation bubble near the leading edge on the lower surface, terminated by a weak shock. As the angle of attack is increased, transition moves forward on the upper surface and aft on the lower surface and the shock on the lower surface disappears (fig. 4(a)). At an angle of attack of −0.50° (fig. 4(b)), a short laminar separation bubble is evident on the upper surface around 40-percent chord and on the lower surface around 80-percent chord. As the angle of attack is increased, a shock forms on the upper surface. The shock, which terminates the bubble on the upper surface, migrates slowly aft with increasing angle of attack, as does the bubble on the lower surface.

Section Characteristics

The section characteristics of the S411 airfoil with transition free predicted using the method of references 8 and 9 (PROFIL07) and the method of reference 11 (MSES 3.0) are shown in figure 5. The results are in reasonable agreement, except for the profile-drag coefficient and the maximum lift coefficient. The method of reference 11 probably predicts lower drag coefficients because it predicts transition further aft. The maximum lift coefficients estimated using the previously discussed empirical criterion applied to the results from the method of references 8 and 9 are 1.14 at a Mach number of 0.30 and a Reynolds number of 0.97×10^6 (fig. 5(a)) and 1.17 at a Mach number of 0.40 and a Reynolds number of 1.29×10^6

(fig. 5(b)), which are below the design objectives. The maximum lift coefficient predicted by the method of reference 11 is 1.47 both at a Mach number of 0.30 and a Reynolds number of 0.97×10^6 (fig. 5(a)) and at a Mach number of 0.40 and a Reynolds number of 1.29×10^6 (fig. 5(b)), which exceeds the design objectives. The lower limit of the low-drag range at a Mach number of 0.70 and a Reynolds number of 2.26×10^6 (fig. 5(e)) is 0.12, which is above the design objective. The upper limit at a Mach number of 0.45 and a Reynolds number of 1.45×10^6 (fig. 5(c)) exceeds the design objective. The zero-lift pitching-moment coefficient at a Mach number of 0.45 and a Reynolds number of 1.45×10^6 (fig. 5(c)) predicted by the method of references 8 and 9 is 0.002 and, predicted by the method of reference 11, is 0.000, which satisfies the design constraint.

The effect of fixing transition on the section characteristics predicted using the method of references 8 and 9 is shown in figure 6. The maximum lift coefficient is unaffected by fixing transition at 10-percent chord on the upper and lower surfaces but decreases 10 percent at a Mach number of 0.30 and a Reynolds number of 0.97×10^6 (fig. 6(a)) and 15 percent at a Mach number of 0.40 and a Reynolds number of 1.29×10^6 (fig. 6(b)) with transition fixed at 2-percent chord on the upper surface and 7-percent chord on the lower surface. The drag coefficients are, of course, adversely affected by fixing transition.

The effect of fixing transition on the section characteristics predicted using the method of reference 11 is shown in figure 7. The maximum lift coefficient is essentially unaffected by fixing transition at 10-percent chord on the upper and lower surfaces and decreases less than 2 percent at a Mach number of 0.30 and a Reynolds number of 0.97×10^6 (fig. 7(a)) and less than 4 percent at a Mach number of 0.40 and a Reynolds number of 1.29×10^6 (fig. 7(b)) with transition fixed at 2-percent chord on the upper surface and 7-percent chord on the lower surface. The drag coefficients are adversely affected by fixing transition. The zero-lift pitching-moment coefficient at a Mach number of 0.75 and a Reynolds number of 2.42×10^6 (not shown) with transition fixed at 10-percent chord on the upper and lower surfaces predicted by the method of reference 11 is –0.013, which exceeds the design constraint.

S412 AIRFOIL

Pressure Distributions

The pressure distributions for the S412 airfoil predicted using the method of reference 11 at various angles of attack at a Mach number of 0.40 and a Reynolds number of 1.34×10^6 with transition free are shown in figure 8. At an angle of attack of 0.00° (fig. 8(a)), a short laminar separation bubble is evident on the upper and lower surfaces around 60-percent chord. As the angle of attack is increased, transition moves quickly forward on the upper surface, whereas the bubble on the lower surface migrates slowly aft (figs. 8(a) and 8(b)). At an angle of attack of 8.00° (fig. 8(b)), the flow near the leading edge on the upper surface is supersonic. At an angle of attack of 10.00° (fig. 8(c)), turbulent, trailing-edge separation occurs on the upper surface and the flow along the entire lower surface is laminar. The amount of upper-surface separation increases with increasing angle of attack. The maximum lift coefficient occurs at an angle of attack of about 11° (fig. 8(c)).

The pressure distributions predicted at various angles of attack at a Mach number of 0.58 and a Reynolds number of 1.88×10^6 with transition free are shown in figure 9. At an angle of attack of 0.00° (fig. 9(a)), a short laminar separation bubble is evident on the upper and lower surfaces around 60-percent chord. At an angle of attack of 1.00° (fig. 9(a)), which corresponds to the upper limit of the low-drag range, transition occurs on the upper surface around 55-percent chord and the bubble on the lower surface has migrated aft. As the angle of attack is increased, transition moves quickly forward on the upper surface, whereas the bubble on the lower surface migrates slowly aft (fig. 9(a)). At an angle of attack of 3.00° (fig. 9(a)), the flow near the leading edge on the upper surface is supersonic. As the angle of attack is increased, a shock forms on the upper surface (fig. 9(b)). The shock, which causes laminar separation, resulting in a bubble, migrates aft with increasing angle of attack, as does the bubble on the lower surface.

The pressure distributions predicted at various angles of attack at a Mach number of 0.70 and a Reynolds number of 2.26×10^6 with transition free are shown in figure 10. At an angle of attack of 0.00° (fig. 10(a)), a short laminar separation bubble is evident on the upper and lower surfaces around 60-percent chord. At an angle of attack of 1.00° (fig. 10(a)), transition occurs on the upper surface around 45-percent chord, the bubble on the lower surface has migrated aft, and the flow near the leading edge on the upper surface is supersonic. As the angle of attack is increased, transition moves quickly forward on the upper surface, whereas the bubble on the lower surface migrates slowly aft (fig. 10(a)). At an angle of attack of 2.00° (fig. 10(b)), a shock has formed on the upper surface. The shock, which causes laminar separation, resulting in a bubble, moves aft with increasing angle of attack.

The pressure distributions predicted at various angles of attack at a Mach number of 0.78 and a Reynolds number of 2.51×10^6 with transition free are shown in figure 11. At an angle of attack of 0.00° (fig. 11(a)), a short laminar separation bubble is evident on the upper and lower surfaces around 55-percent chord and the flow over roughly the forward half of the airfoil is supersonic. As the angle of attack is increased, a shock forms on the upper surface (fig. 11(a)). The shock, which causes laminar separation, resulting in a bubble, migrates slowly aft with increasing angle of attack, as does the bubble on the lower surface (fig. 11(b)).

Section Characteristics

The section characteristics of the S412 airfoil with transition free predicted using the method of references 8 and 9 and the method of reference 11 are shown in figure 12. It should be remembered that the section characteristics predicted using the method of references 8 and 9 are limited to conditions at which the flow is everywhere subsonic. The results are in reasonable agreement, except for the width of the low-drag range. The method of reference 11 probably predicts wider low-drag ranges because it predicts transition later. The maximum lift coefficient predicted by the method of reference 11 at a Mach number of 0.40 and a Reynolds number of 1.34×10^6 (fig. 12(a)) is 1.13, which exceeds the design objective. The upper limit of the low-drag range at a Mach number of 0.58 and a Reynolds number of 1.88×10^6 (fig. 12(b)) is lower than the design objective. At a Mach number of 0.78 and a Reynolds

number of 2.51×10^6 (fig. 12(d)), the lower limit meets the design objective and the zero-lift pitching-moment coefficient, 0.000, satisfies the design constraint.

The effect of fixing transition on the section characteristics predicted using the method of references 8 and 9 is shown in figure 13. The section characteristics, with the exception of the drag coefficient, are essentially unaffected by fixing transition. The drag coefficients are, of course, adversely affected.

The effect of fixing transition on the section characteristics predicted using the method of reference 11 is shown in figure 14. At a Mach number of 0.40 and a Reynolds number of 1.34×10^6 (fig. 14(a)), the maximum lift coefficient increases slightly with transition fixed. For all conditions, the other section characteristics, with the exception of the drag coefficient, are essentially unaffected by fixing transition. The drag coefficients are adversely affected.

S413 AIRFOIL

Pressure Distributions

The pressure distributions for the S413 airfoil predicted using the method of reference 11 at various angles of attack at a Mach number of 0.40 and a Reynolds number of 1.34×10^6 with transition free are shown in figure 15. At an angle of attack of 0.00° (fig. 15(a)), a short laminar separation bubble is evident on the upper and lower surfaces around 65-percent chord. At an angle of attack of 1.00° (fig. 15(a)), transition occurs on the upper surface around 55-percent chord and the bubble on the lower surface has migrated aft. As the angle of attack is increased, transition moves quickly forward on the upper surface, whereas the bubble on the lower surface migrates slowly aft (figs. 15(a) and 15(b)). At an angle of attack of 8.00° (fig. 15(c)), the flow near the leading edge on the upper surface is supersonic and the flow along the entire lower surface is laminar. At an angle of attack of 10.00° (fig. 15(c)), which corresponds to the maximum lift coefficient, turbulent, trailing-edge separation occurs on the upper surface. The amount of separation increases with increasing angle of attack.

The pressure distributions predicted at various angles of attack at a Mach number of 0.61 and a Reynolds number of 1.98×10^6 with transition free are shown in figure 16. At an angle of attack of 0.00° (fig. 16(a)), a short laminar separation bubble is evident on the upper and lower surfaces around 60-percent chord. At an angle of attack of 1.00° (fig. 16(a)), which already exceeds the upper limit of the low-drag range, transition occurs on the upper surface around 30-percent chord and the bubble on the lower surface has migrated aft to about 65-percent chord. As the angle of attack is increased, transition moves further forward on the upper surface, whereas the bubble on the lower surface migrates slowly aft (fig. 16(a)). At an angle of attack of 2.00° (fig. 16(a)), the flow near the leading edge on the upper surface is supersonic. As the angle of attack is increased, a shock forms on the upper surface (fig. 16(a)). The shock, which causes laminar separation, resulting in a bubble, migrates aft with increasing angle of attack, as does the bubble on the lower surface (fig. 16(b)).

The pressure distributions predicted at various angles of attack at a Mach number of 0.70 and a Reynolds number of 2.28×10^6 with transition free are shown in figure 17. At an angle of attack of 0.00° (fig. 17(a)), a short laminar separation bubble is evident on the upper and lower surfaces around 55-percent chord. At an angle of attack of 0.50° (fig. 17(a)), transition occurs on the upper surface around 40-percent chord, the bubble on the lower surface has migrated aft to about 60-percent chord, and the flow near the leading edge on the upper surface is supersonic. As the angle of attack is increased, transition moves further forward on the upper surface, whereas the bubble on the lower surface migrates slowly aft (fig. 17(a)). At an angle of attack of 1.50° (fig. 17(a)), a shock has formed on the upper surface. The shock, which causes laminar separation, resulting in a bubble, moves aft with increasing angle of attack (fig. 17(b)).

The pressure distributions predicted at various angles of attack at a Mach number of 0.80 and a Reynolds number of 2.61×10^6 with transition free are shown in figure 18. At an angle of attack of 0.00° (fig. 18(a)), a short laminar separation bubble is evident on the upper and lower surfaces around 50-percent chord and the flow over roughly the forward half of the airfoil is supersonic. As the angle of attack is increased, a shock forms on the upper surface (fig. 18(a)). The shock, which causes laminar separation, resulting in a bubble, migrates aft with increasing angle of attack, as does the bubble on the lower surface (fig. 18(b)).

Section Characteristics

The section characteristics of the S413 airfoil with transition free predicted using the method of references 8 and 9 and the method of reference 11 are shown in figure 19. It should be remembered that the section characteristics predicted using the method of references 8 and 9 are limited to conditions at which the flow is everywhere subsonic. The results are in reasonable agreement, except for the width of the low-drag range and the maximum lift coefficient. The method of reference 11 probably predicts wider low-drag ranges because it predicts transition later. At a Mach number of 0.40 and a Reynolds number of 1.34×10^6 (fig. 19(a)), the maximum lift coefficient predicted by the method of references 8 and 9 is 0.80, which is below the design objective; the maximum lift coefficient predicted by the method of reference 11 is 1.08, which exceeds the design objective. The upper limit of the low-drag range at a Mach number of 0.61 and a Reynolds number of 1.98×10^6 (fig. 19(b)) is lower than the design objective. At a Mach number of 0.80 and a Reynolds number of 2.61×10^6 (fig. 19(d)), the lower limit meets the design objective and the zero-lift pitching-moment coefficient, 0.000, satisfies the design constraint.

The effect of fixing transition on the section characteristics predicted using the method of references 8 and 9 is shown in figure 20. The section characteristics, with the exception of the maximum lift coefficient and the drag coefficient, are essentially unaffected by fixing transition. At a Mach number of 0.40 and a Reynolds number of 1.34×10^6 (fig. 20(a)), the maximum lift coefficient increases with transition fixed. The drag coefficients are, of course, adversely affected.

The effect of fixing transition on the section characteristics predicted using the method of reference 11 is shown in figure 21. At a Mach number of 0.40 and a Reynolds number of 1.34×10^6 (fig. 21(a)), the maximum lift coefficient increases slightly with transition fixed. For all conditions, the other section characteristics, with the exception of the drag coefficient, are essentially unaffected by fixing transition. The drag coefficients are adversely affected.

CONCLUDING REMARKS

A family of airfoils, the S411, S412, and S413, intended for rotorcraft applications has been designed and analyzed theoretically. The two primary objectives of a high maximum lift coefficient, relatively insensitive to leading-edge roughness, and low profile-drag coefficients have been achieved. The constraint on the zero-lift pitching-moment coefficient of the primary airfoil, the S411, has been exceeded; those of the outboard and tip airfoils, the S412 and S413, respectively, have been satisfied. The constraints on the airfoil thicknesses have been satisfied. The primary airfoil incorporates a 5-percent-chord tab.

ACKNOWLEDGMENTS

This effort was sponsored by the U.S. Army. Preston B. Martin served as the technical monitor.

REFERENCES

1. Noonan, Kevin W.: Aerodynamic Characteristics of Two Rotorcraft Airfoils Designed for Application to the Inboard Region of a Main Rotor Blade. NASA TP-3009, 1990.

2. Somers, Dan M.; and Maughmer, Mark D.: Design and Experimental Results for the S411 Airfoil. U.S. Army RDECOM TR 10-D-111, 2010. (Available from DTIC.)

3. Abbott, Ira H.; Von Doenhoff, Albert E.; and Stivers, Louis S., Jr.: Summary of Airfoil Data. NACA Rep. 824, 1945. (Supersedes NACA WR L-560.)

4. Eppler, Richard; and Somers, Dan M.: Airfoil Design for Reynolds Numbers Between 50,000 and 500,000. Proceedings of the Conference on Low Reynolds Number Airfoil Aerodynamics, UNDAS-CP-77B123, Univ. of Notre Dame, June 1985, pp. 1–14.

5. Wortmann, F. X.: Experimental Investigations on New Laminar Profiles for Gliders and Helicopters. TIL/T.4906, British Minist. Aviat., Mar. 1960. (Translated from Z. Flugwissenschaften, Bd. 5, Heft 8, Aug. 1957, S. 228–243.)

6. Maughmer, Mark D.; and Somers, Dan M.: Design and Experimental Results for a High-Altitude, Long-Endurance Airfoil. J. Aircr., vol. 26, no. 2, Feb. 1989, pp. 148–153.

7. Eppler, R.: Laminar Airfoils for Reynolds Numbers Greater Than 4×10^6. B-819-35, Apr. 1969. (Available from NTIS as N69-28178; translated from Ingenieur-Archiv, Bd. 38, Heft 4/5, 1969, S. 232–240.)

8. Eppler, Richard: Airfoil Design and Data. Springer-Verlag (Berlin), 1990.

9. Eppler, Richard: Airfoil Program System “PROFIL07.” User’s Guide. Richard Eppler, c.2007.

10. Somers, Dan M.: Subsonic Natural-Laminar-Flow Airfoils. Natural Laminar Flow and Laminar Flow Control, R. W. Barnwell and M. Y. Hussaini, eds., Springer-Verlag New York, Inc., 1992, pp. 143–176.

11. Drela, M.: Design and Optimization Method for Multi-Element Airfoils. AIAA Paper 93-0969, Feb. 1993.

12. Labrujere, Th. E.; Loeve, W.; and Sloof, J. W.: An Approximate Method for the Determination of the Pressure Distribution on Wings in the Lower Critical Speed Range. Transonic Aerodynamics. AGARD CP No. 35, Sept. 1968, pp. 17-1–17-10.

TABLE I.- AIRFOIL DESIGN SPECIFICATIONS

(a) Primary airfoil

Parameter	Objective/ Constraint	Mach Number M	Reynolds Number R	Priority
Minimum lift coefficient $c_{l,min}$	0.00[1]	0.70	2.26×10^6	Low
Maximum lift coefficient $c_{l,max}$	1.25 1.20	0.30 0.40	0.97×10^6 1.29×10^6	High
Lower limit of low-drag, lift-coefficient range $c_{l,ll}$	0.10	0.70	2.26×10^6	Medium
Upper limit of low-drag, lift-coefficient range $c_{l,ul}$	0.65	0.45	1.45×10^6	Medium
Zero-lift pitching-moment coefficient $c_{m,0}$	0 ± 0.002[1] 0 ± 0.005[2]	0.75 0.45	2.42×10^6 1.45×10^6	High
Thickness t/c	0.14 with tab			Medium
Other requirements: Maximum lift coefficient $c_{l,max}$ independent of leading-edge roughness Docile stall characteristics 5-percent-chord tab with thickness of 0.352-percent chord				

[1]With transition fixed at 10-percent chord on upper and lower surfaces.

[2]With transition free.

TABLE I.- Continued

(b) Outboard airfoil

Parameter	Objective/ Constraint	Mach Number M	Reynolds Number R	Priority
Minimum lift coefficient $c_{l,\min}$	–0.05	0.78	2.51×10^6	Low
Maximum lift coefficient $c_{l,\max}$	1.00	0.40	1.34×10^6	High
Lower limit of low-drag, lift-coefficient range $c_{l,\mathrm{ll}}$	0.00	0.78	2.51×10^6	High
Upper limit of low-drag, lift-coefficient range $c_{l,\mathrm{ul}}$	0.50	0.58	1.88×10^6	Medium
Zero-lift pitching-moment coefficient $c_{m,0}$	0 ± 0.002	0.78	2.51×10^6	High
Thickness t/c	0.12			Medium
Other requirements: Maximum lift coefficient $c_{l,\max}$ relatively independent of leading-edge roughness Docile stall characteristics Trailing-edge thickness of 0.352-percent chord				

TABLE I.- Concluded

(c) Tip airfoil

Parameter	Objective/ Constraint	Mach Number M	Reynolds Number R	Priority
Minimum lift coefficient $c_{l,\min}$	–0.10	0.80	2.61×10^6	Low
Maximum lift coefficient $c_{l,\max}$	1.00	0.40	1.34×10^6	Medium
Lower limit of low-drag, lift-coefficient range $c_{l,\mathrm{ll}}$	0.00	0.80	2.61×10^6	High
Upper limit of low-drag, lift-coefficient range $c_{l,\mathrm{ul}}$	0.50	0.61	1.98×10^6	High
Zero-lift pitching-moment coefficient $c_{m,0}$	0 ± 0.002	0.80	2.61×10^6	High
Thickness t/c	0.10			Medium
Other requirements: Maximum lift coefficient $c_{l,\max}$ relatively independent of leading-edge roughness Docile stall characteristics Trailing-edge thickness of 0.352-percent chord				

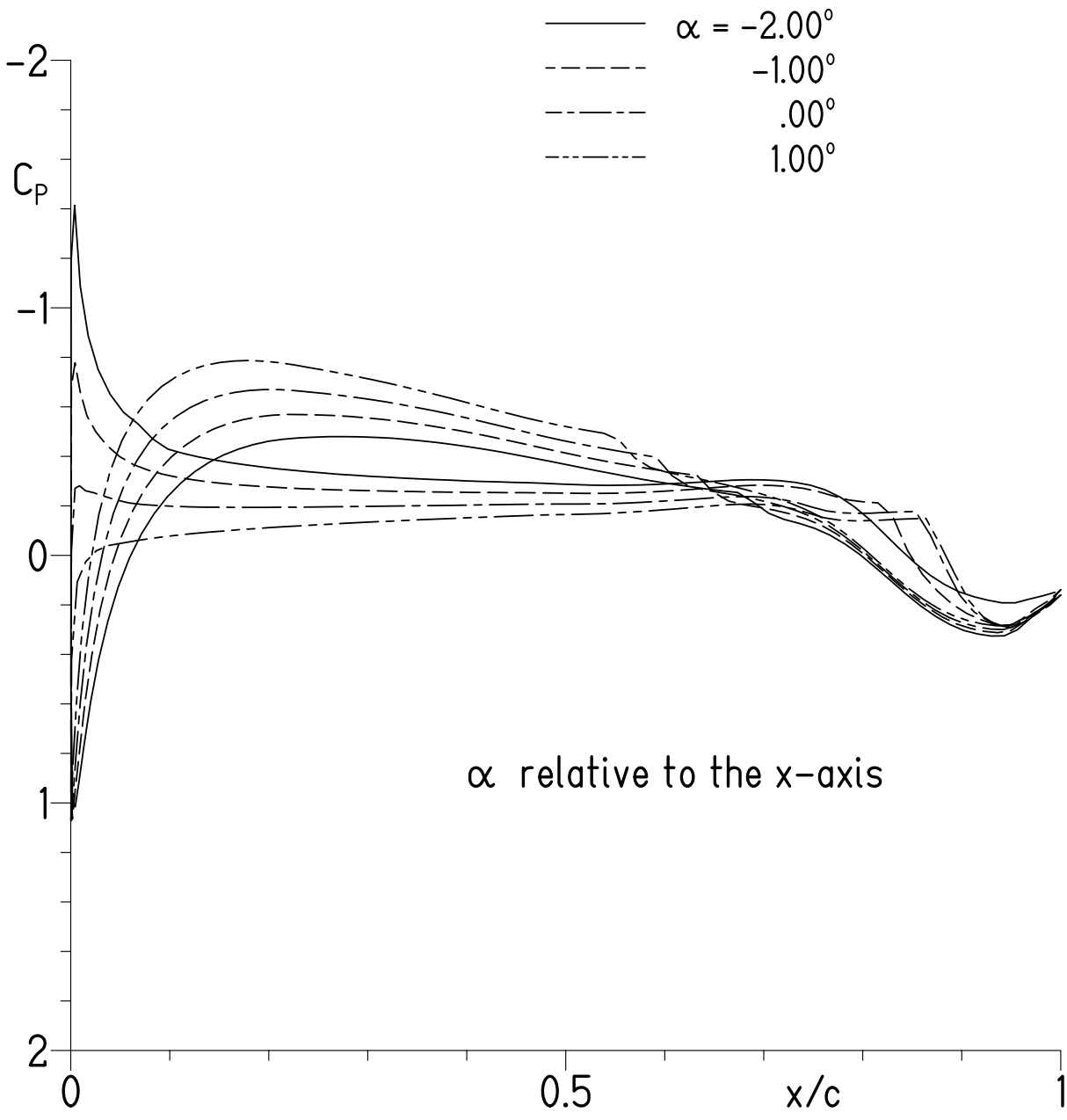

(a) $\alpha = -2.00°, -1.00°, 0.00°$, and $1.00°$.

Figure 1.- Pressure distributions for S411 airfoil at $M = 0.30$ and $R = 0.97 \times 10^6$ with transition free.

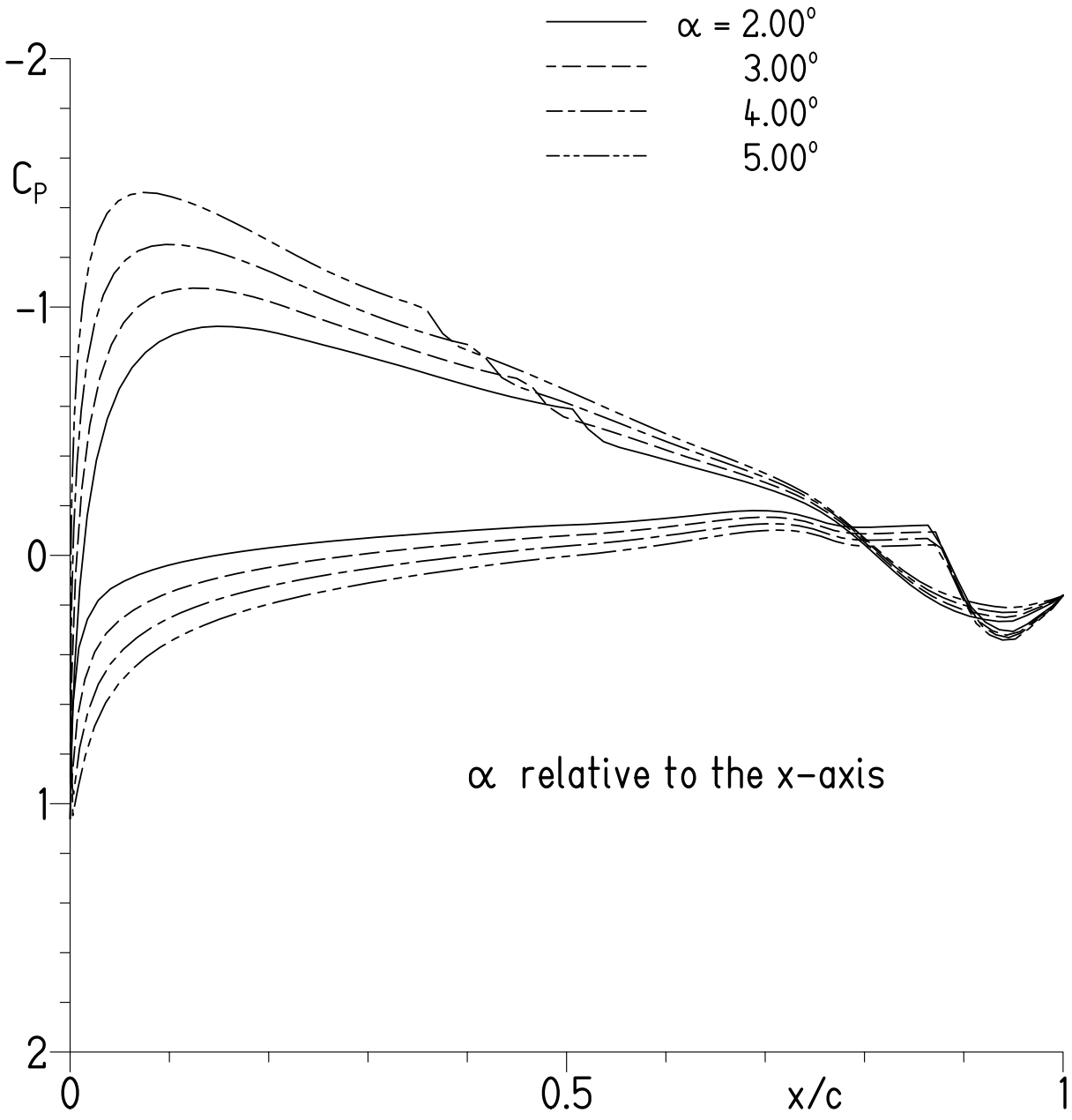

(b) $\alpha = 2.00°$, 3.00°, 4.00°, and 5.00°.

Figure 1.- Continued.

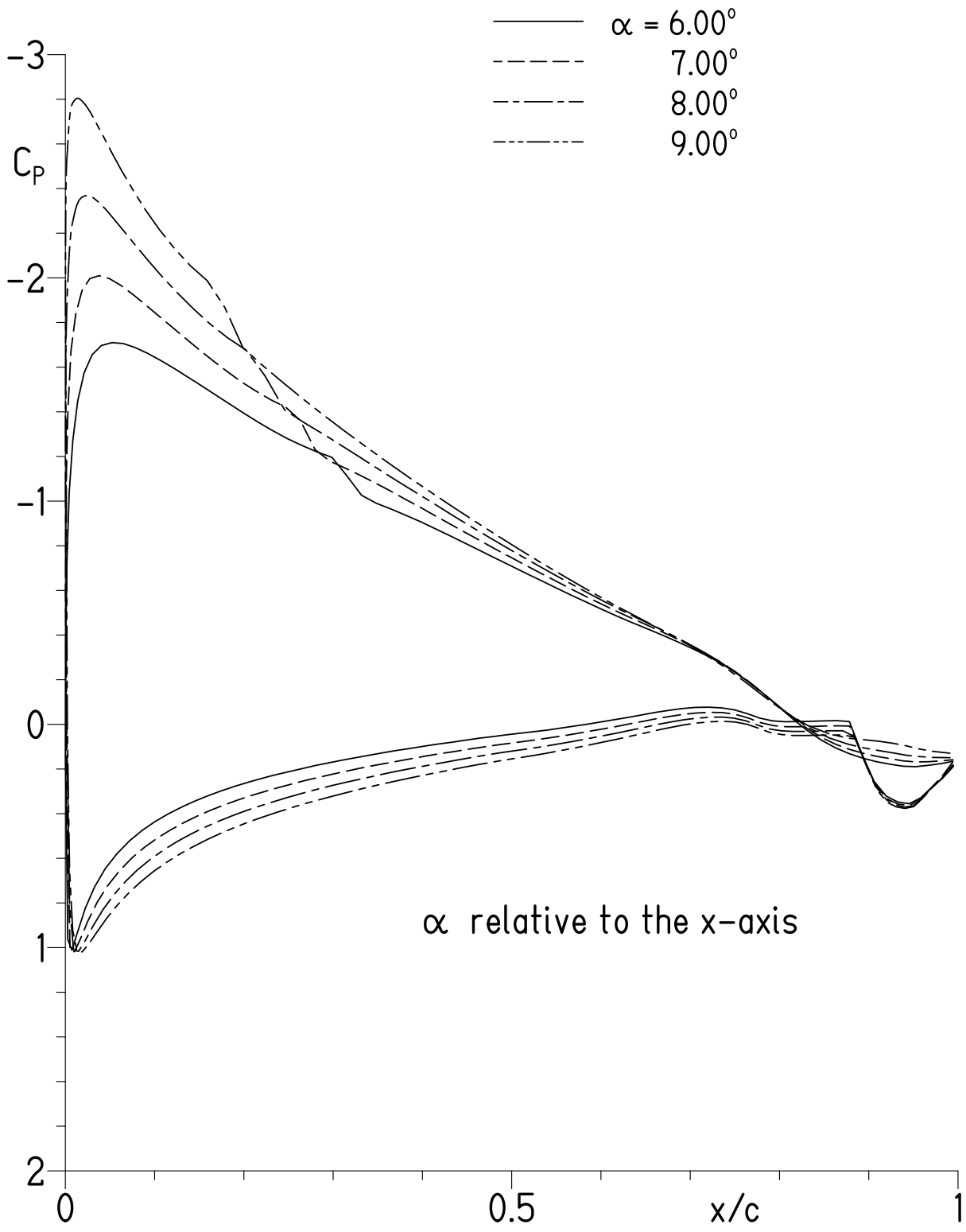

(c) $\alpha = 6.00°$, 7.00°, 8.00°, and 9.00°.

Figure 1.- Continued.

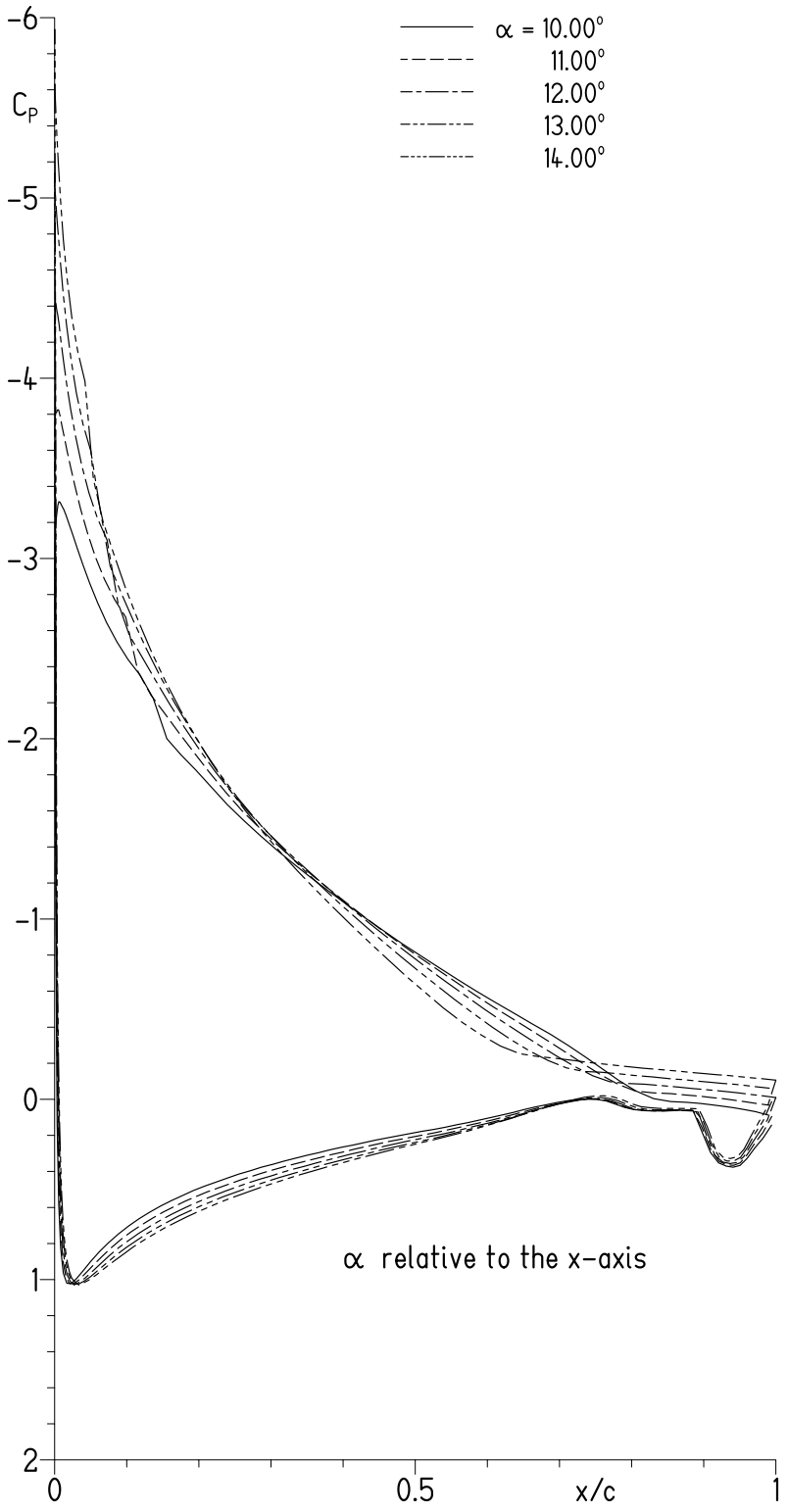

(d) $\alpha = 10.00°, 11.00°, 12.00°, 13.00°$, and $14.00°$.

Figure 1.- Concluded.

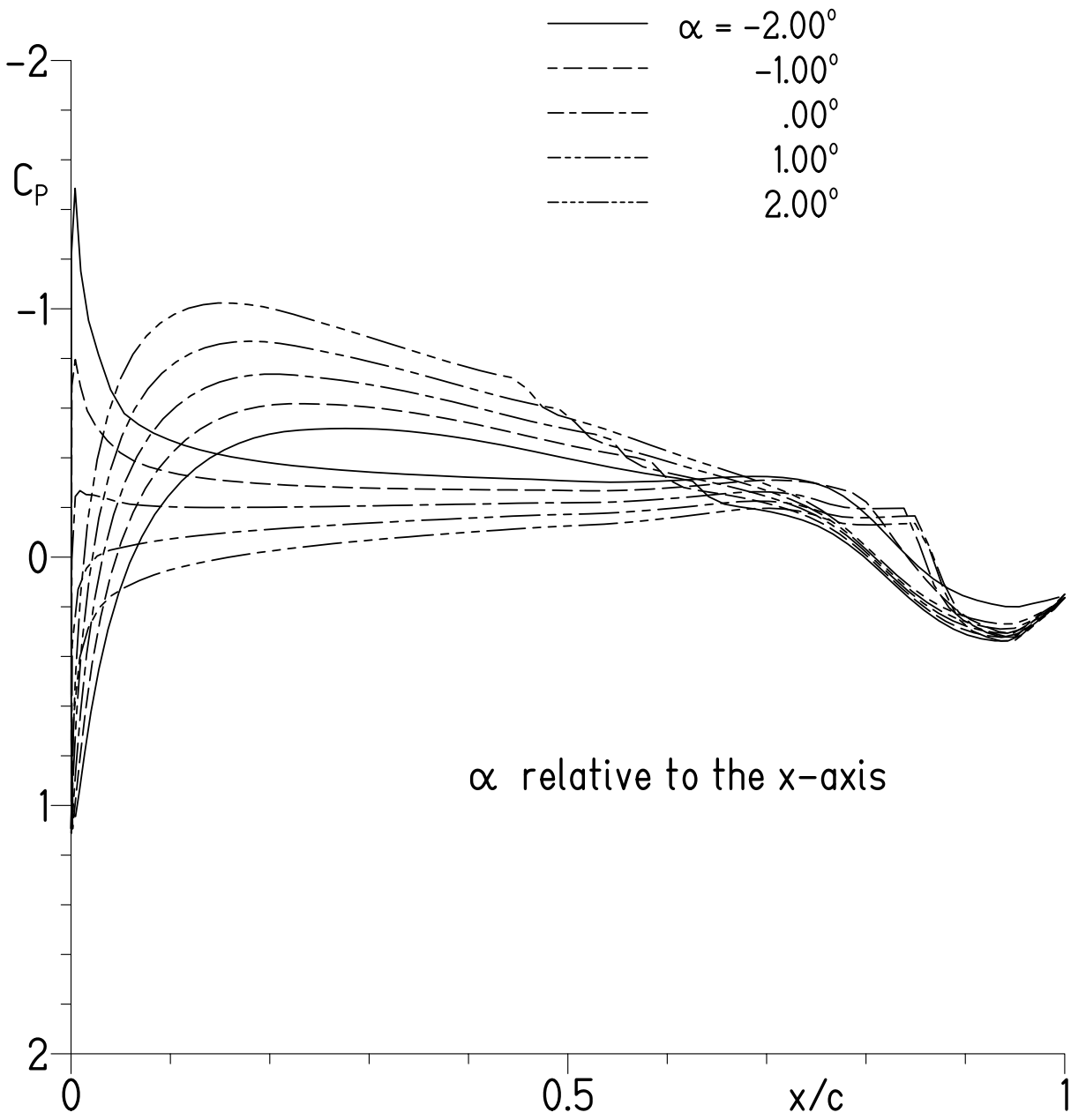

(a) $\alpha = -2.00°, -1.00°, 0.00°, 1.00°$, and $2.00°$.

Figure 2.- Pressure distributions for S411 airfoil at $M = 0.45$ and $R = 1.45 \times 10^6$ with transition free.

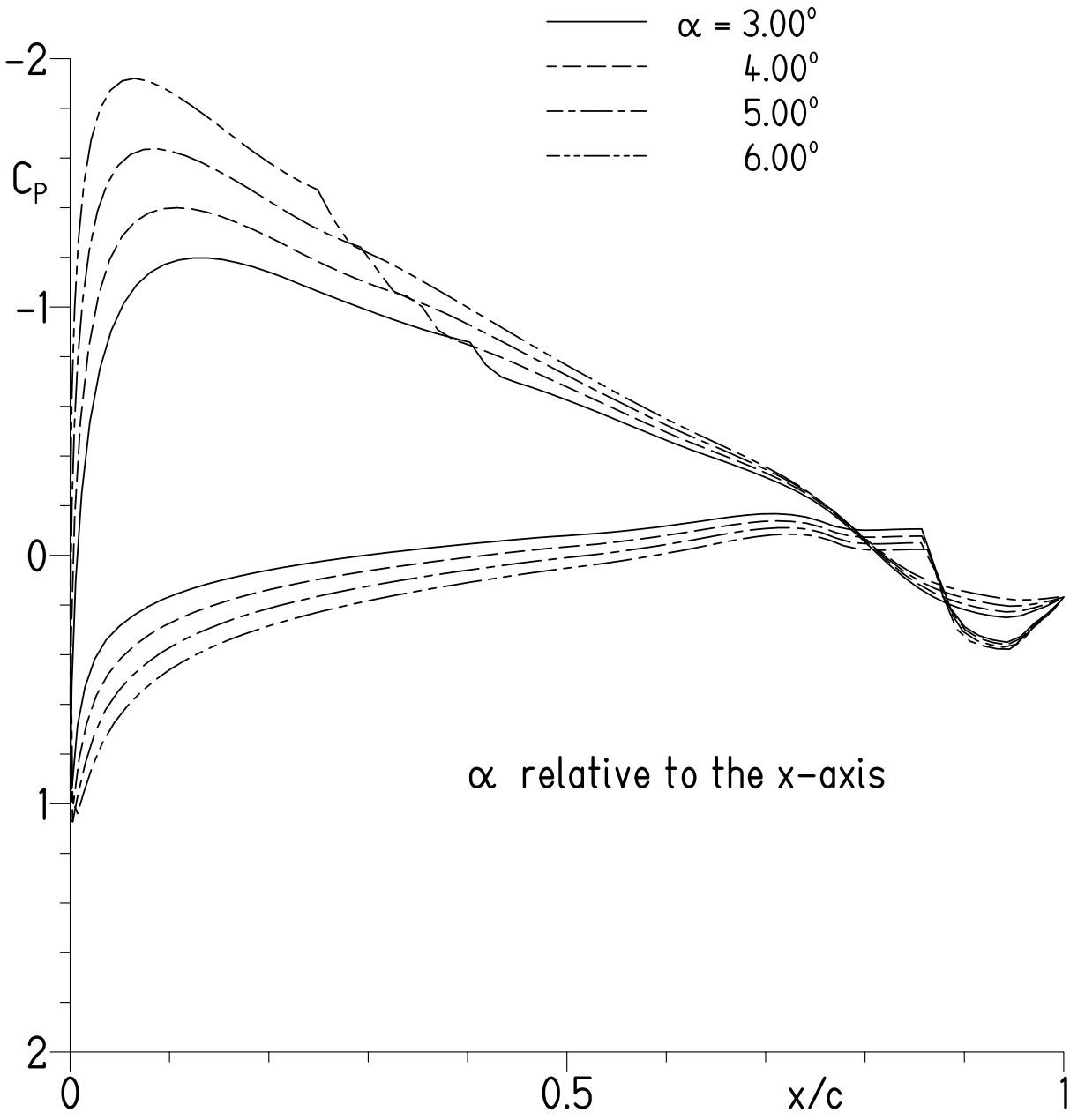

(b) $\alpha = 3.00°$, 4.00°, 5.00°, and 6.00°.

Figure 2.- Concluded.

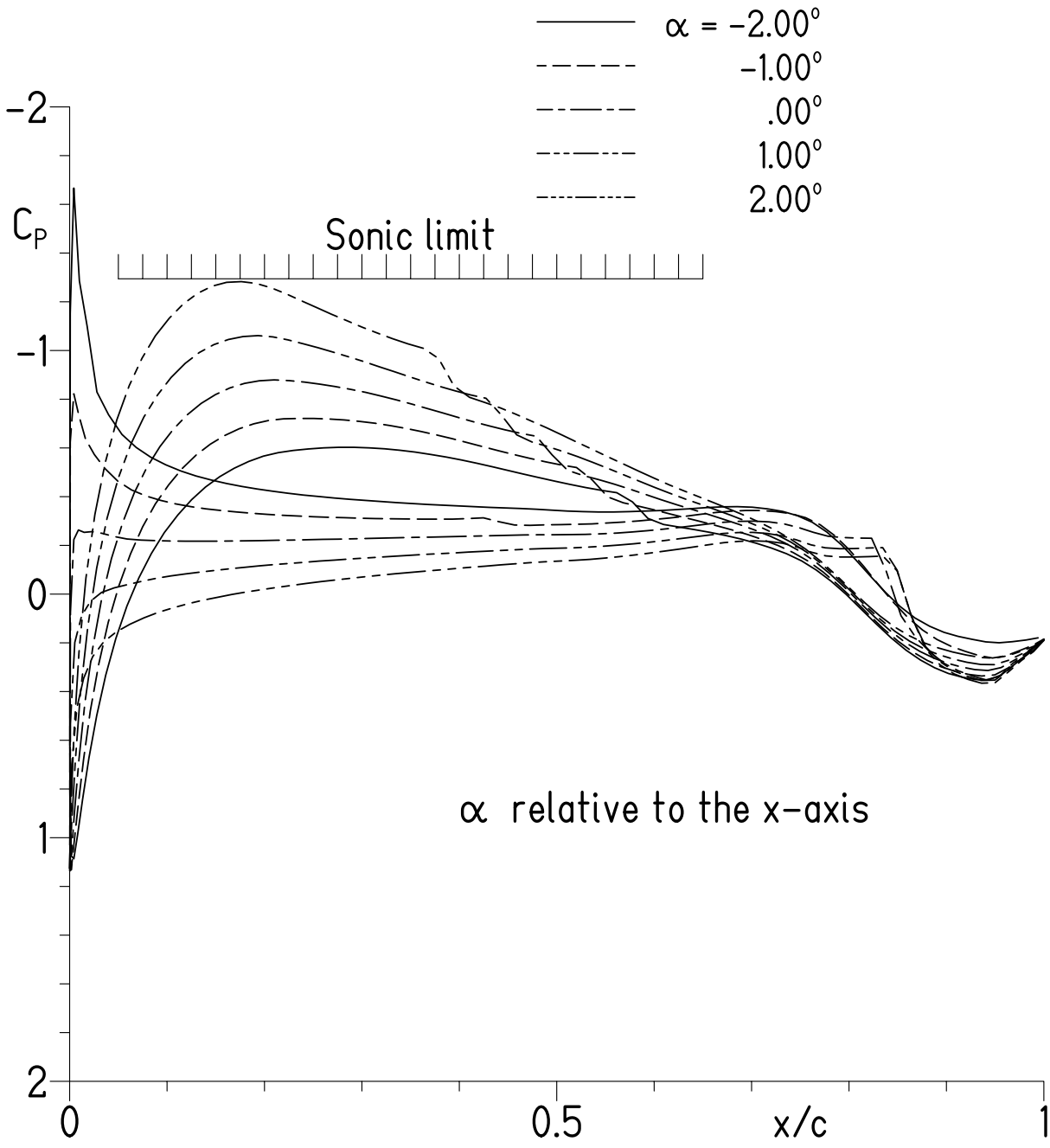

Figure 3.- Pressure distributions for S411 airfoil at $M = 0.60$ and $R = 1.94 \times 10^6$ with transition free.

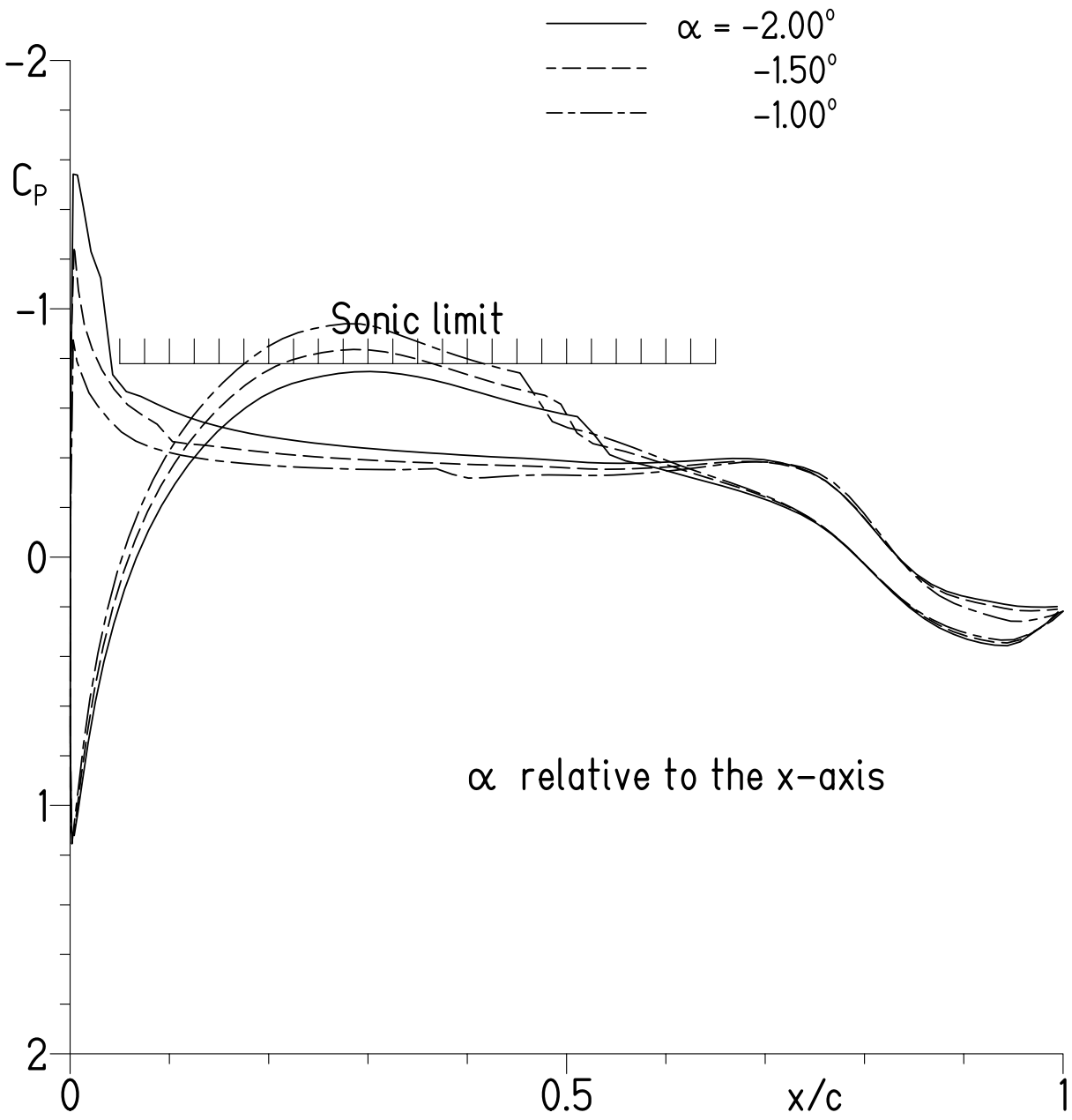

(a) $\alpha = -2.00°, -1.50°$, and $-1.00°$.

Figure 4.- Pressure distributions for S411 airfoil at $M = 0.70$ and $R = 2.26 \times 10^6$ with transition free.

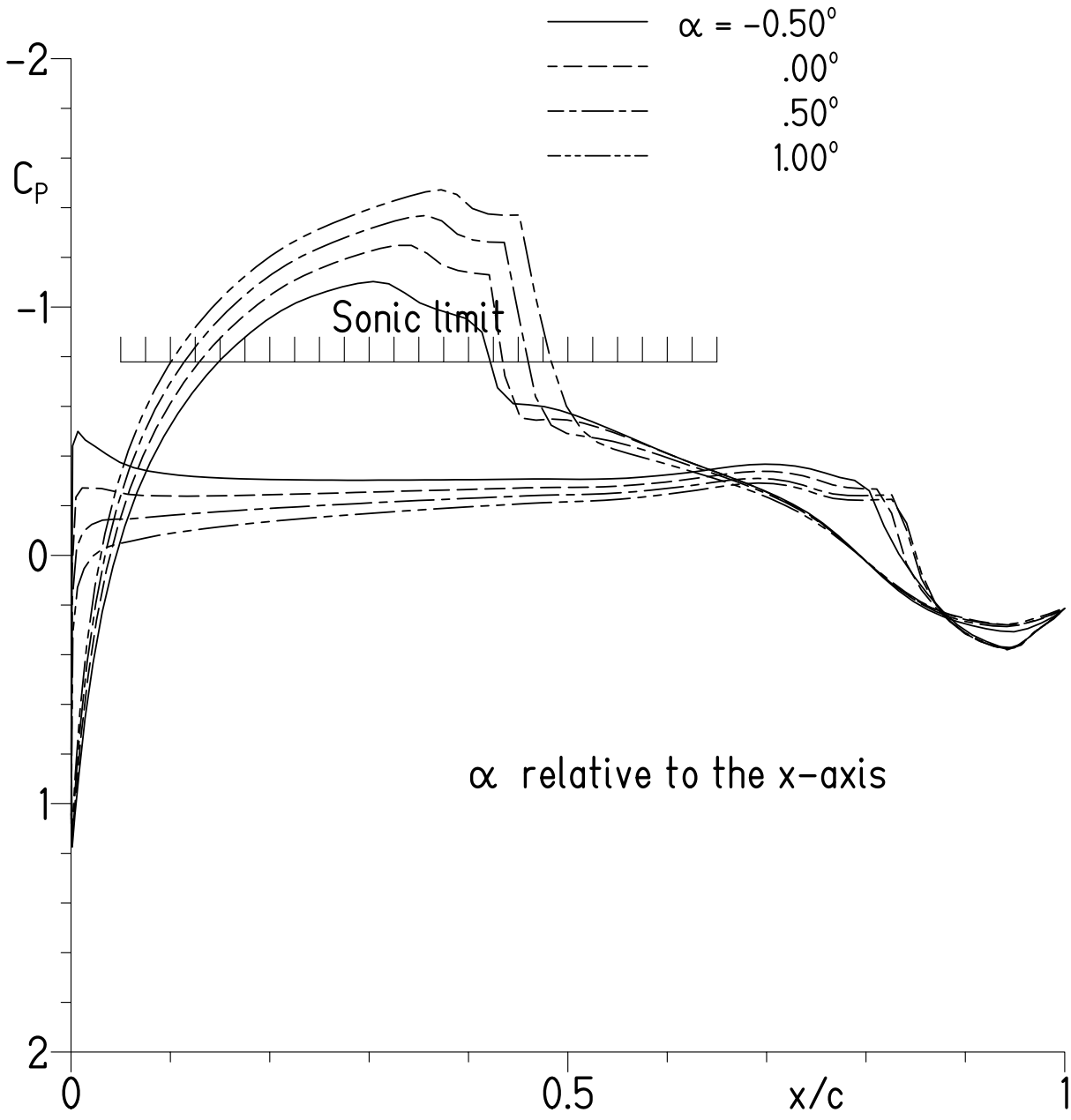

(b) $\alpha = -0.50°$, 0.00°, 0.50°, and 1.00°.

Figure 4.- Concluded.

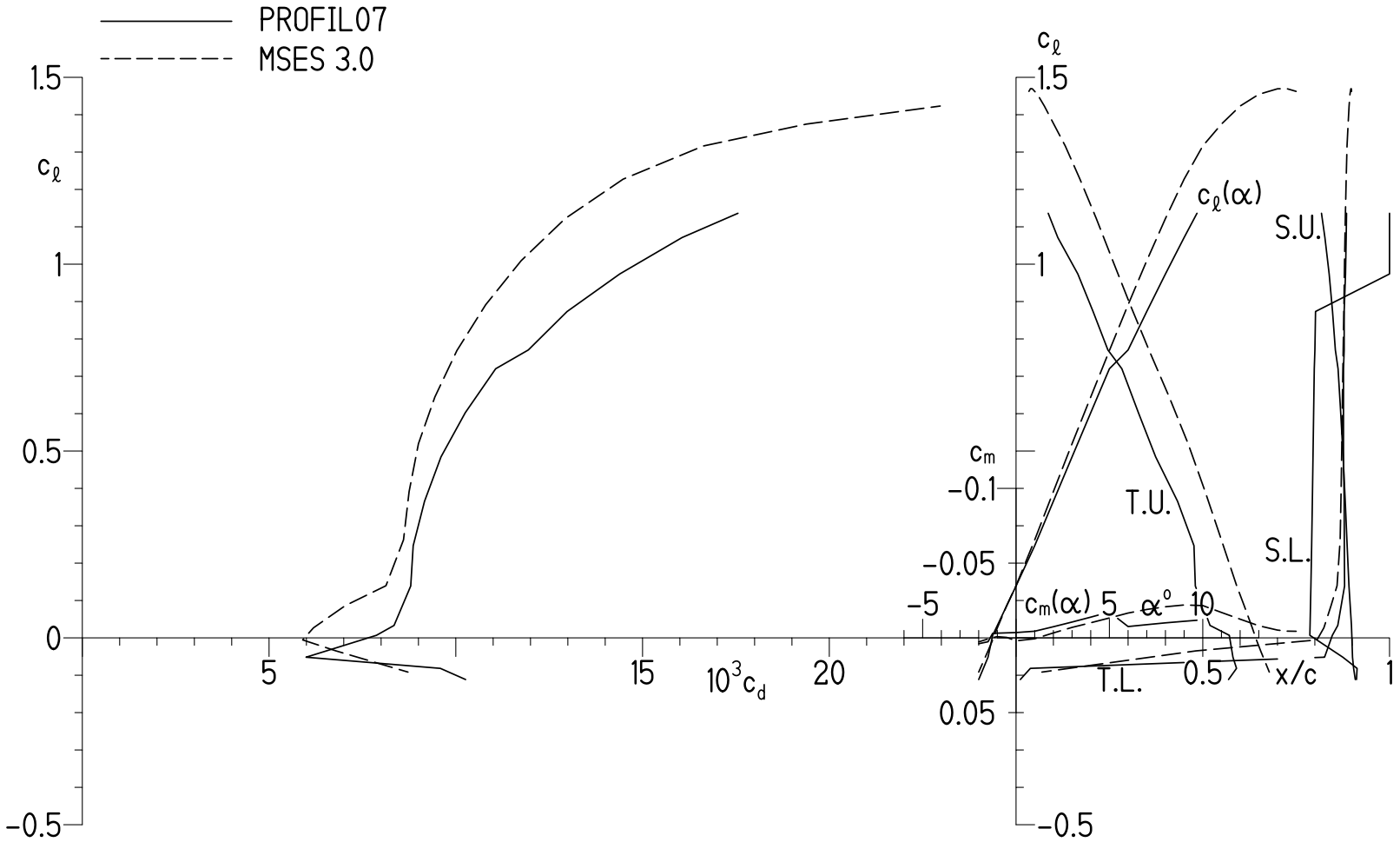

(a) M = 0.30 and R = 0.97×10^6.

Figure 5.- Section characteristics of S411 airfoil with transition free.

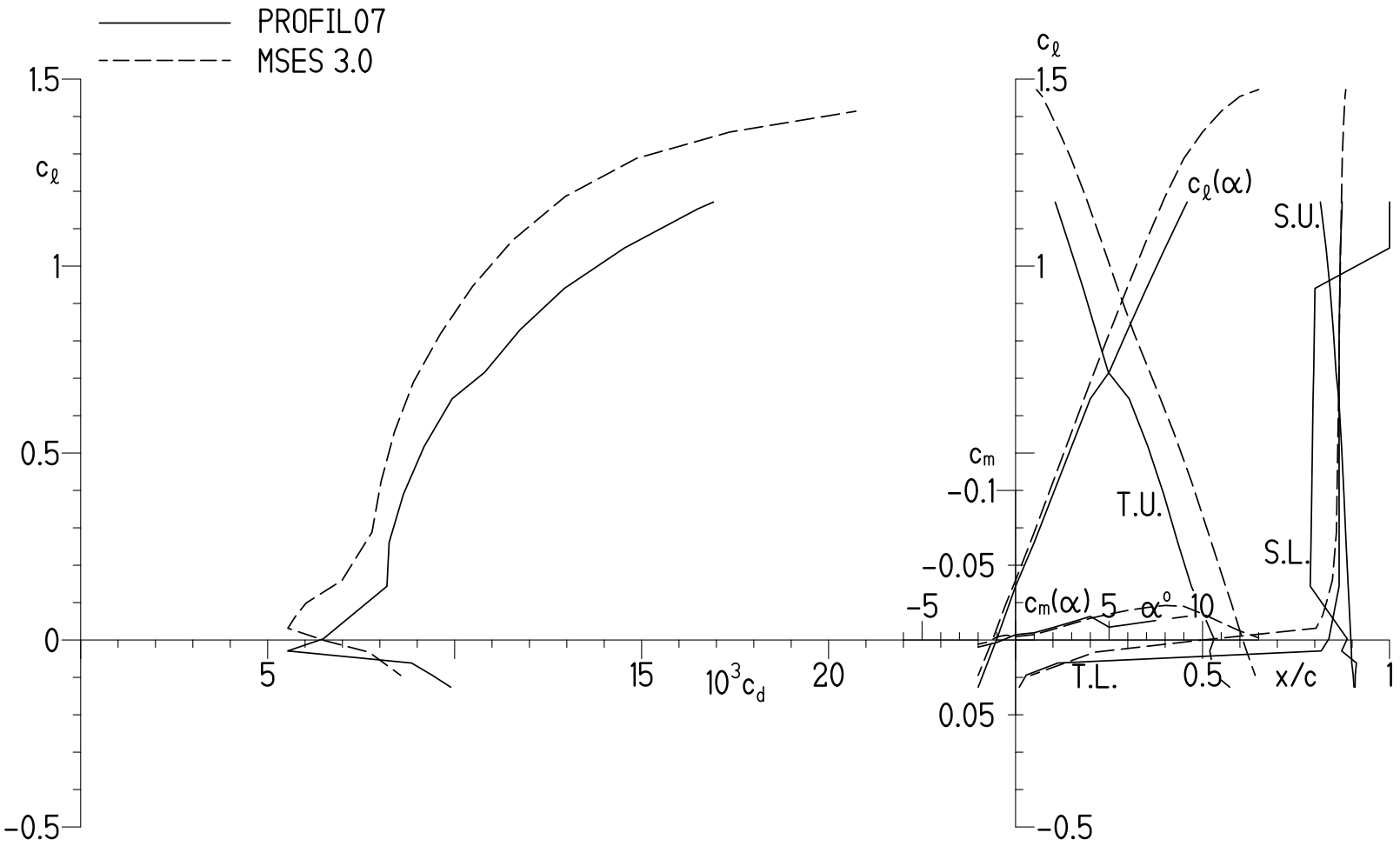

(b) M = 0.40 and R = 1.29×10^6.

Figure 5.- Continued.

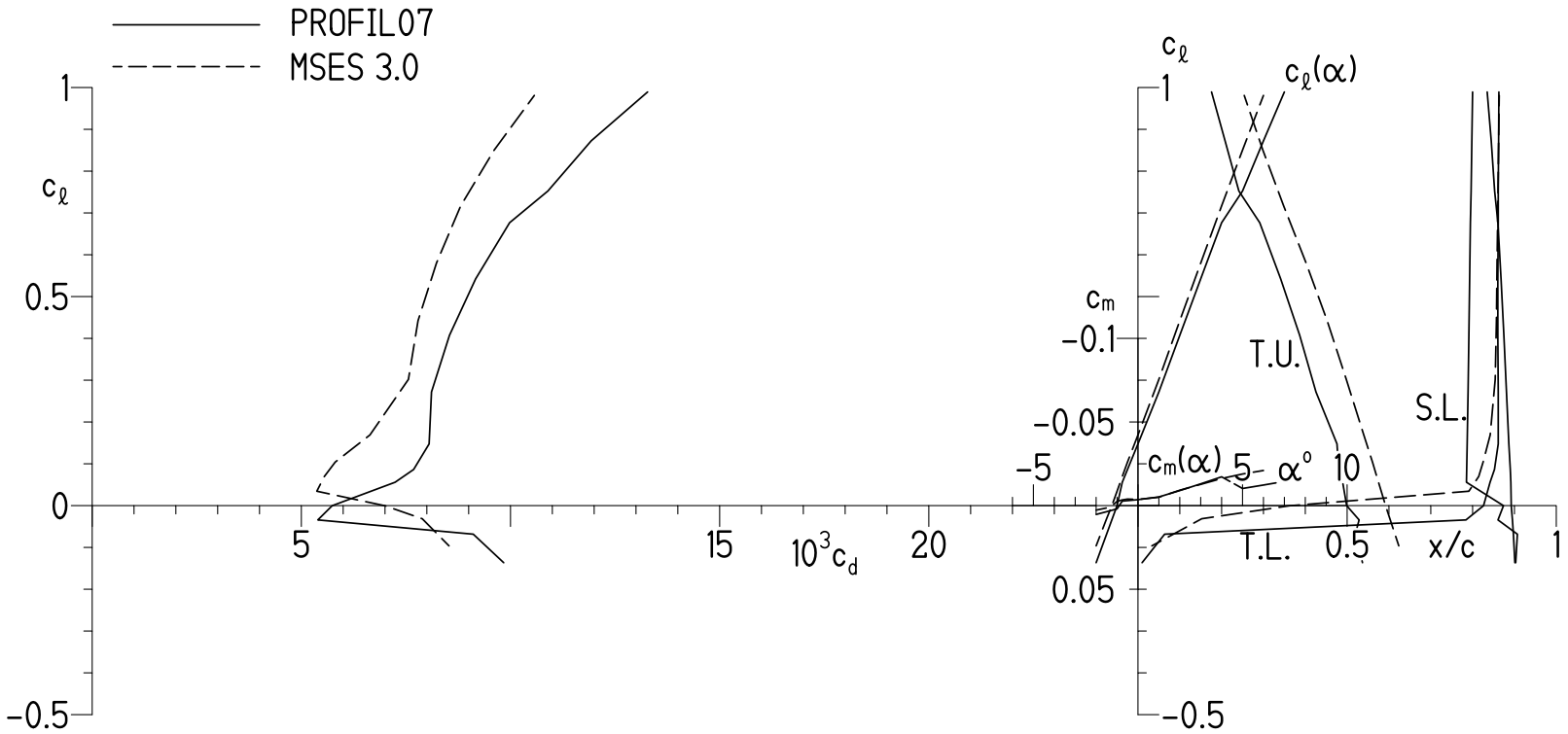

(c) M = 0.45 and R = 1.45×10^6.

Figure 5.- Continued.

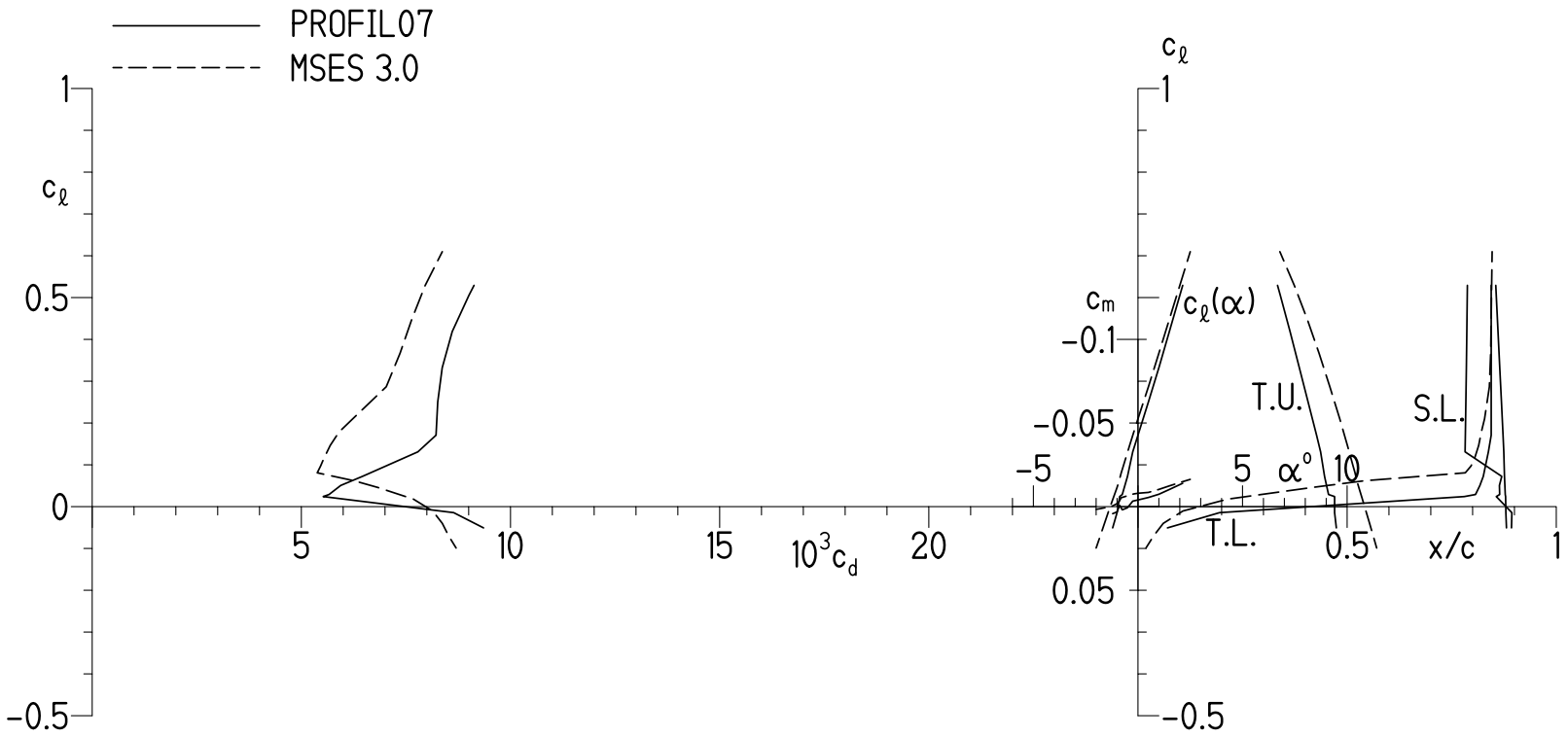

(d) M = 0.60 and R = 1.94×10^6.

Figure 5.- Continued.

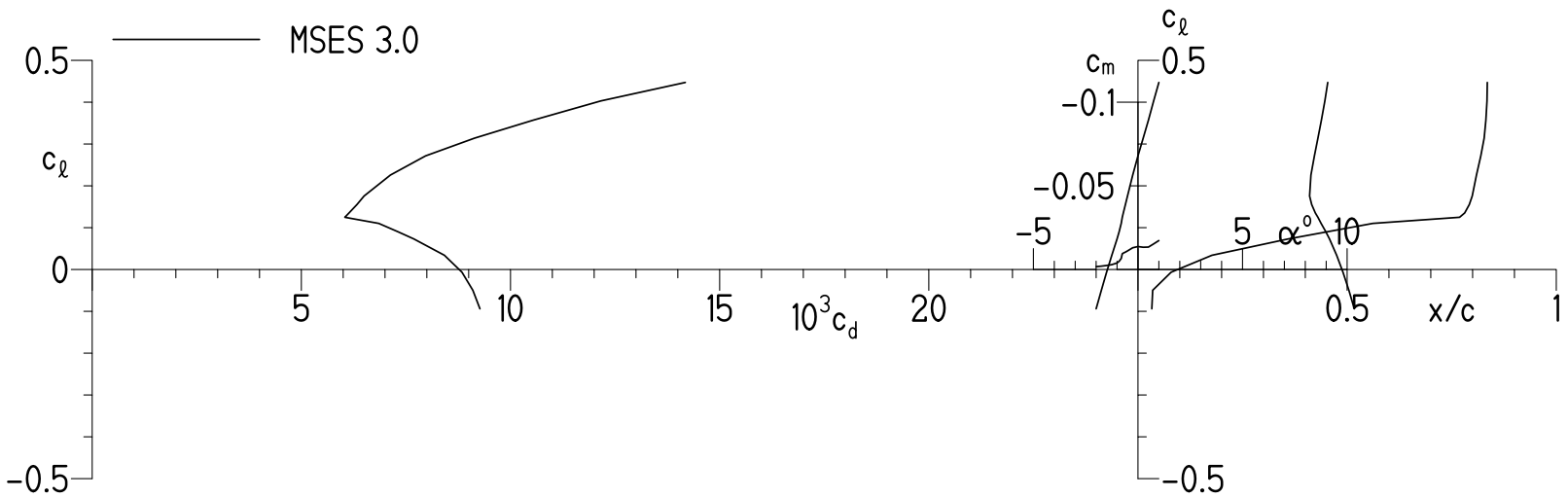

(e) M = 0.70 and R = 2.26×10^6.

Figure 5.- Concluded.

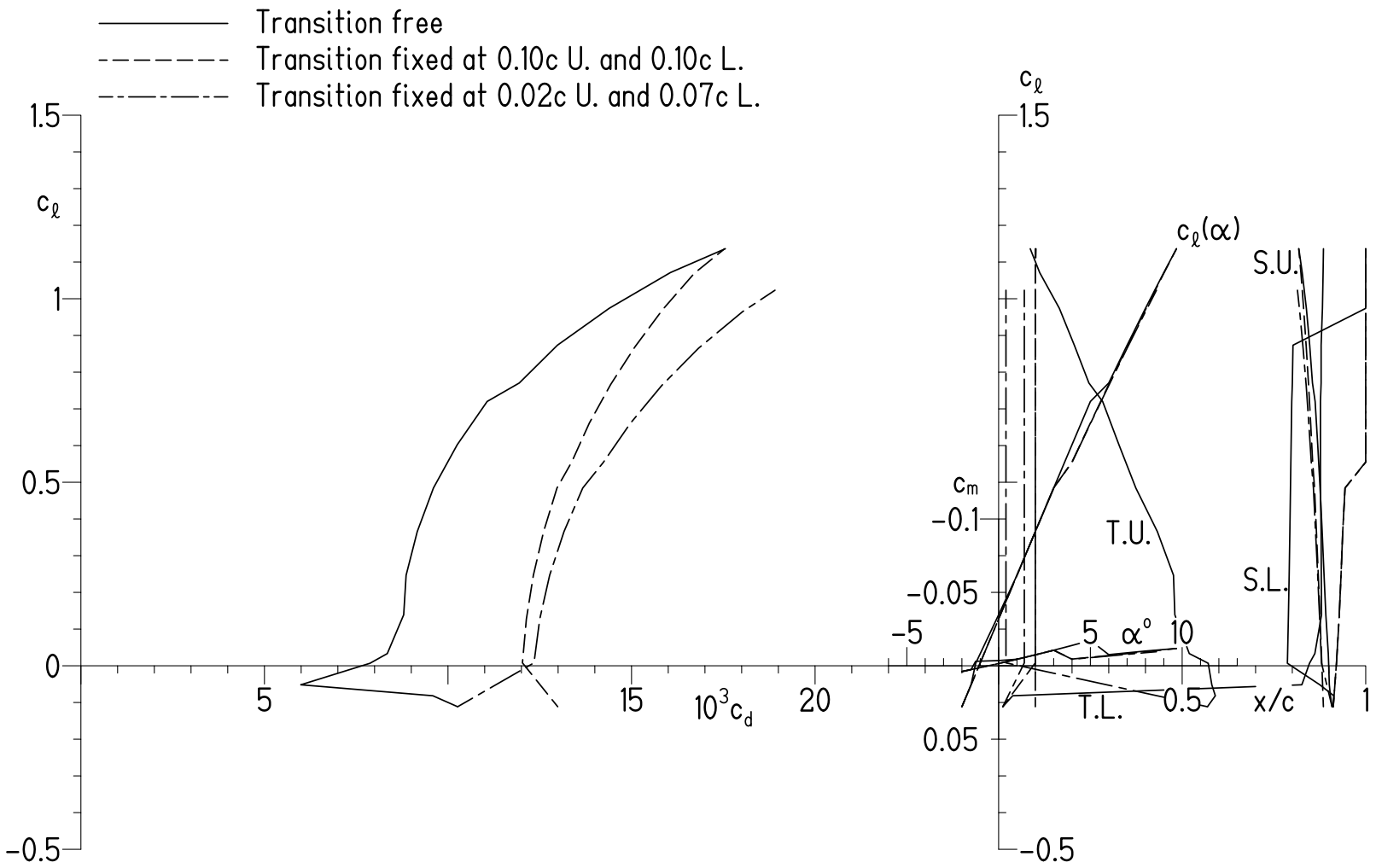

(a) $M = 0.30$ and $R = 0.97 \times 10^6$.

Figure 6.- Effect of fixing transition on section characteristics of S411 airfoil predicted using method of references 8 and 9.

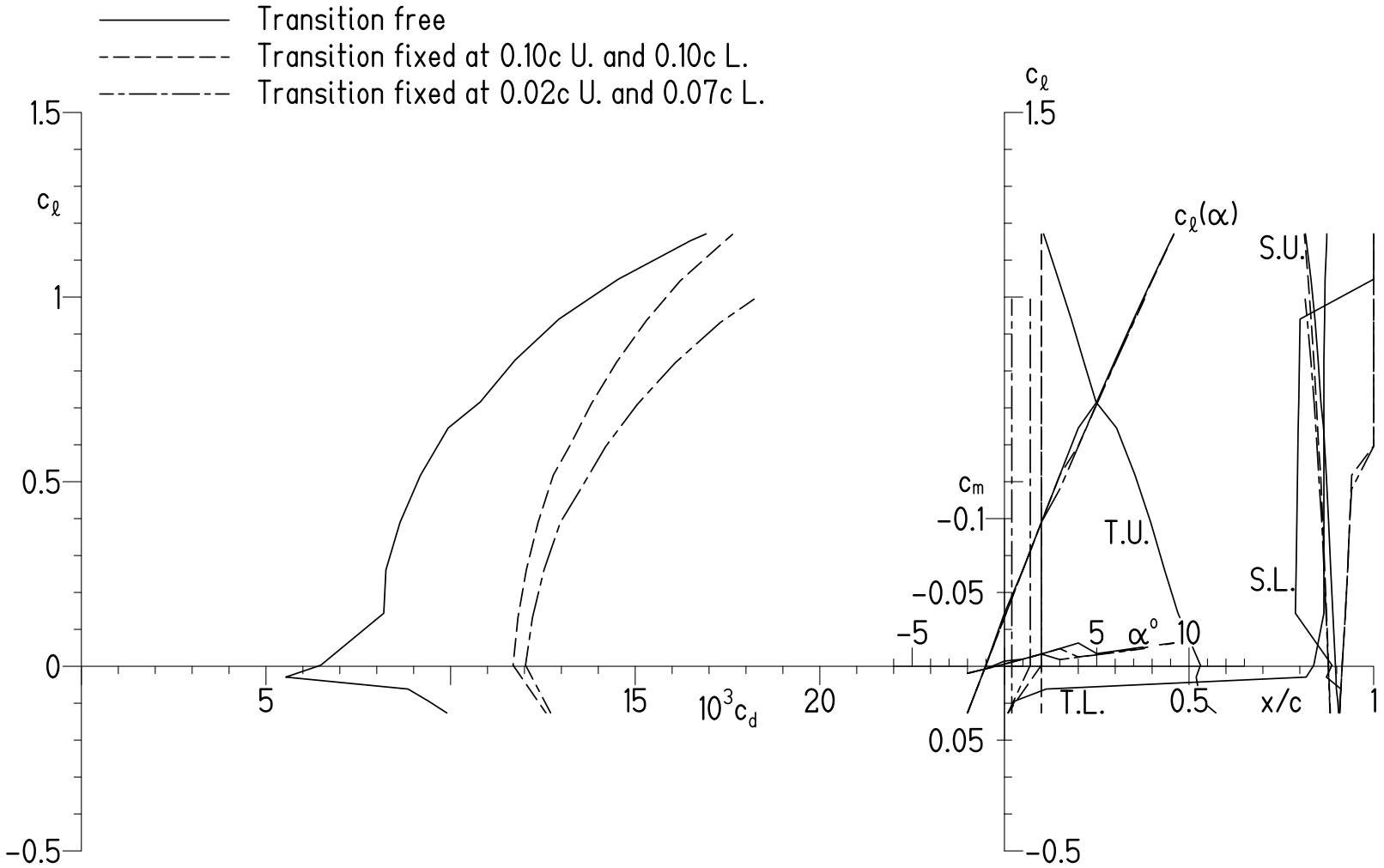

(b) M = 0.40 and R = 1.29×10^6.

Figure 6.- Continued.

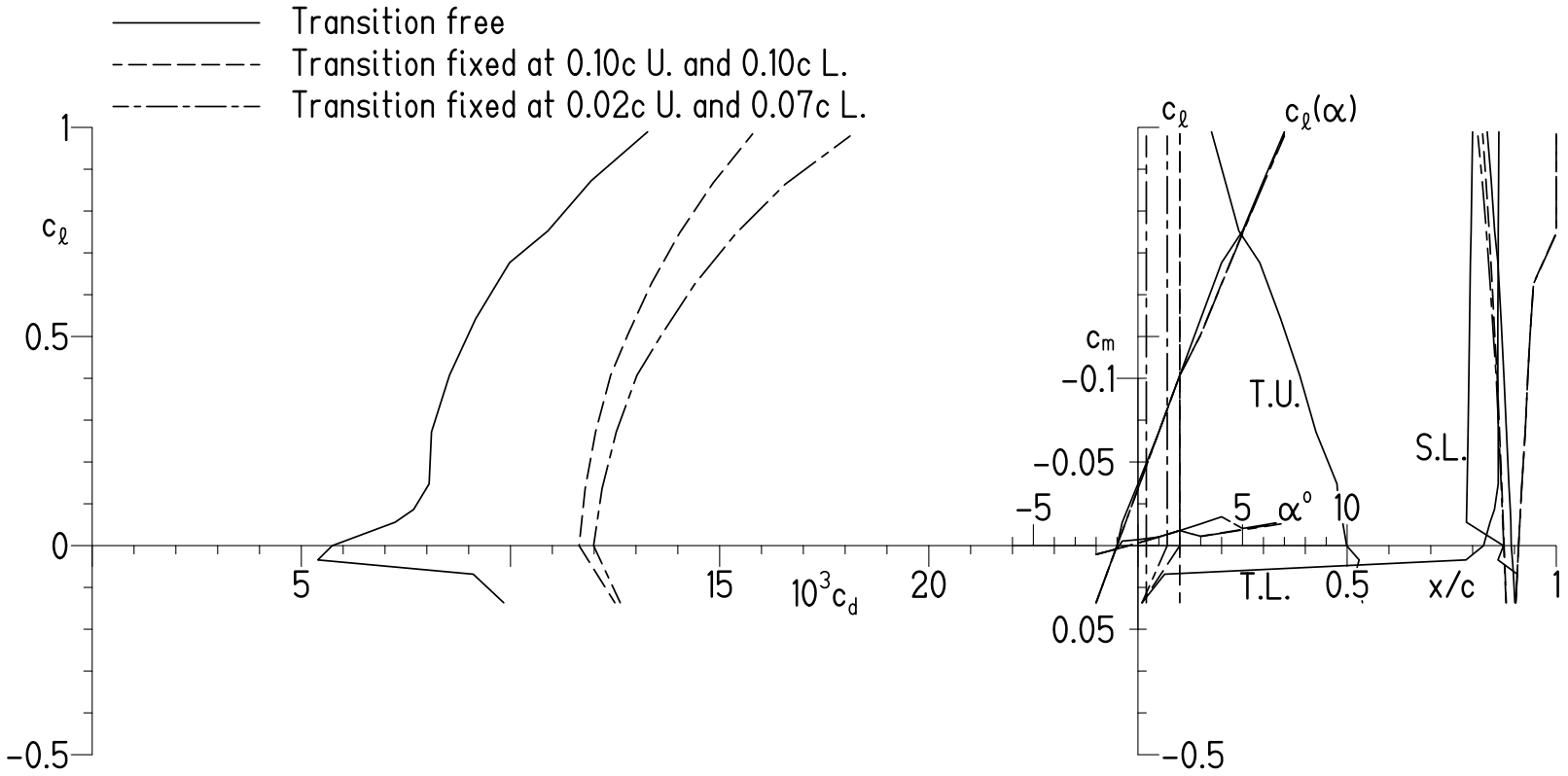

(c) M = 0.45 and R = 1.45×10^6.

Figure 6.- Continued.

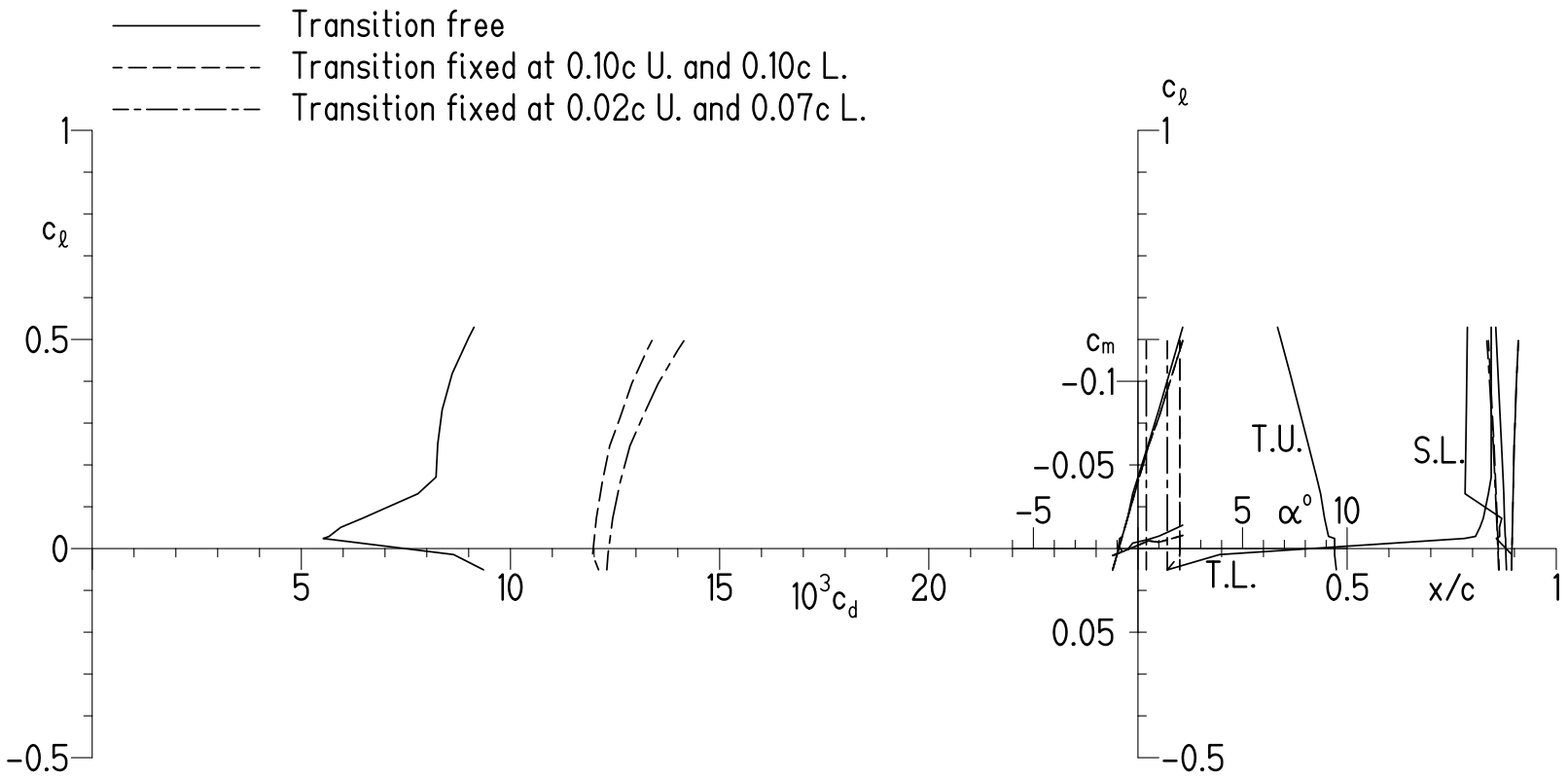

(d) M = 0.60 and R = 1.94×10^6.

Figure 6.- Concluded.

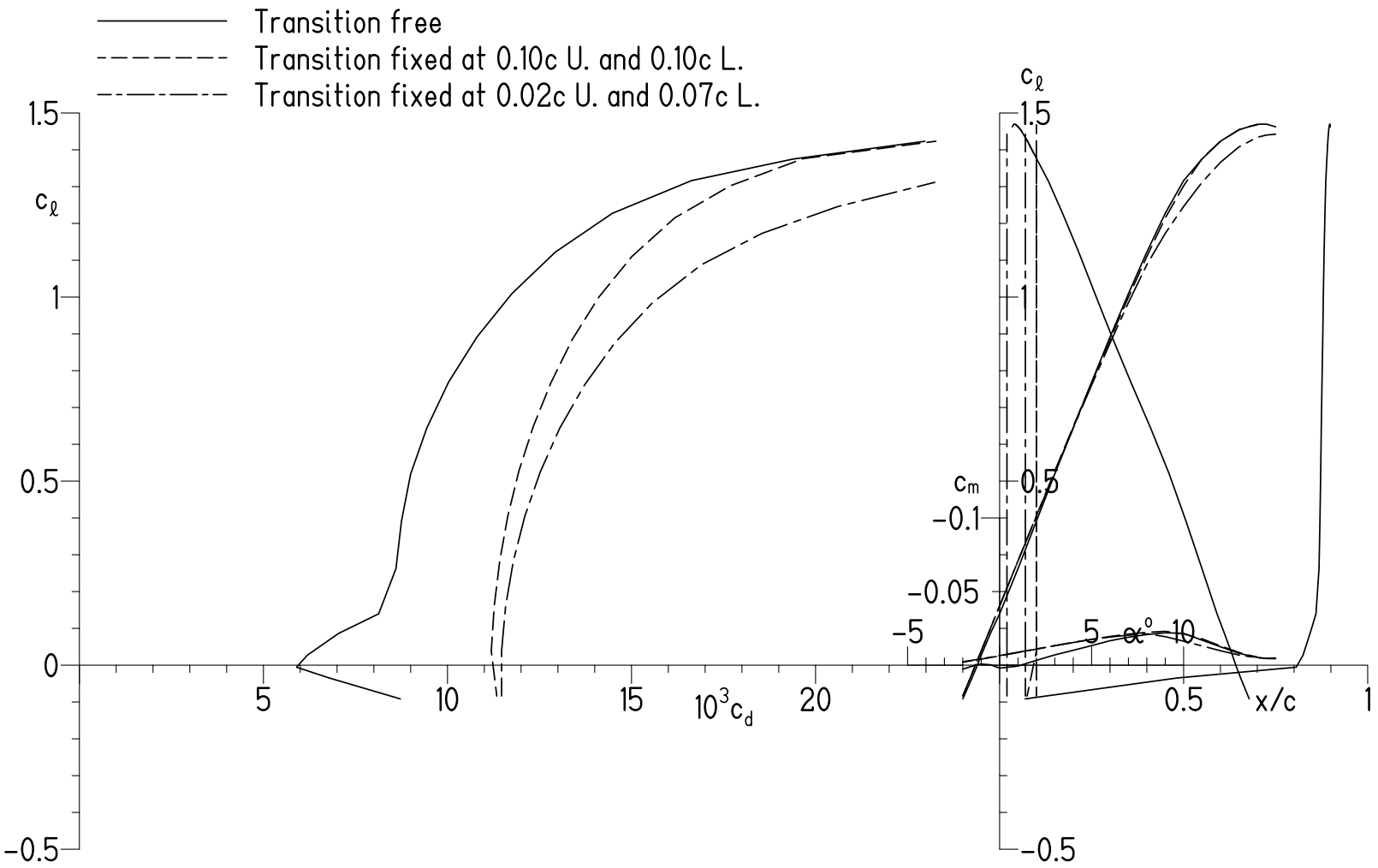

(a) M = 0.30 and R = 0.97×10^6.

Figure 7.- Effect of fixing transition on section characteristics of S411 airfoil predicted using method of reference 11.

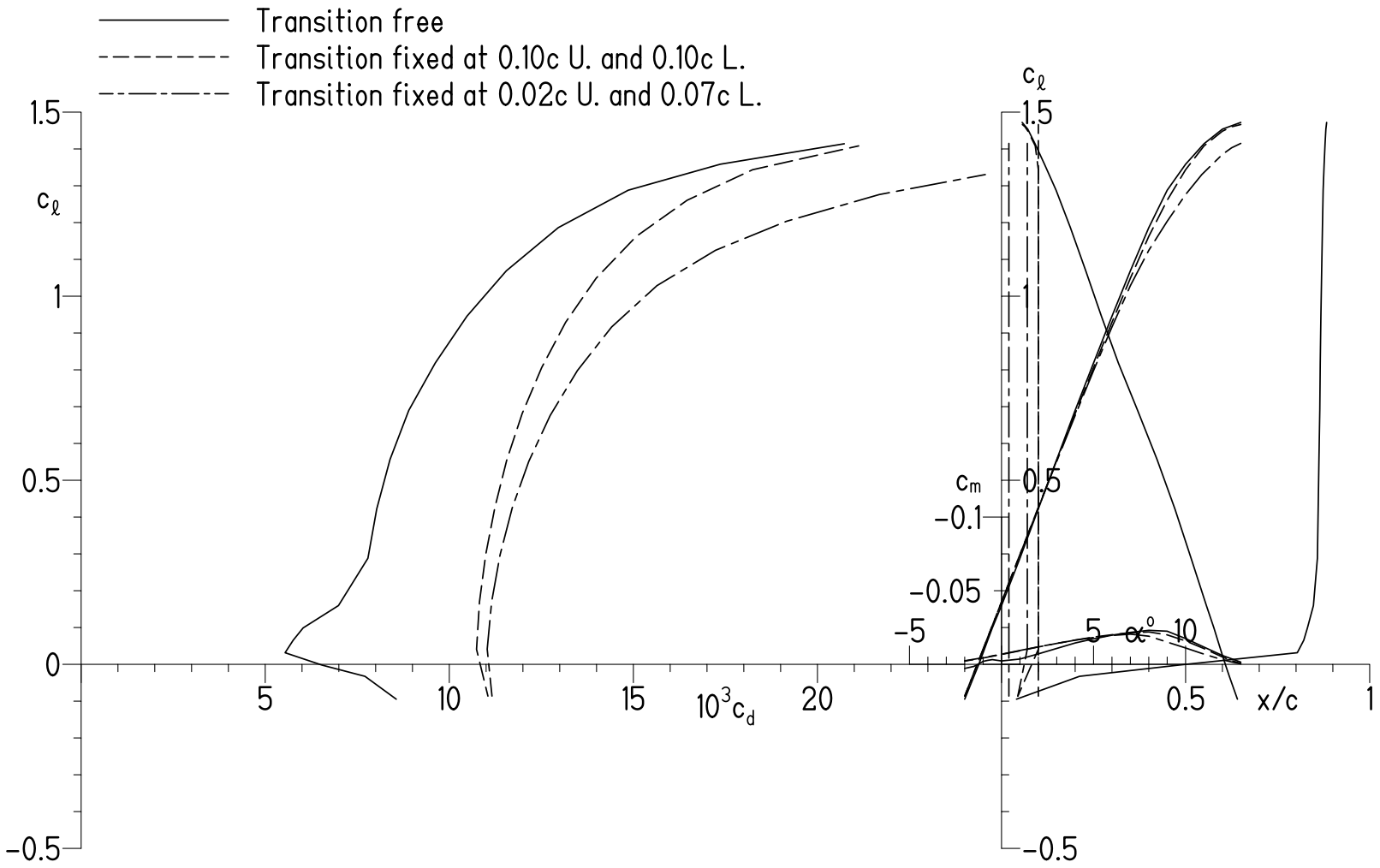

(b) M = 0.40 and R = 1.29×10^6.

Figure 7.- Continued.

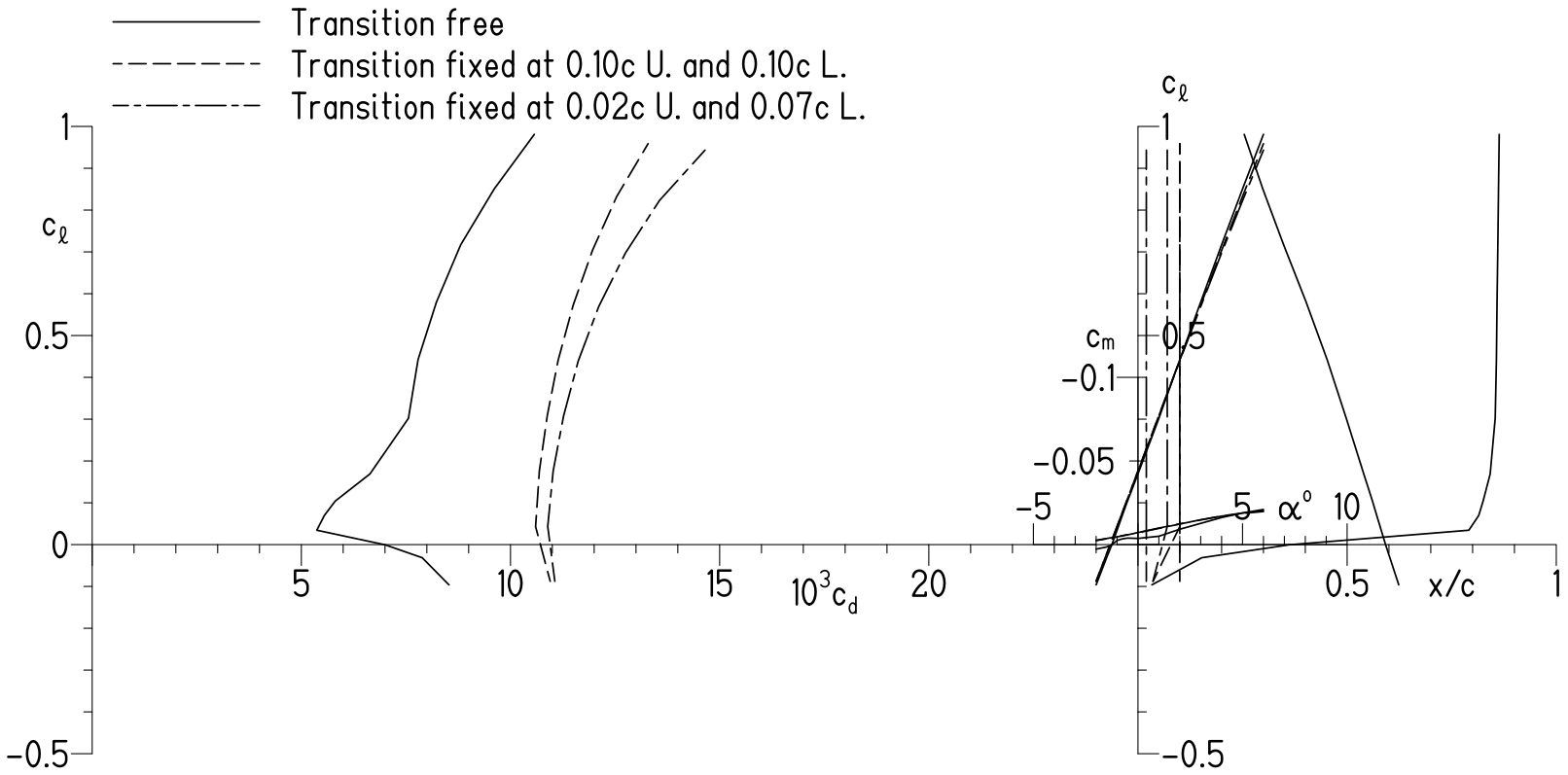

(c) $M = 0.45$ and $R = 1.45 \times 10^6$.

Figure 7.- Continued.

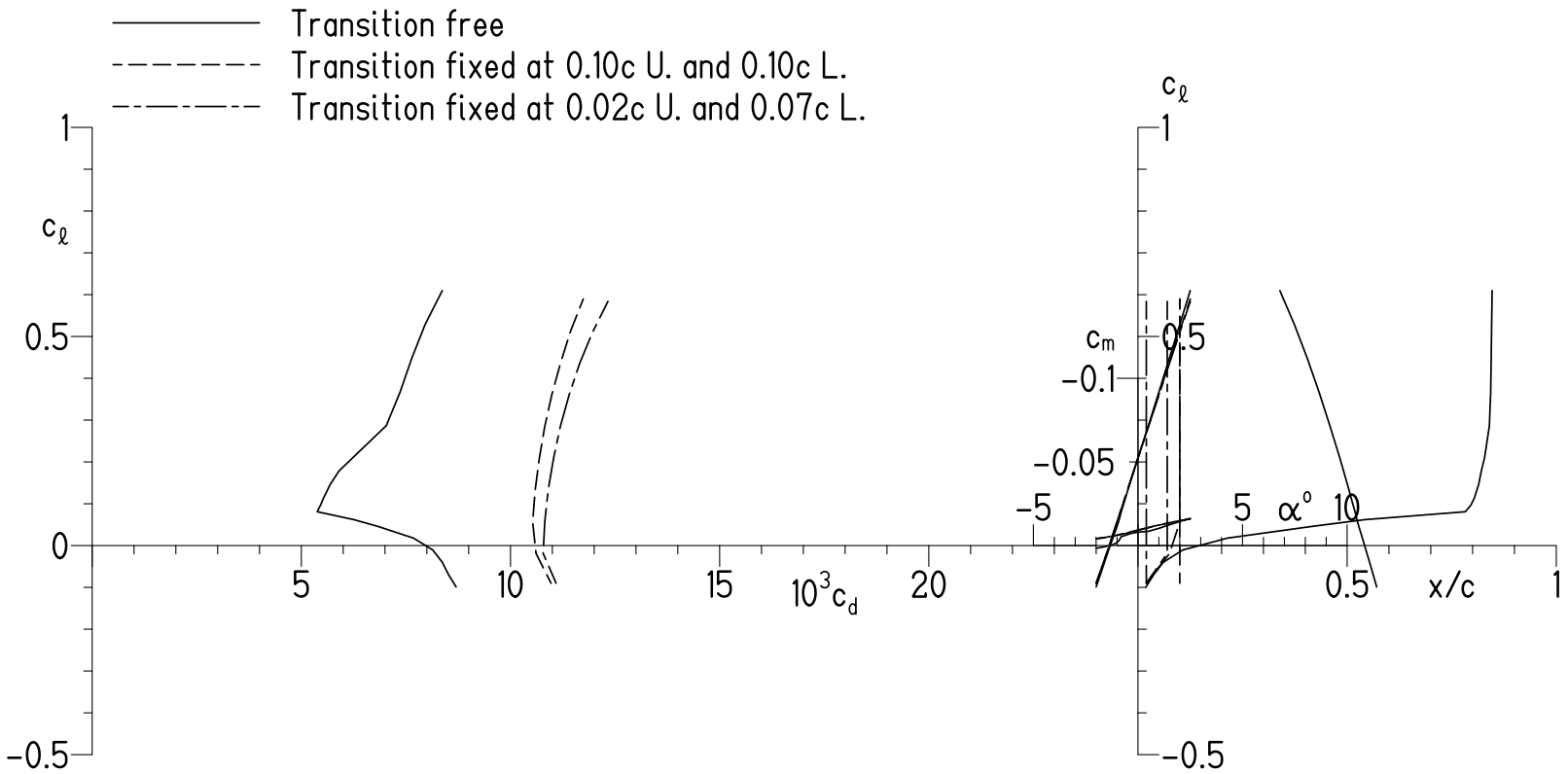

(d) M = 0.60 and R = 1.94×10^6.

Figure 7.- Continued.

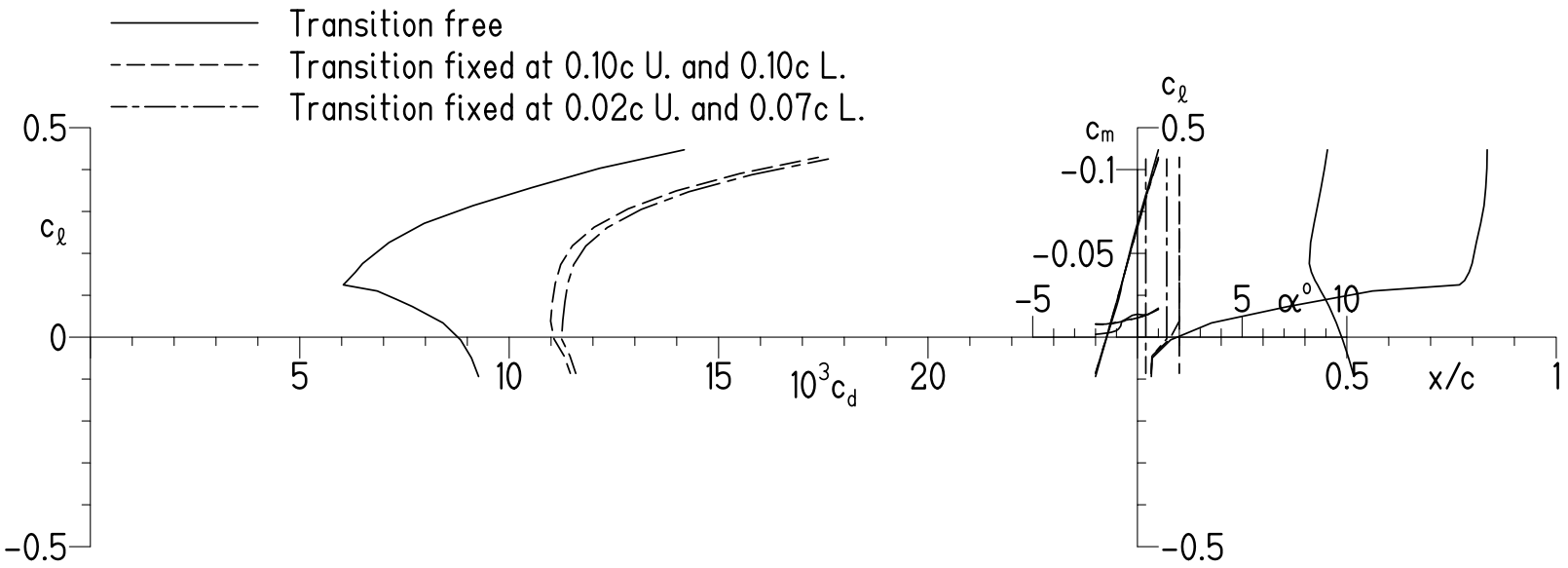

(e) $M = 0.70$ and $R = 2.26 \times 10^6$.

Figure 7.- Concluded.

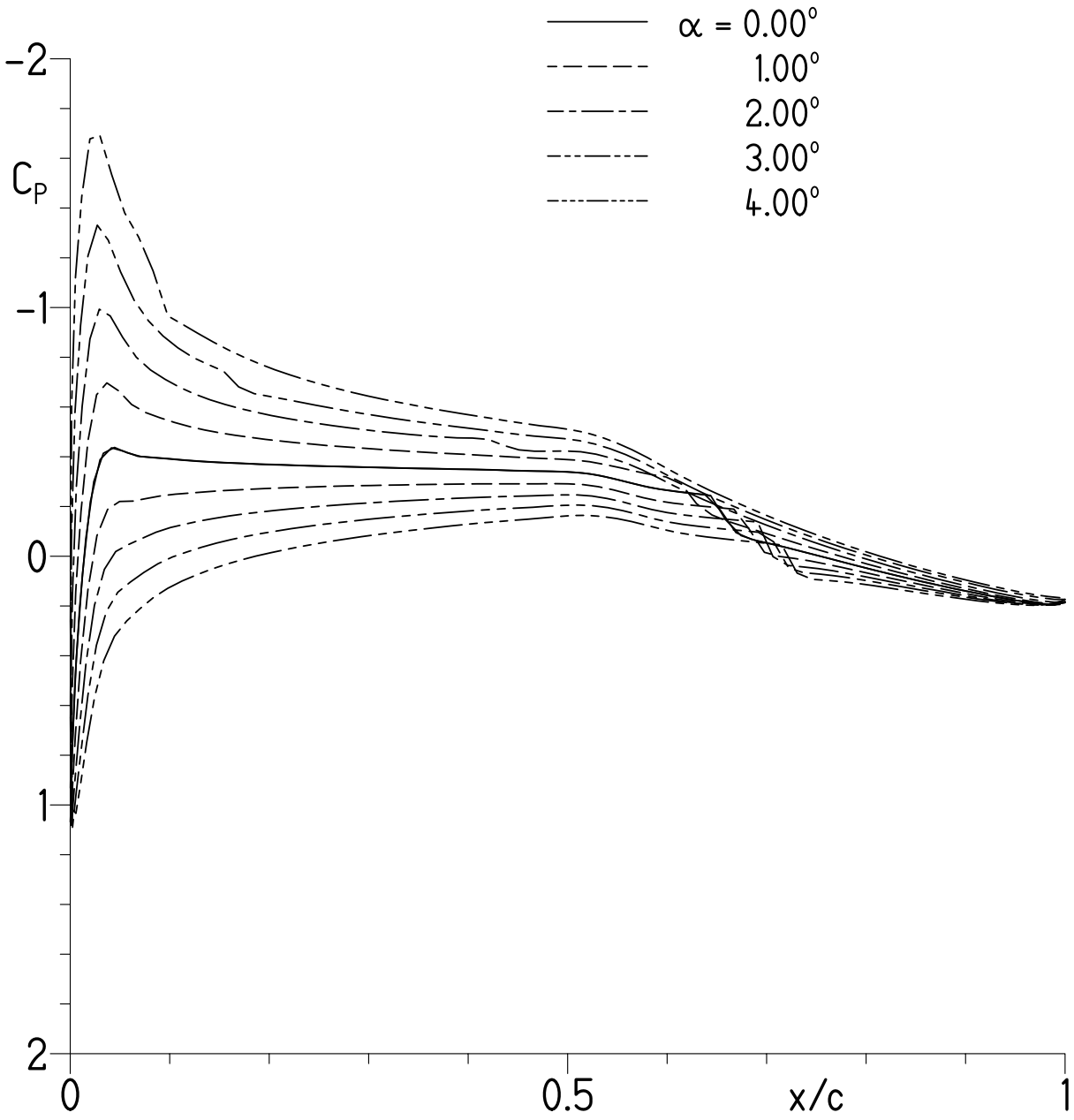

(a) $\alpha = 0.00°$, 1.00°, 2.00°, 3.00°, and 4.00°.

Figure 8.- Pressure distributions for S412 airfoil at $M = 0.40$ and $R = 1.34 \times 10^6$ with transition free.

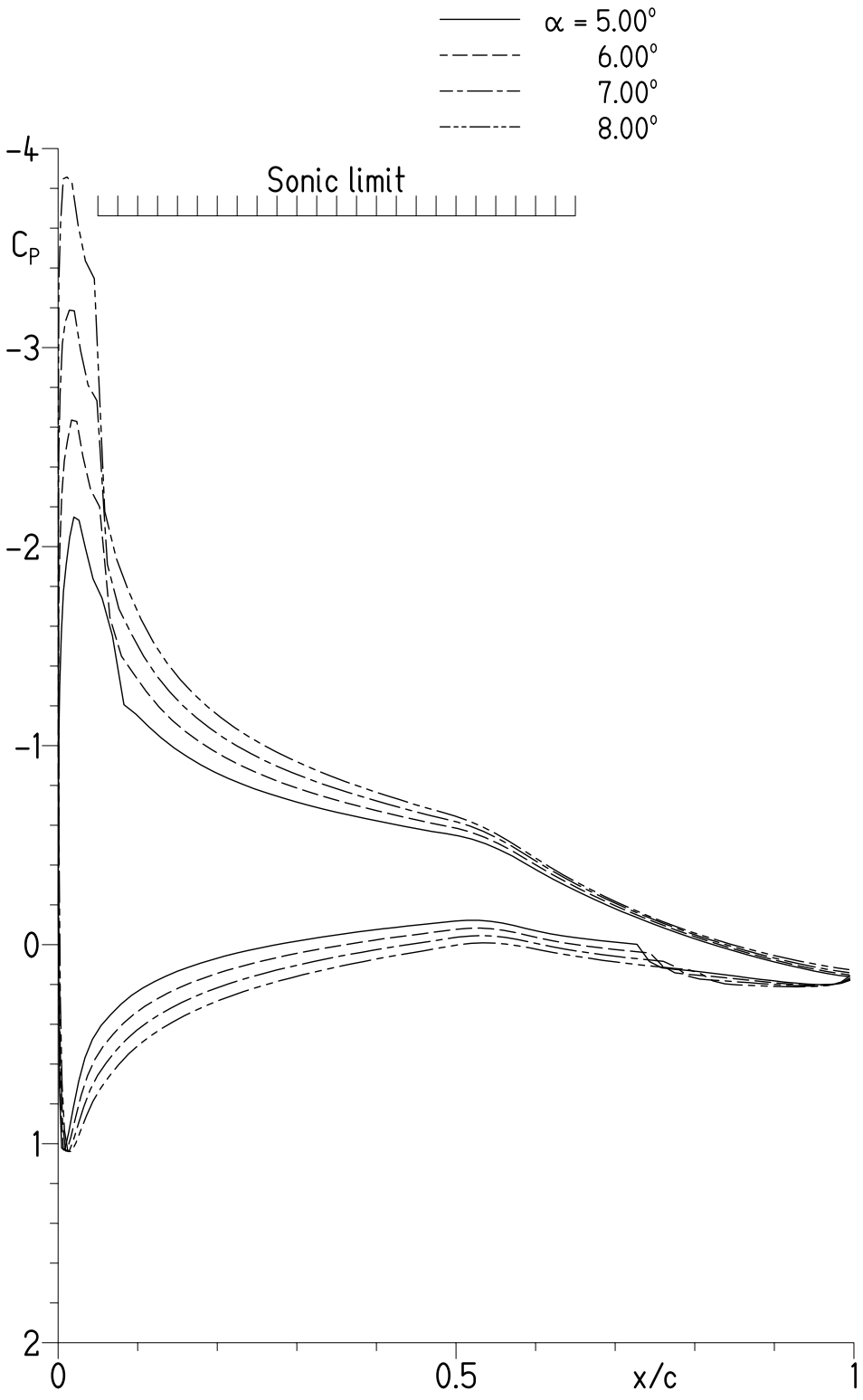

(b) $\alpha = 5.00°$, 6.00°, 7.00°, and 8.00°.

Figure 8.- Continued.

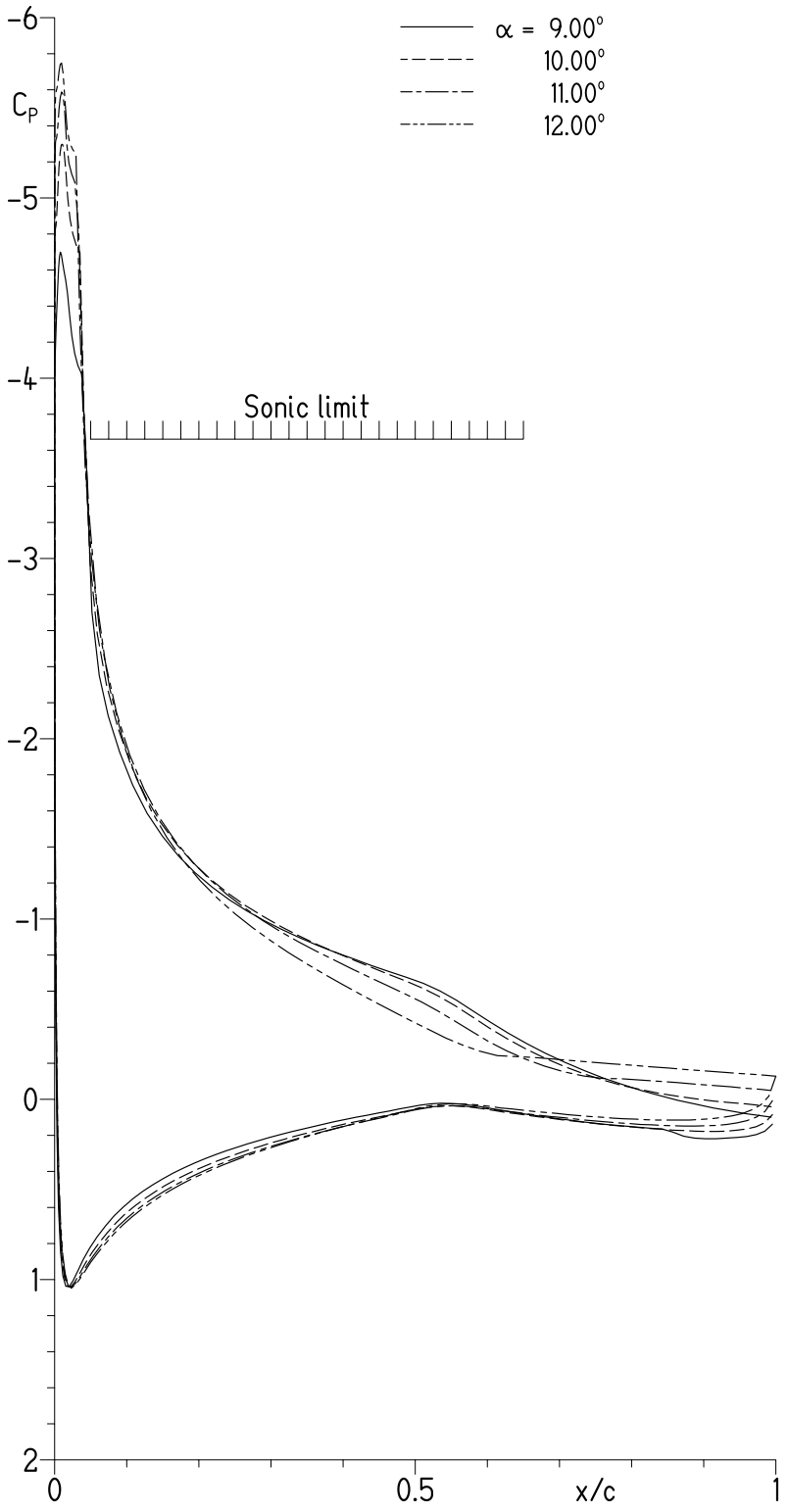

(c) $\alpha = 9.00°$, 10.00°, 11.00°, and 12.00°.

Figure 8.- Concluded.

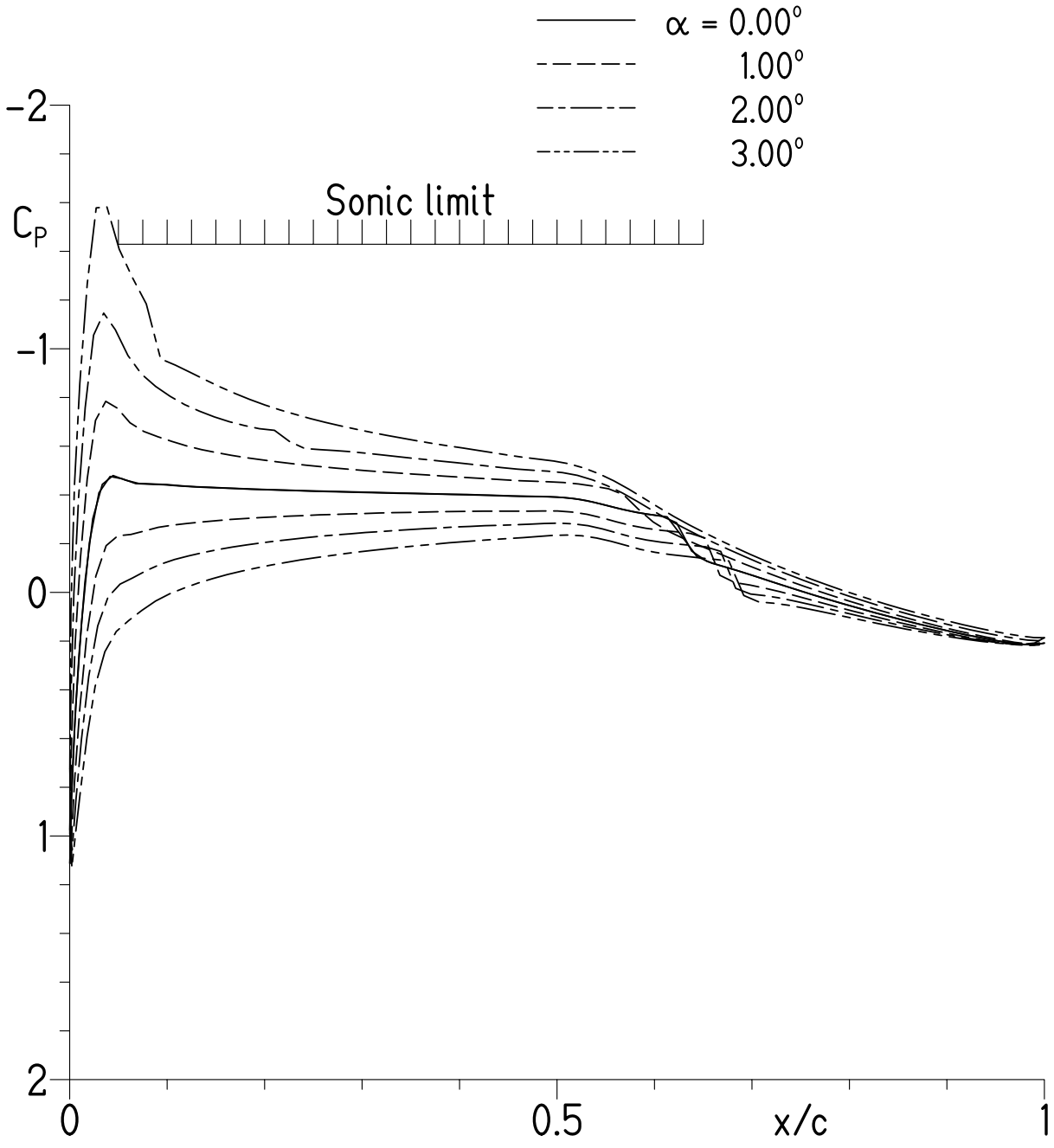

(a) $\alpha = 0.00°$, 1.00°, 2.00°, and 3.00°.

Figure 9.- Pressure distributions for S412 airfoil at $M = 0.58$ and $R = 1.88 \times 10^6$ with transition free.

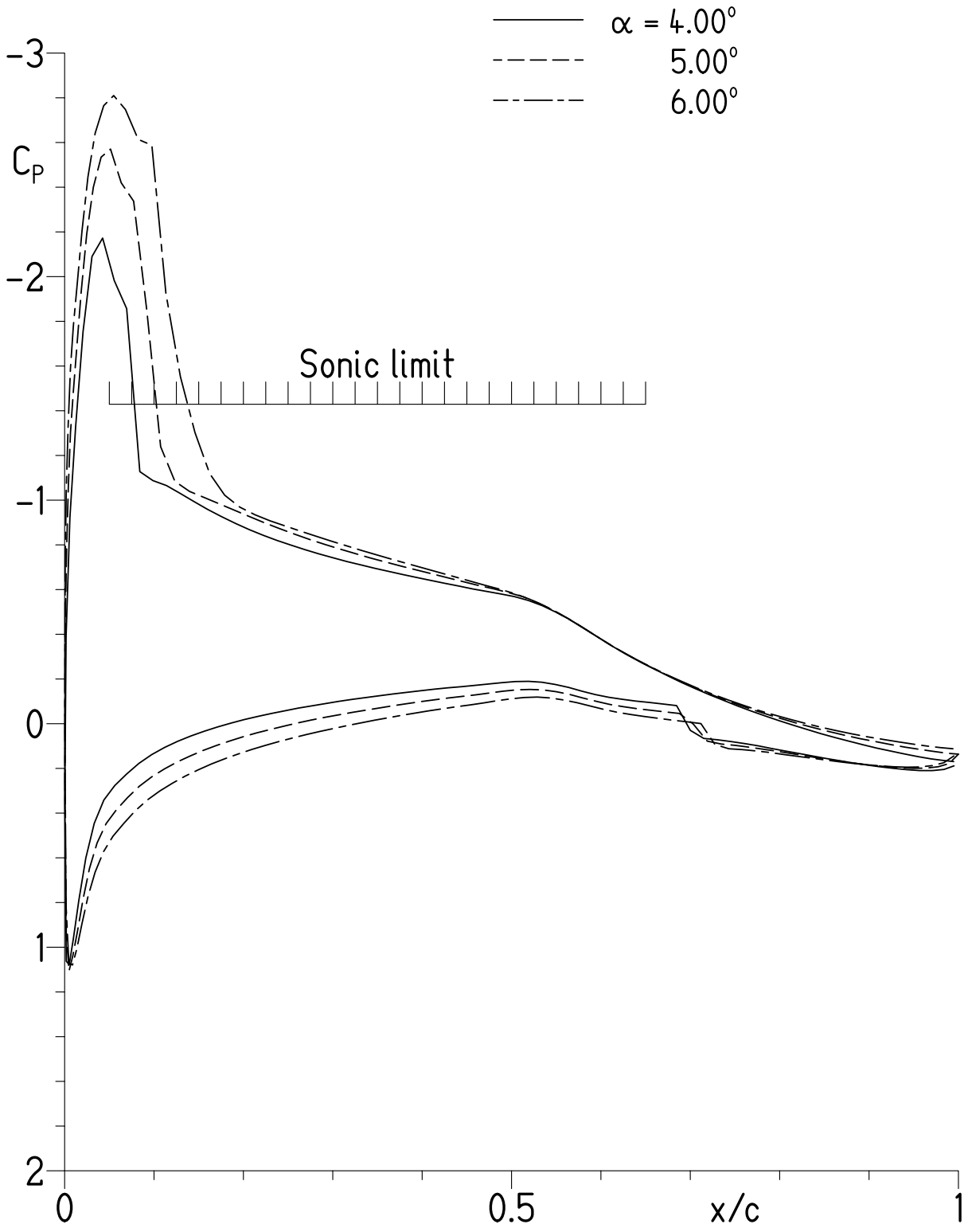

(b) $\alpha = 4.00°$, 5.00°, and 6.00°.

Figure 9.- Concluded.

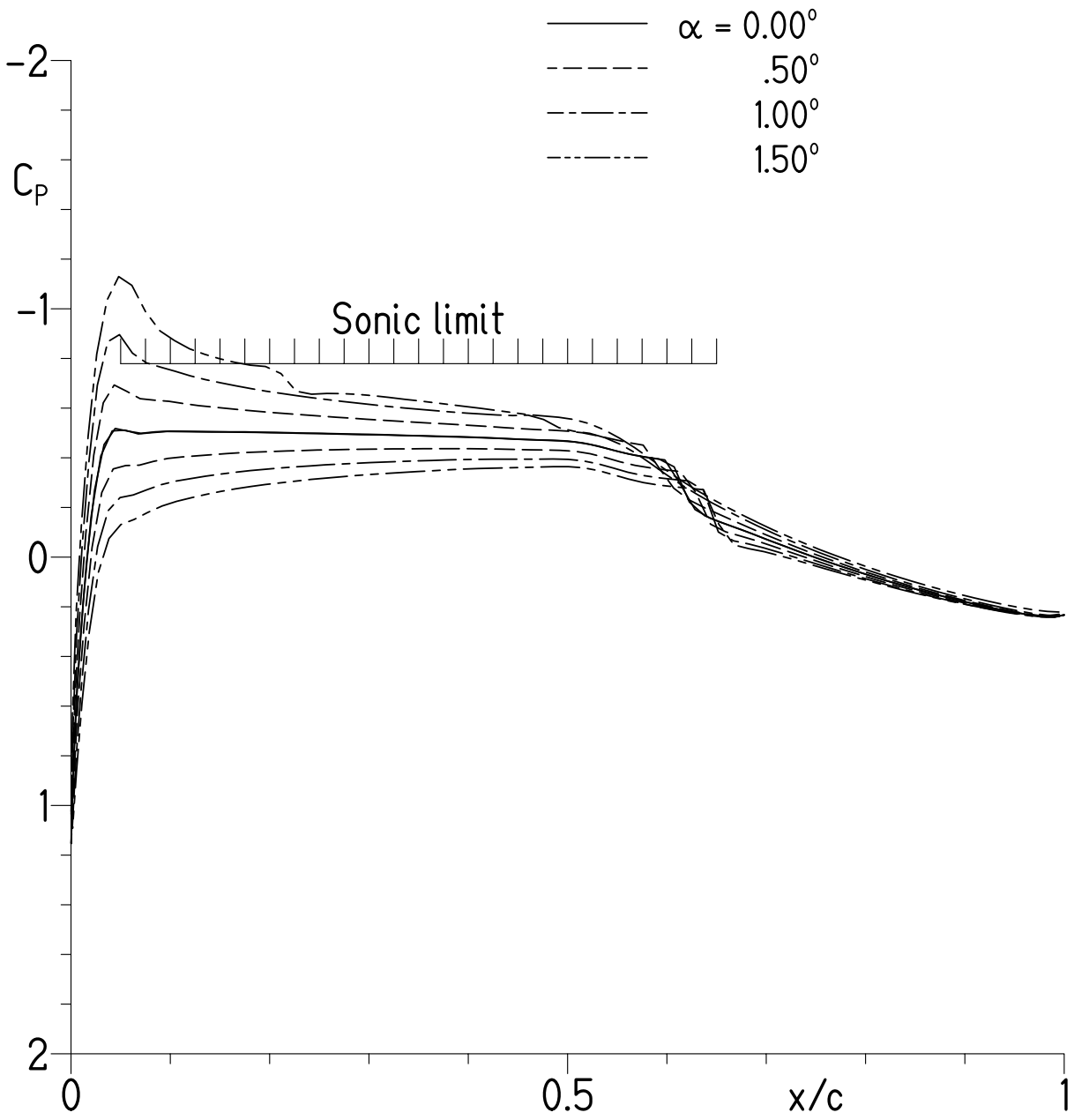

(a) $\alpha = 0.00°$, 0.50°, 1.00°, and 1.50°.

Figure 10.- Pressure distributions for S412 airfoil at $M = 0.70$ and $R = 2.26 \times 10^6$ with transition free.

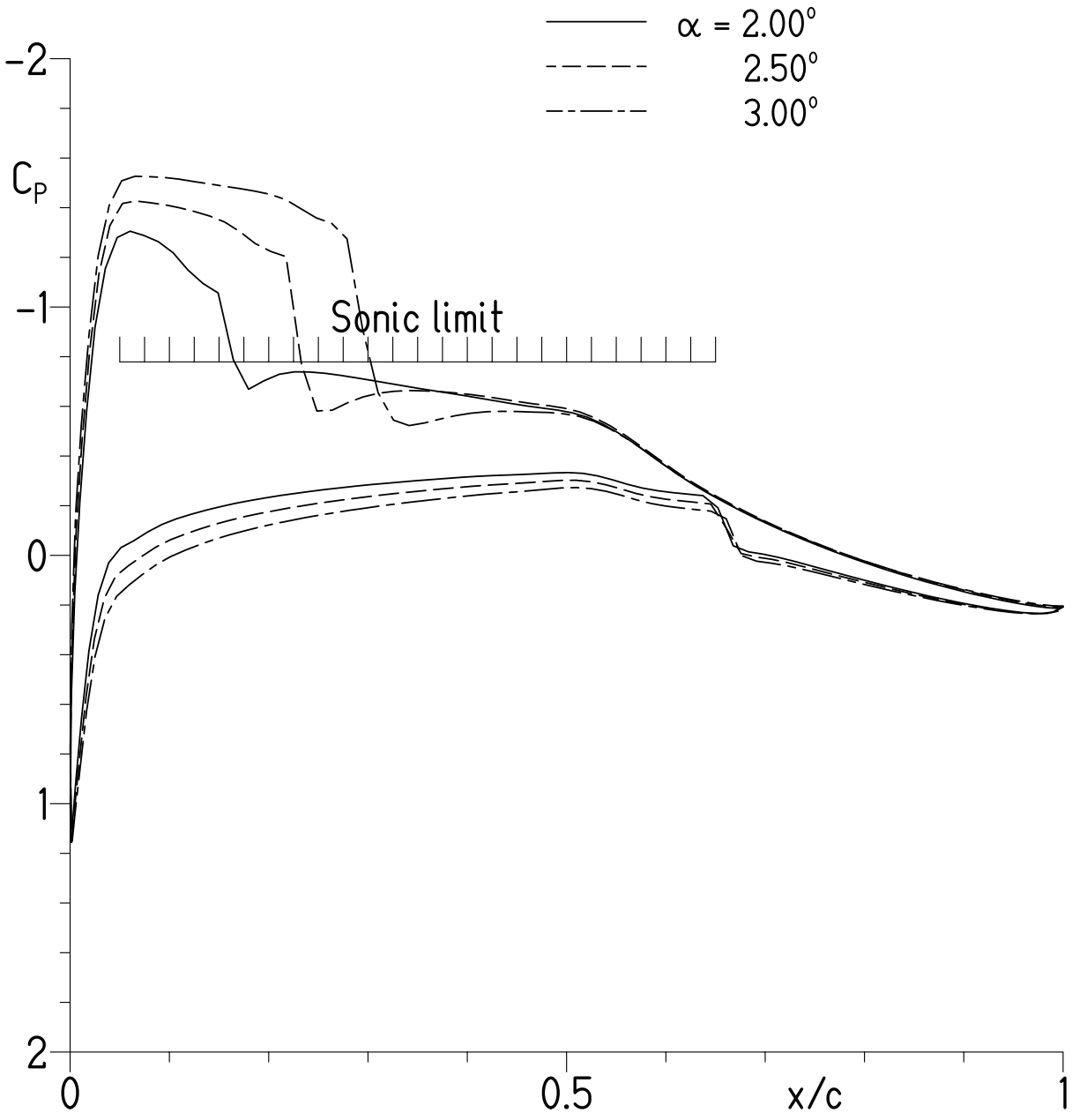

(b) $\alpha = 2.00°$, 2.50°, and 3.00°.

Figure 10.- Concluded.

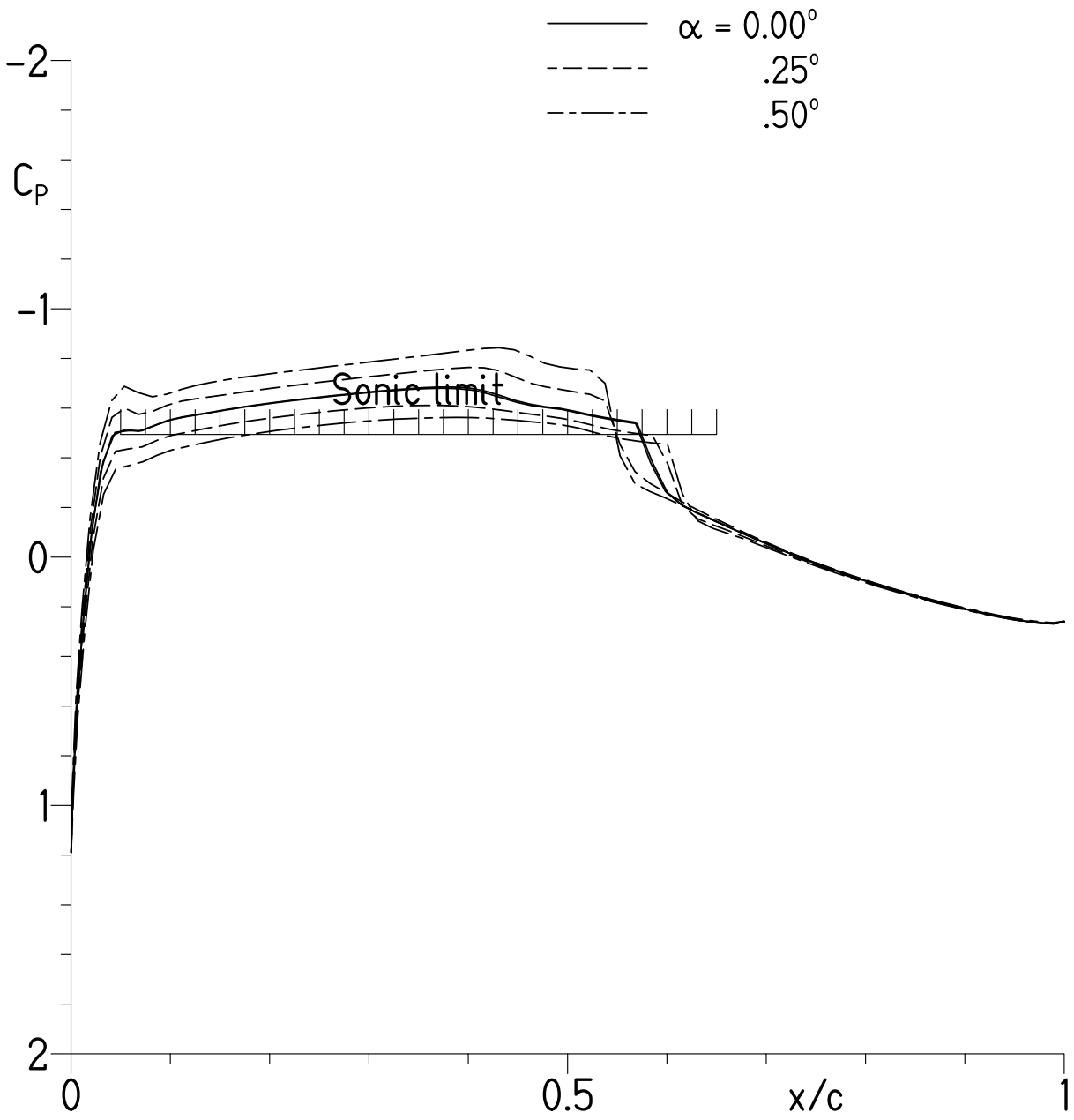

(a) $\alpha = 0.00°$, 0.25°, and 0.50°.

Figure 11.- Pressure distributions for S412 airfoil at $M = 0.78$ and $R = 2.51 \times 10^6$ with transition free.

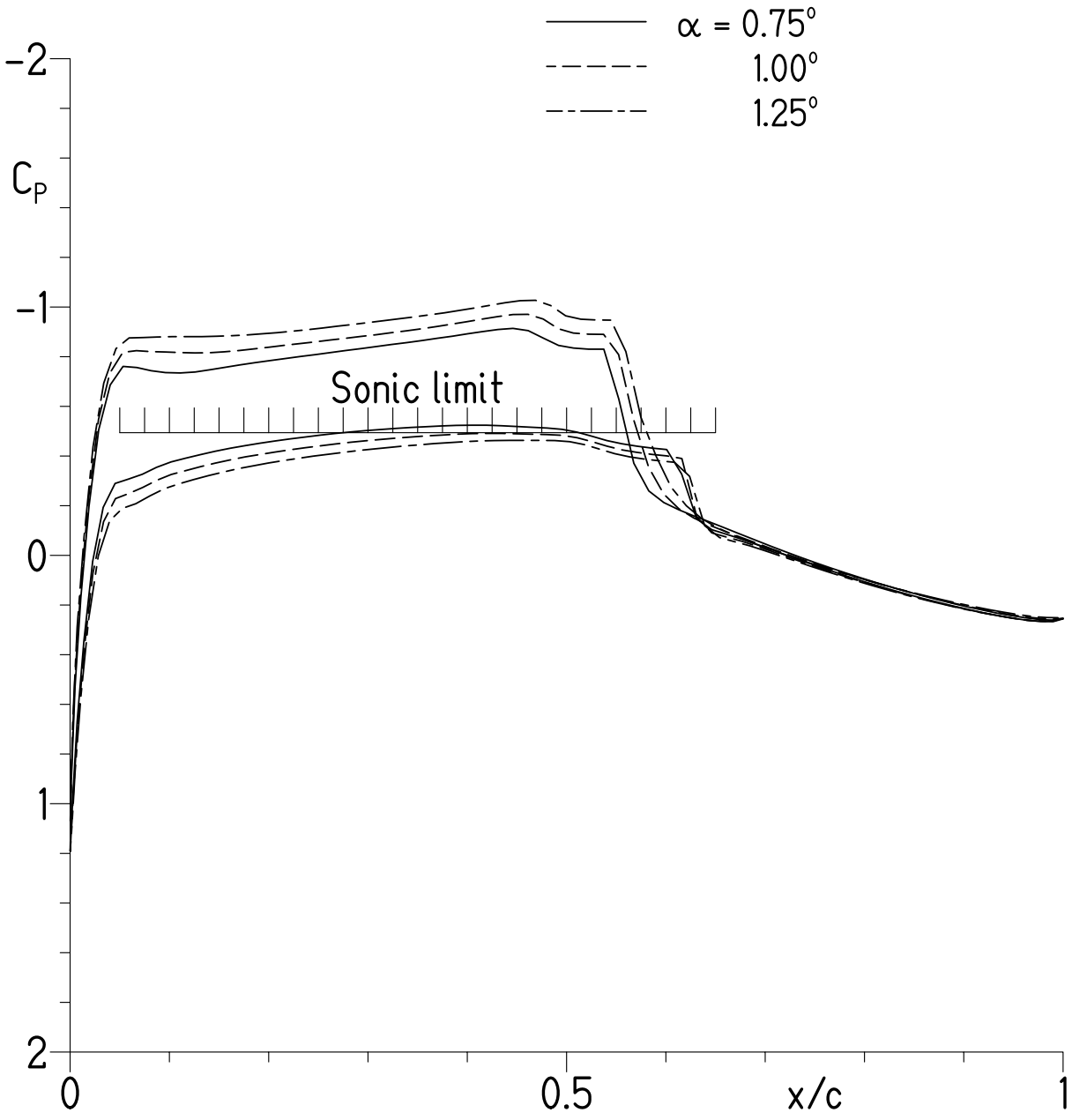

(b) $\alpha = 0.75°$, 1.00°, and 1.25°.

Figure 11.- Concluded.

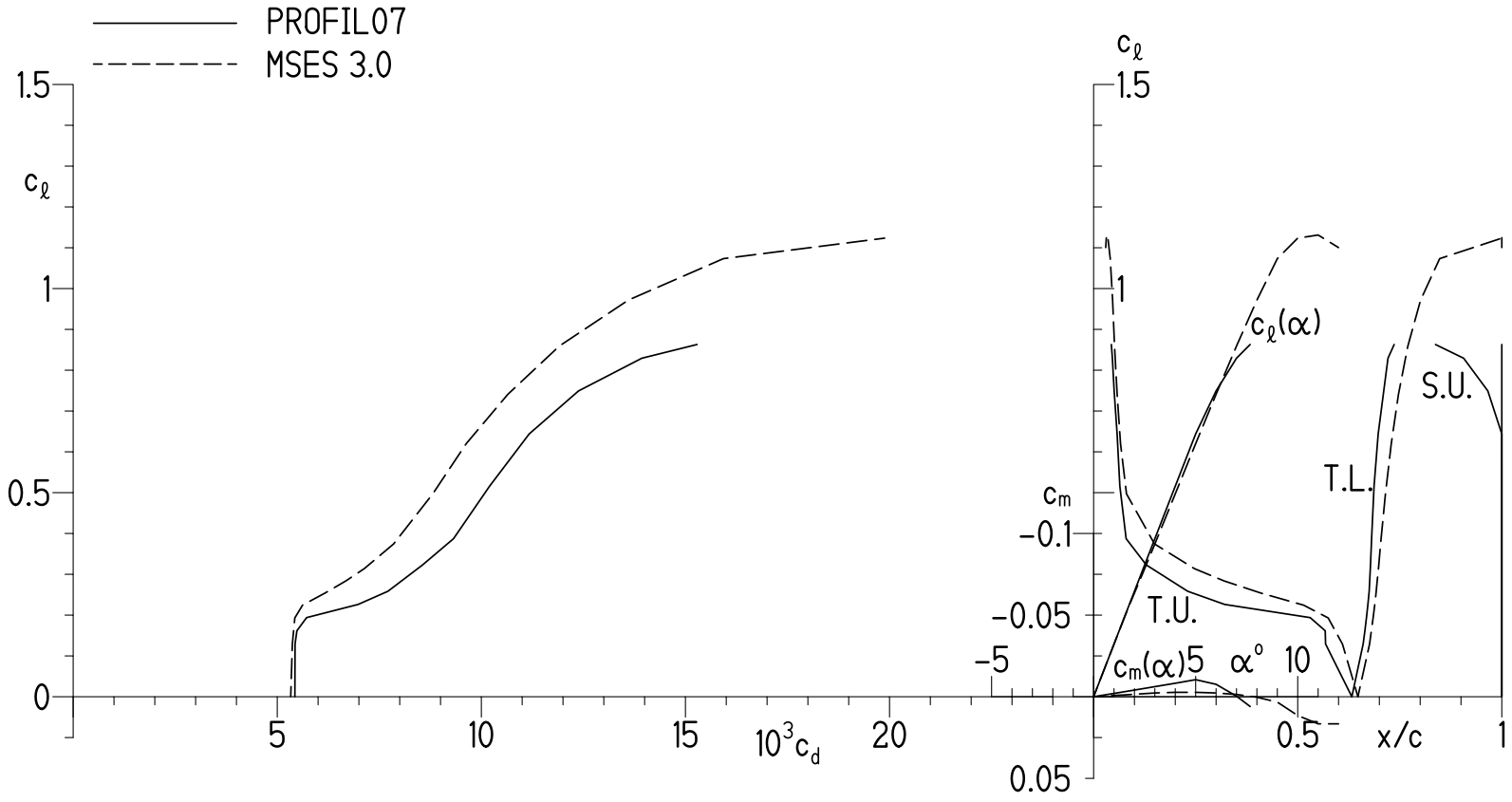

(a) M = 0.40 and R = 1.34×10^6.

Figure 12.- Section characteristics of S412 airfoil with transition free.

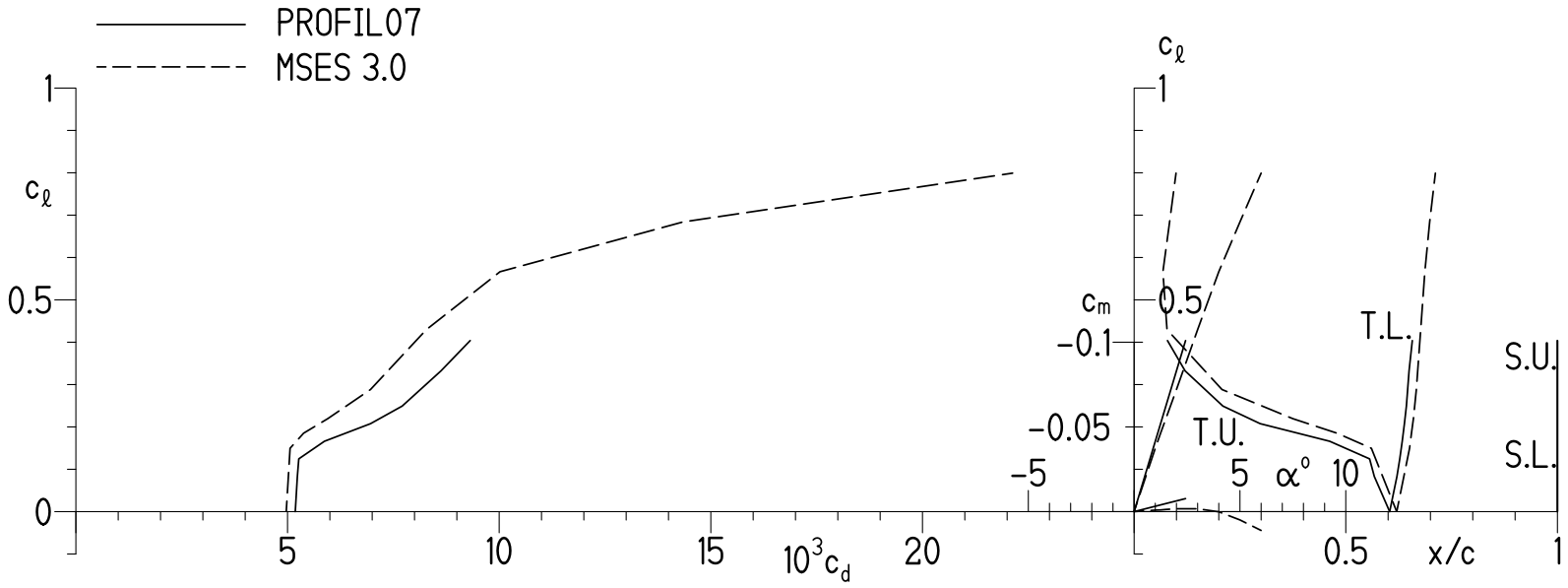

(b) M = 0.58 and R = 1.88×10^6.

Figure 12.- Continued.

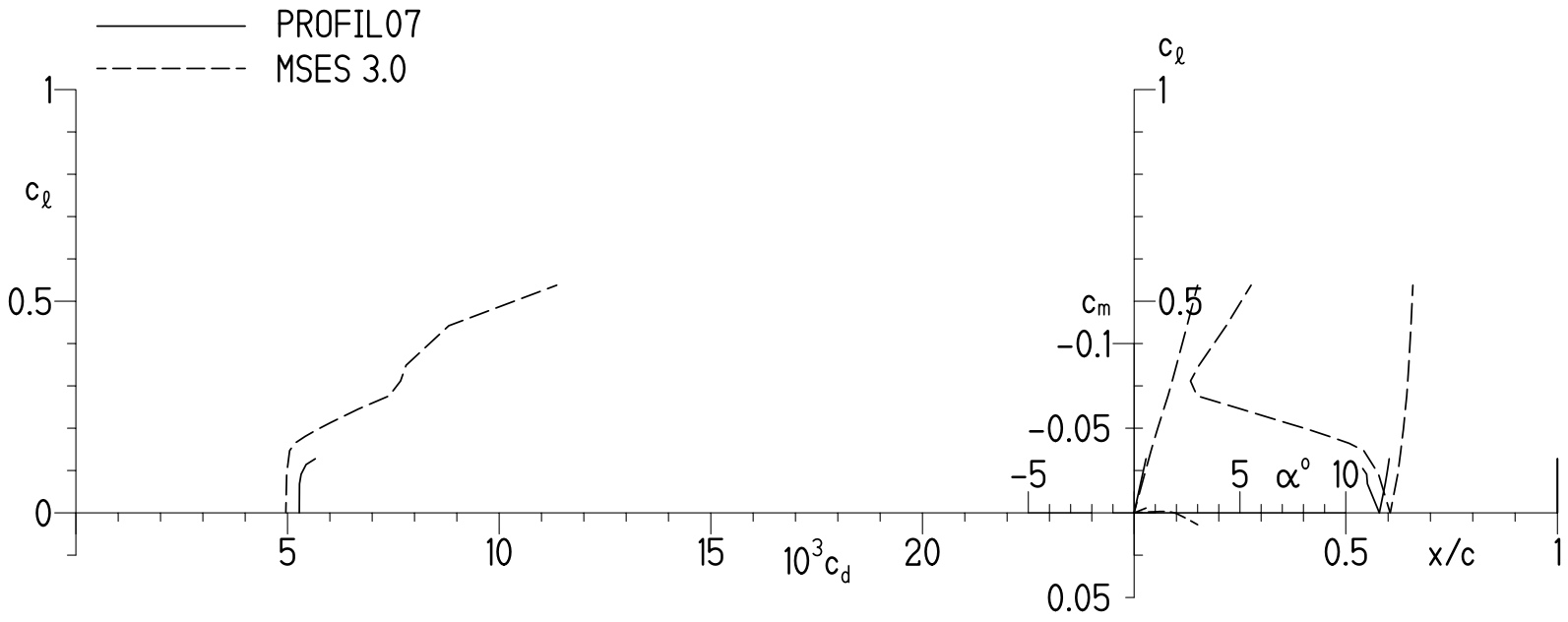

(c) $M = 0.70$ and $R = 2.26 \times 10^6$.

Figure 12.- Continued.

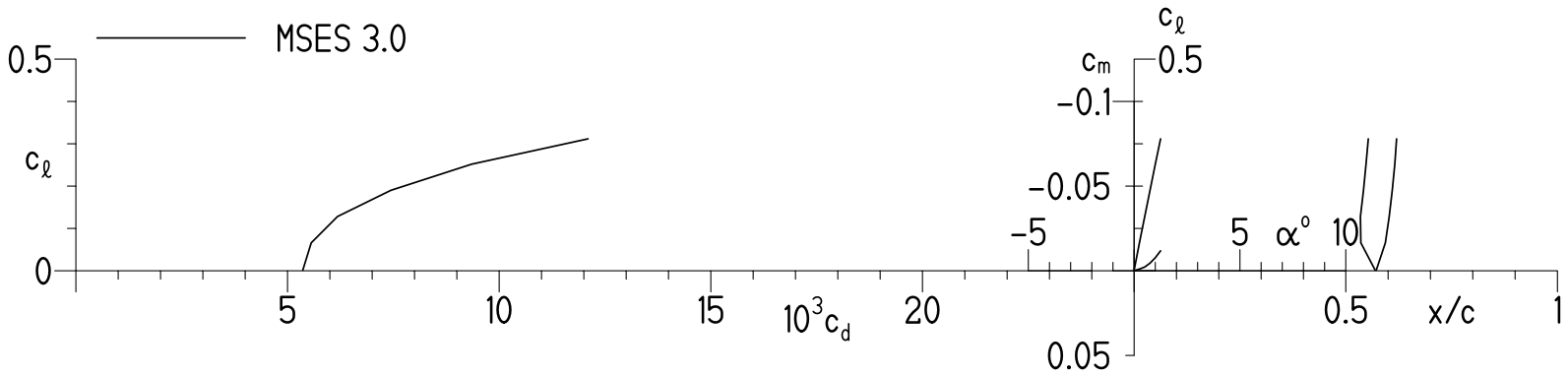

(d) M = 0.78 and R = 2.51×10^6.

Figure 12.- Concluded.

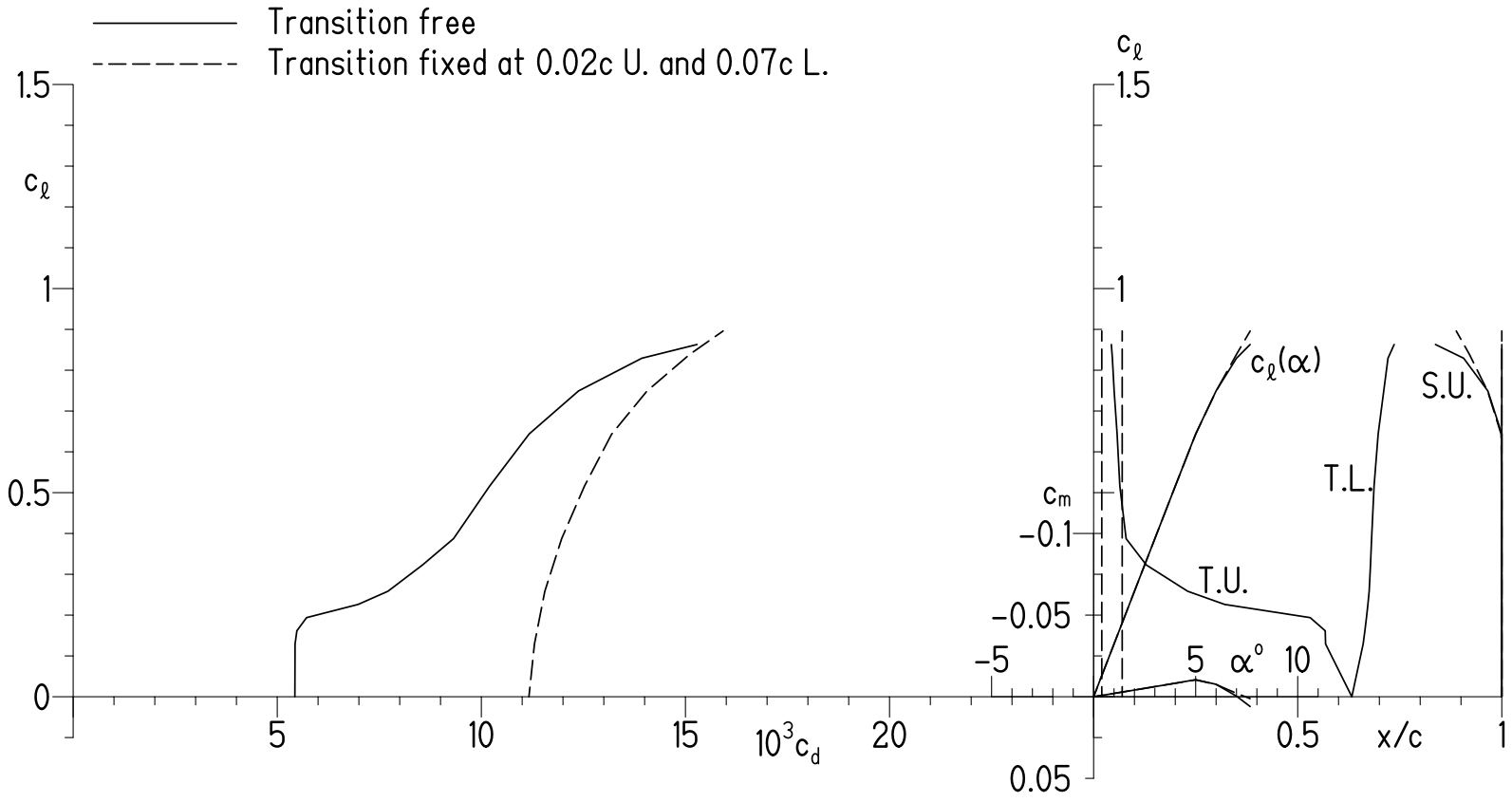

(a) M = 0.40 and R = 1.34×10^6.

Figure 13.- Effect of fixing transition on section characteristics of S412 airfoil predicted using method of references 8 and 9.

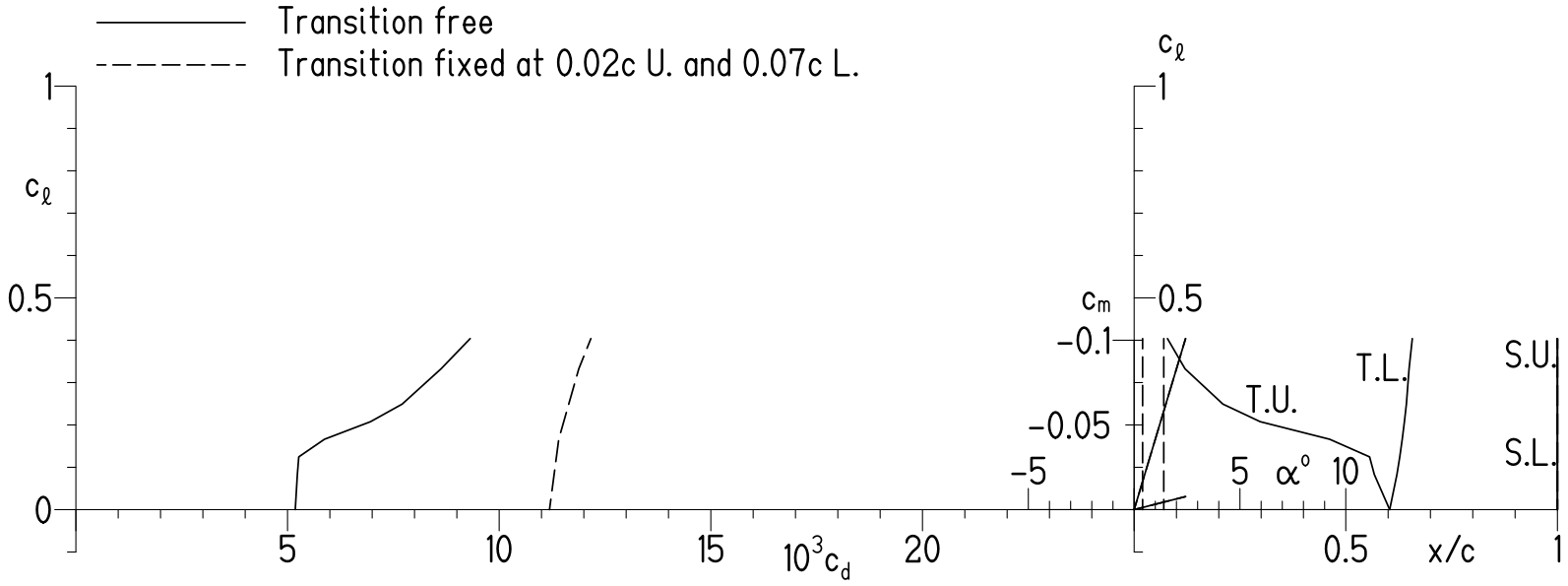

(b) M = 0.58 and R = 1.88×10^6.

Figure 13.- Continued.

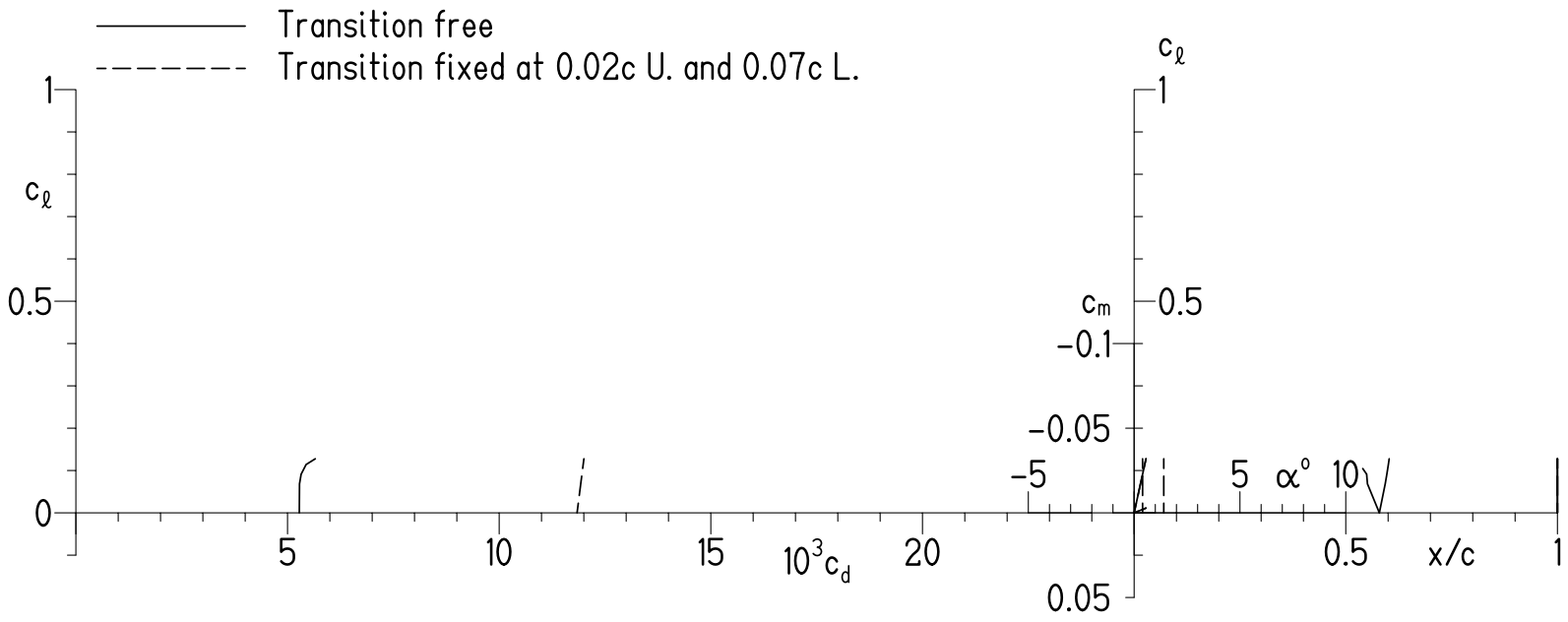

(c) $M = 0.70$ and $R = 2.26 \times 10^6$.

Figure 13.- Concluded.

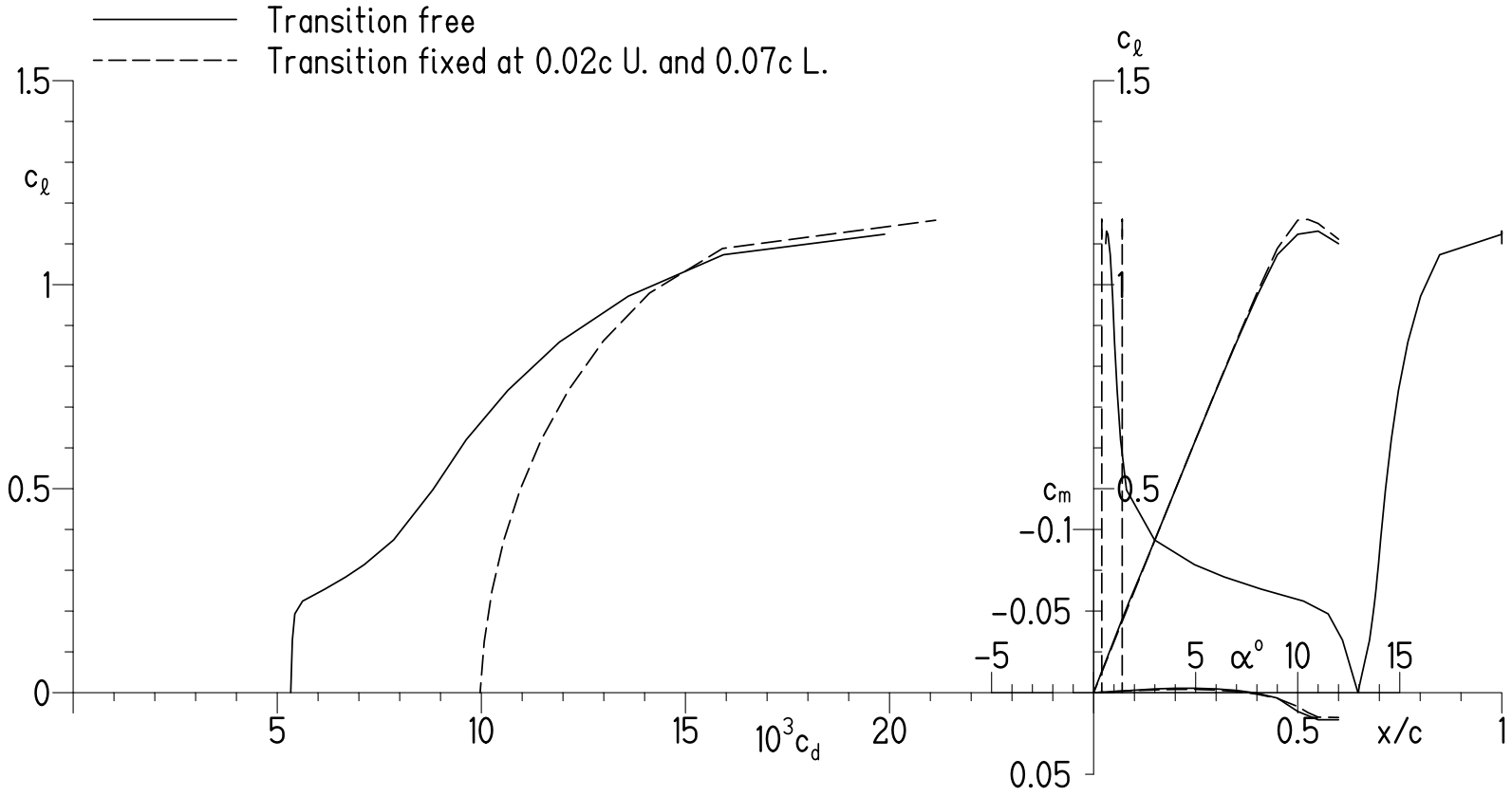

(a) M = 0.40 and R = 1.34×10^6.

Figure 14.- Effect of fixing transition on section characteristics of S412 airfoil predicted using method of reference 11.

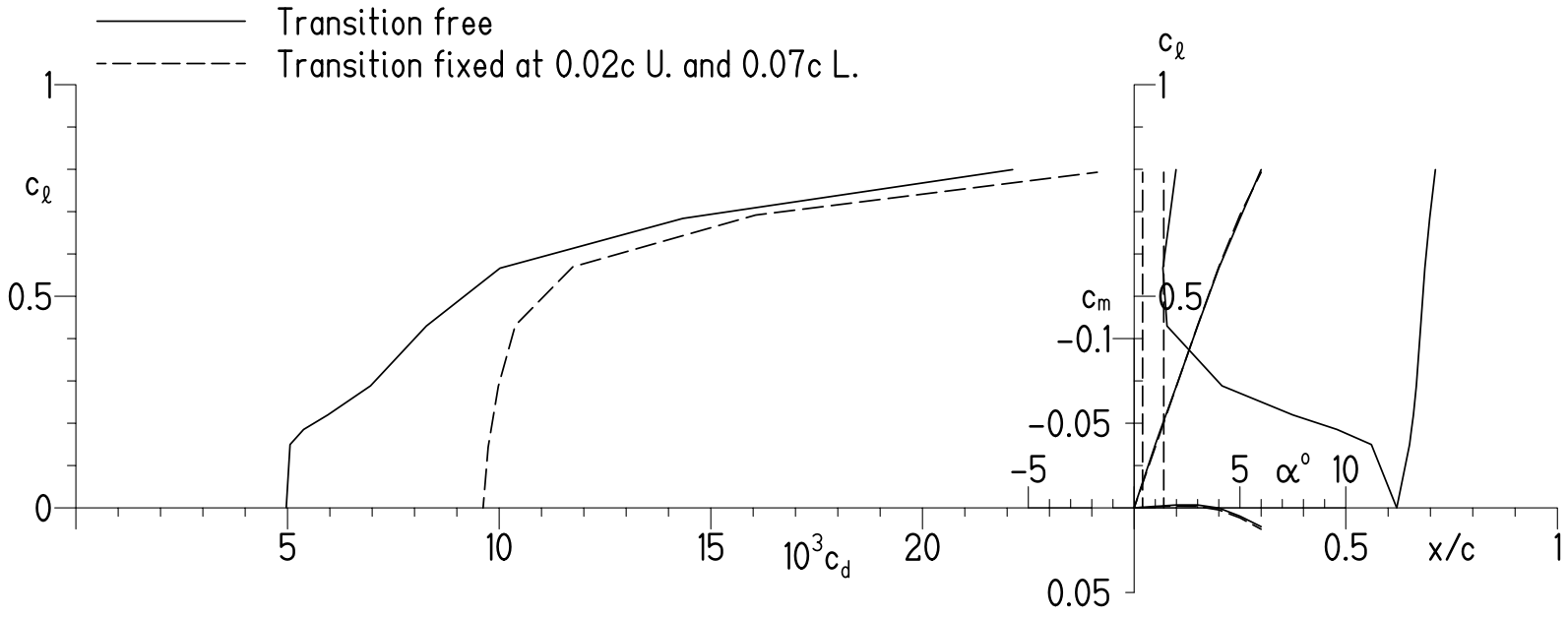

(b) M = 0.58 and R = 1.88×10^6.

Figure 14.- Continued.

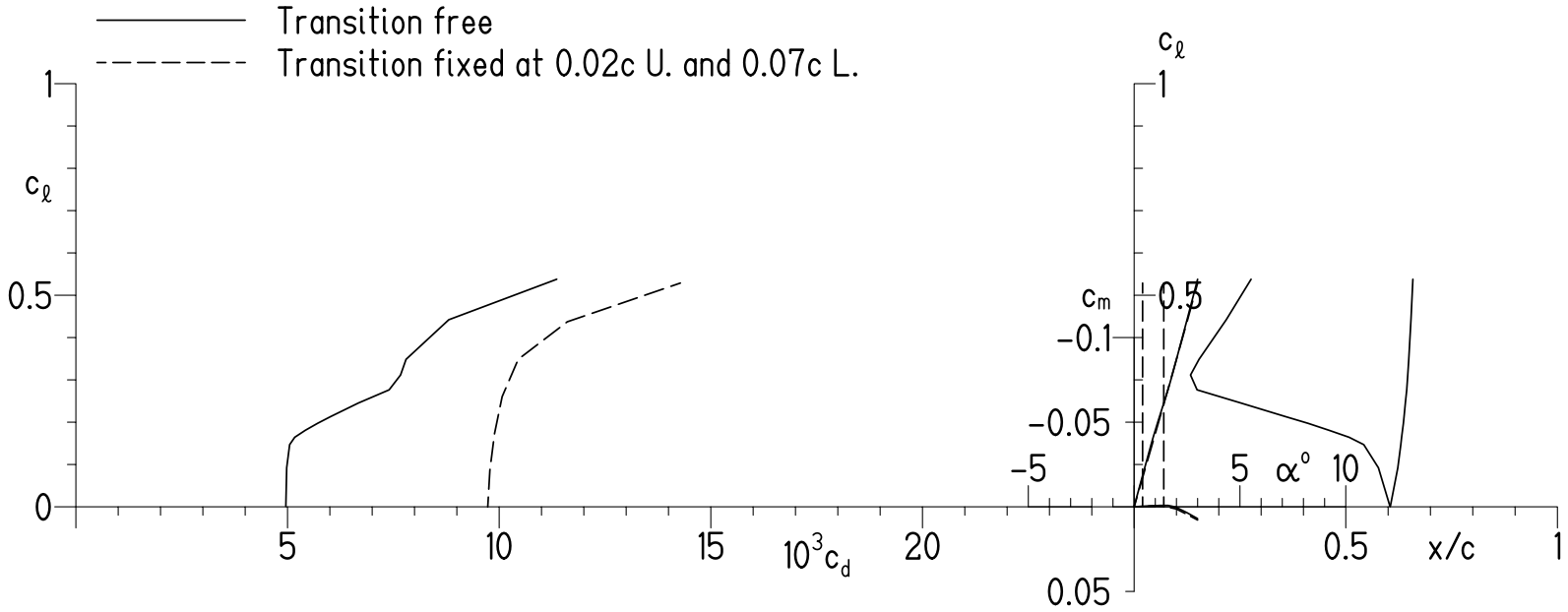

(c) M = 0.70 and R = 2.26×10^6.

Figure 14.- Continued.

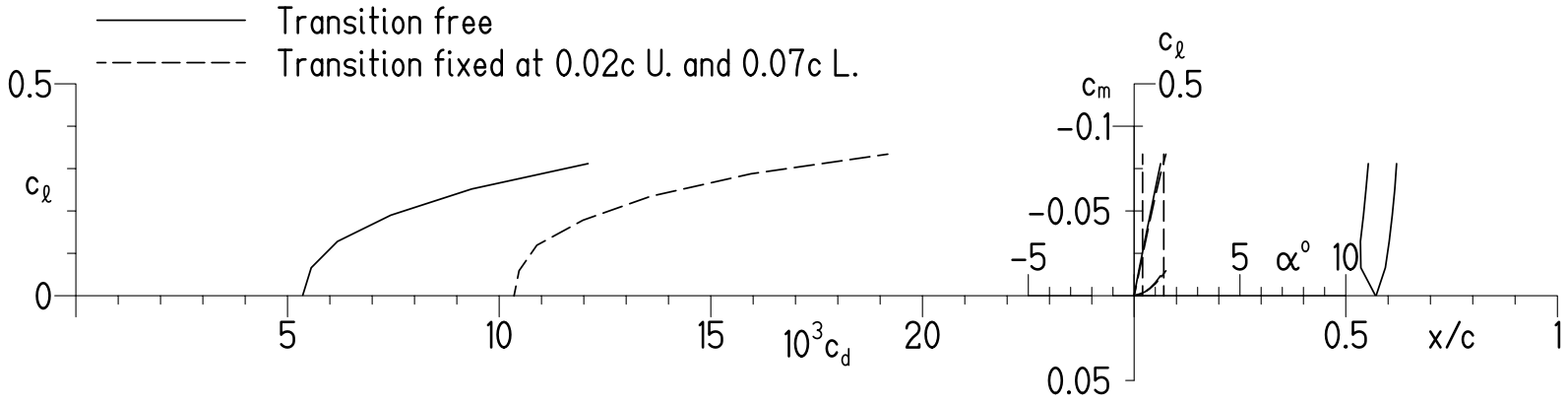

(d) $M = 0.78$ and $R = 2.51 \times 10^6$.

Figure 14.- Concluded.

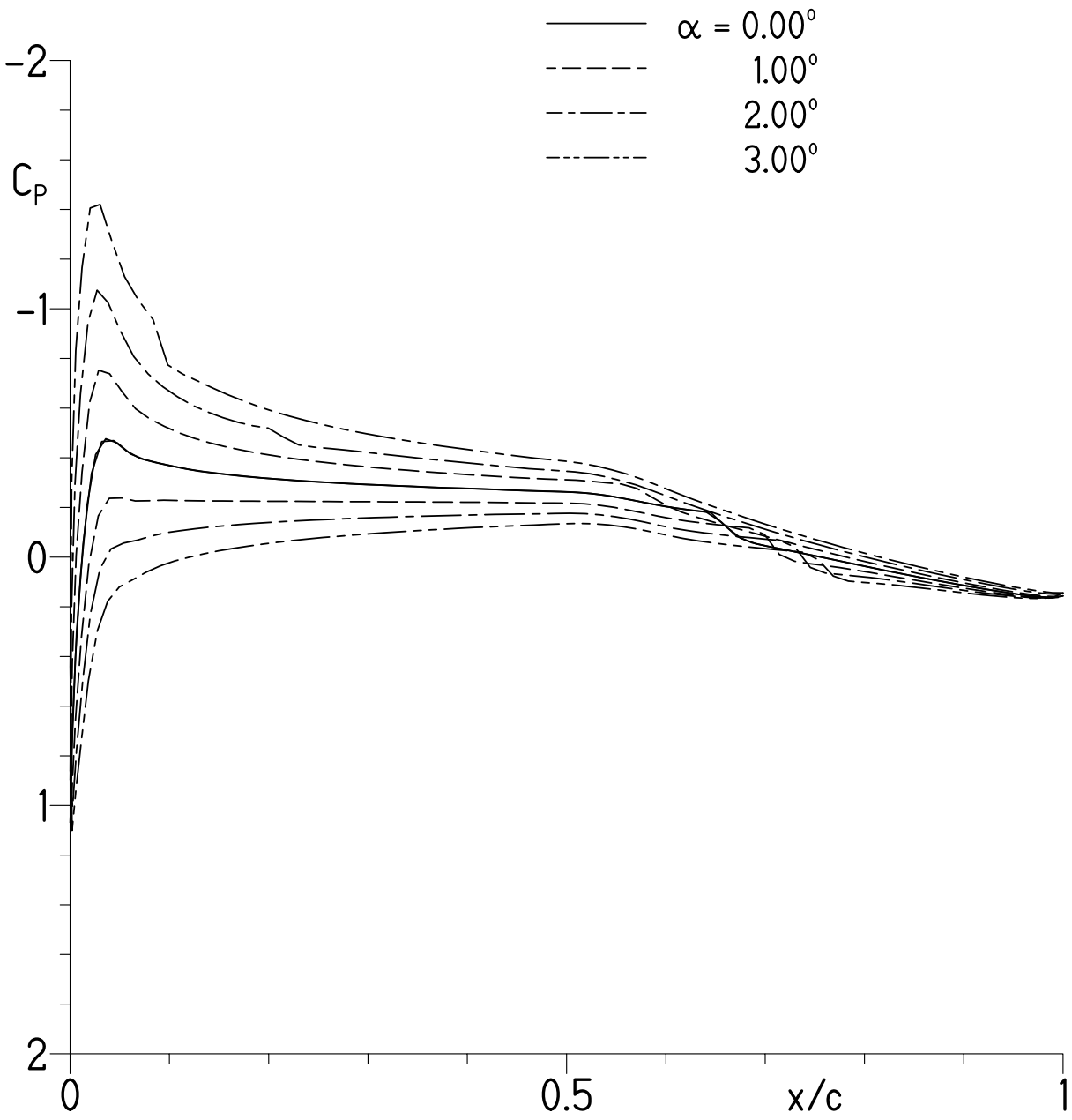

(a) $\alpha = 0.00°$, 1.00°, 2.00°, and 3.00°.

Figure 15.- Pressure distributions for S413 airfoil at $M = 0.40$ and $R = 1.34 \times 10^6$ with transition free.

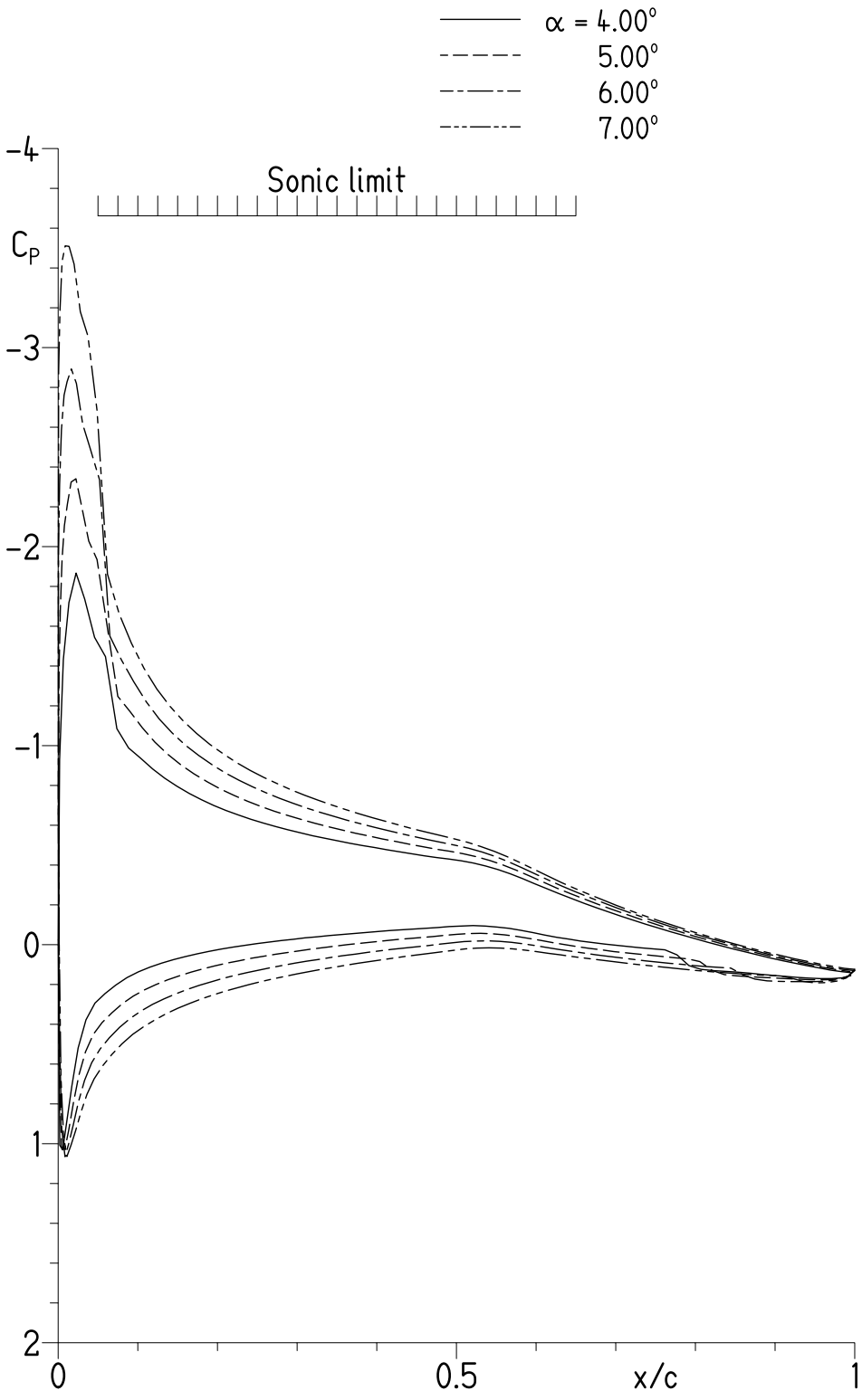

(b) $\alpha = 4.00°$, 5.00°, 6.00°, and 7.00°.

Figure 15.- Continued.

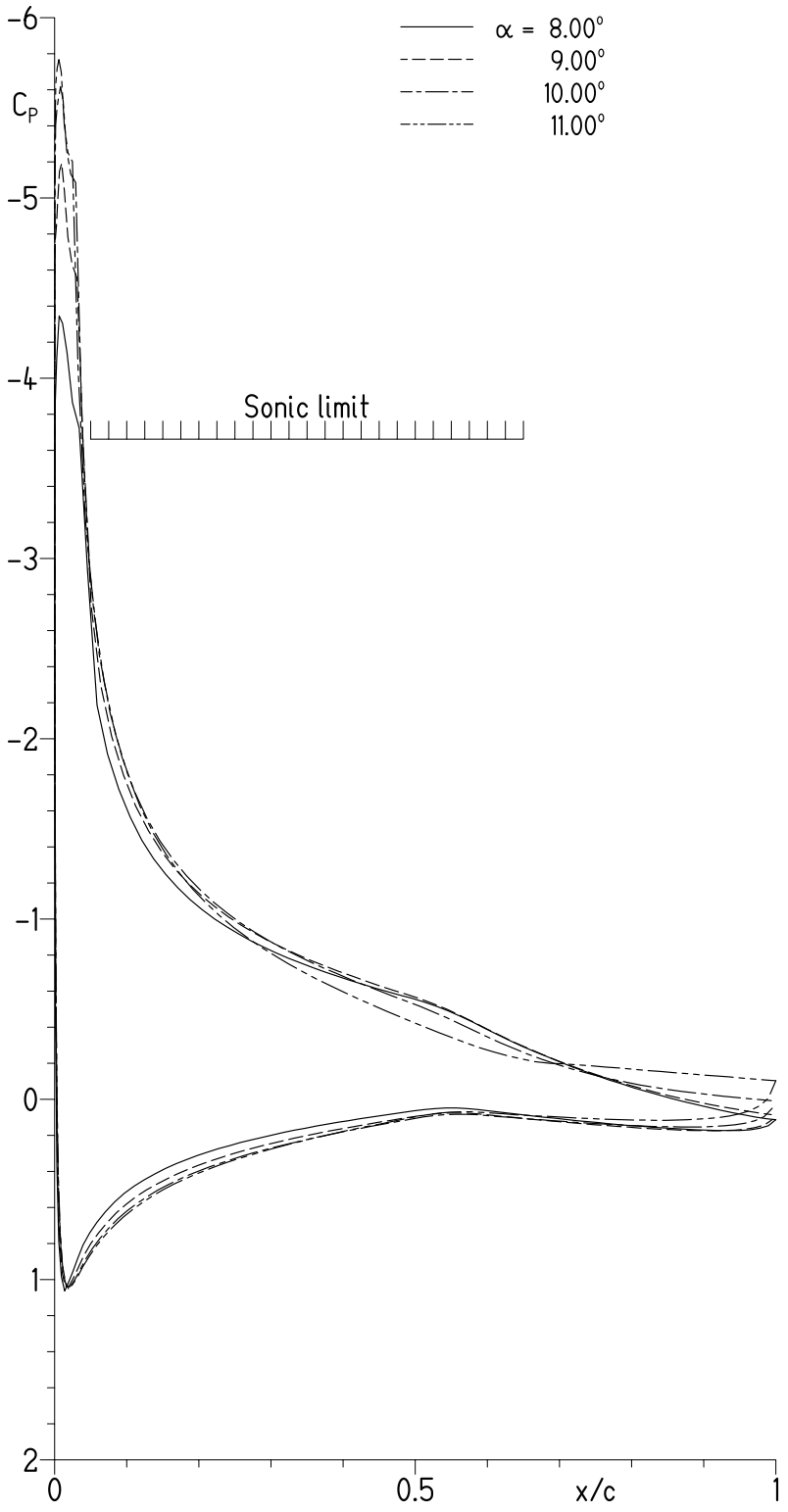

(c) $\alpha = 8.00°$, 9.00°, 10.00°, and 11.00°.

Figure 15.- Concluded.

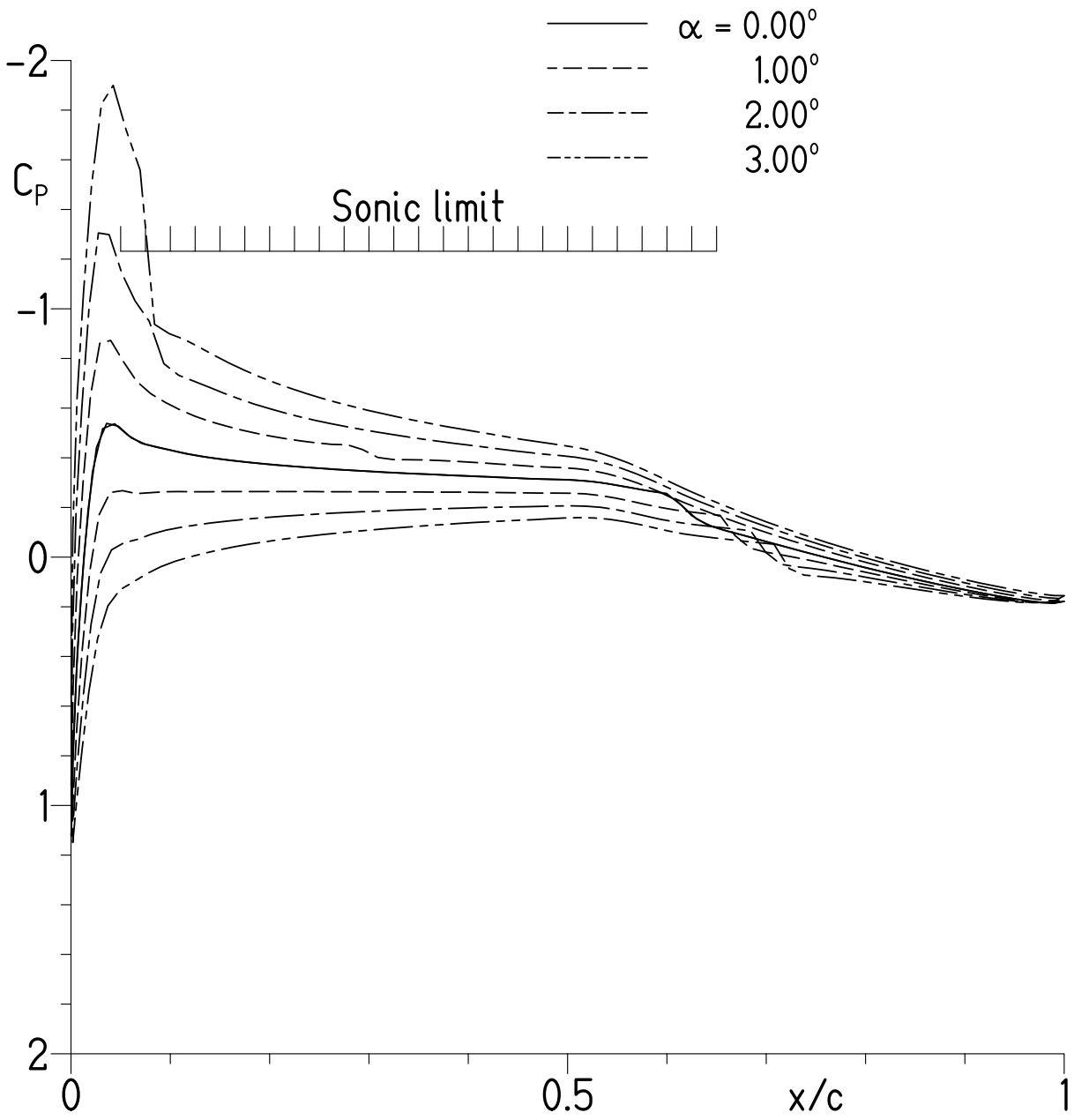

(a) $\alpha = 0.00°$, 1.00°, 2.00°, and 3.00°.

Figure 16.- Pressure distributions for S413 airfoil at $M = 0.61$ and $R = 1.98 \times 10^6$ with transition free.

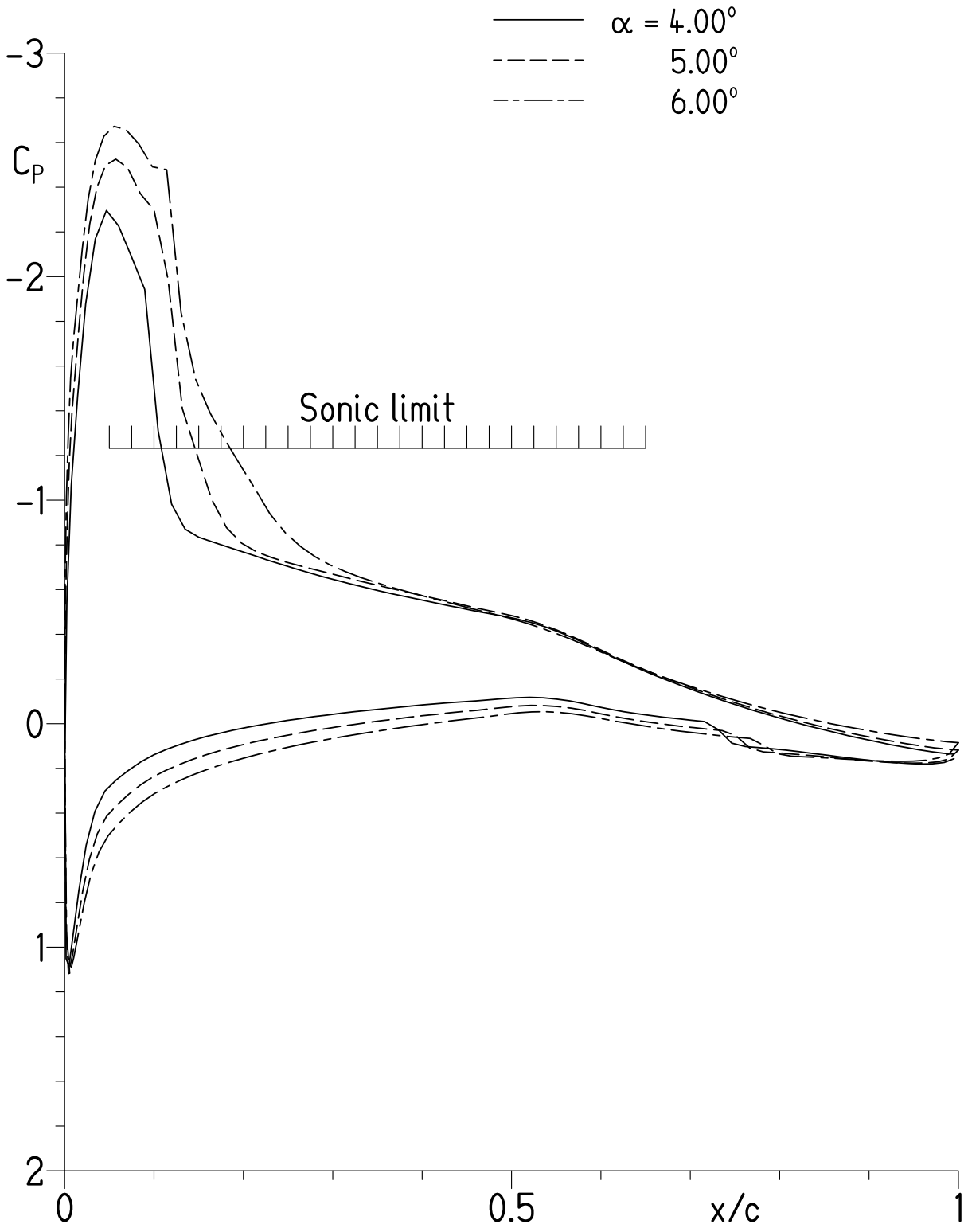

(b) $\alpha = 4.00°$, 5.00°, and 6.00°.

Figure 16.- Concluded.

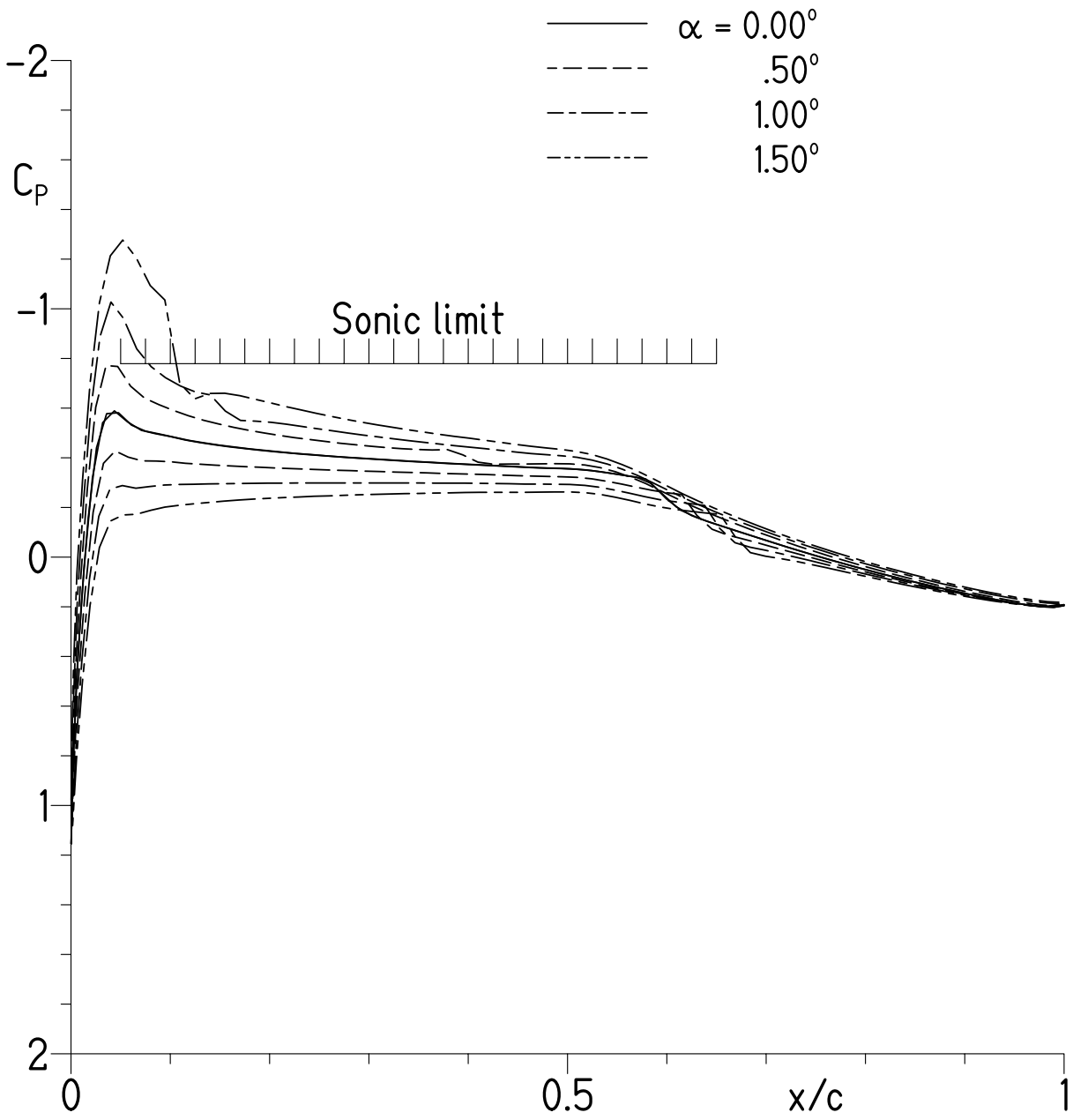

(a) $\alpha = 0.00°$, 0.50°, 1.00°, and 1.50°.

Figure 17.- Pressure distributions for S413 airfoil at $M = 0.70$ and $R = 2.28 \times 10^6$ with transition free.

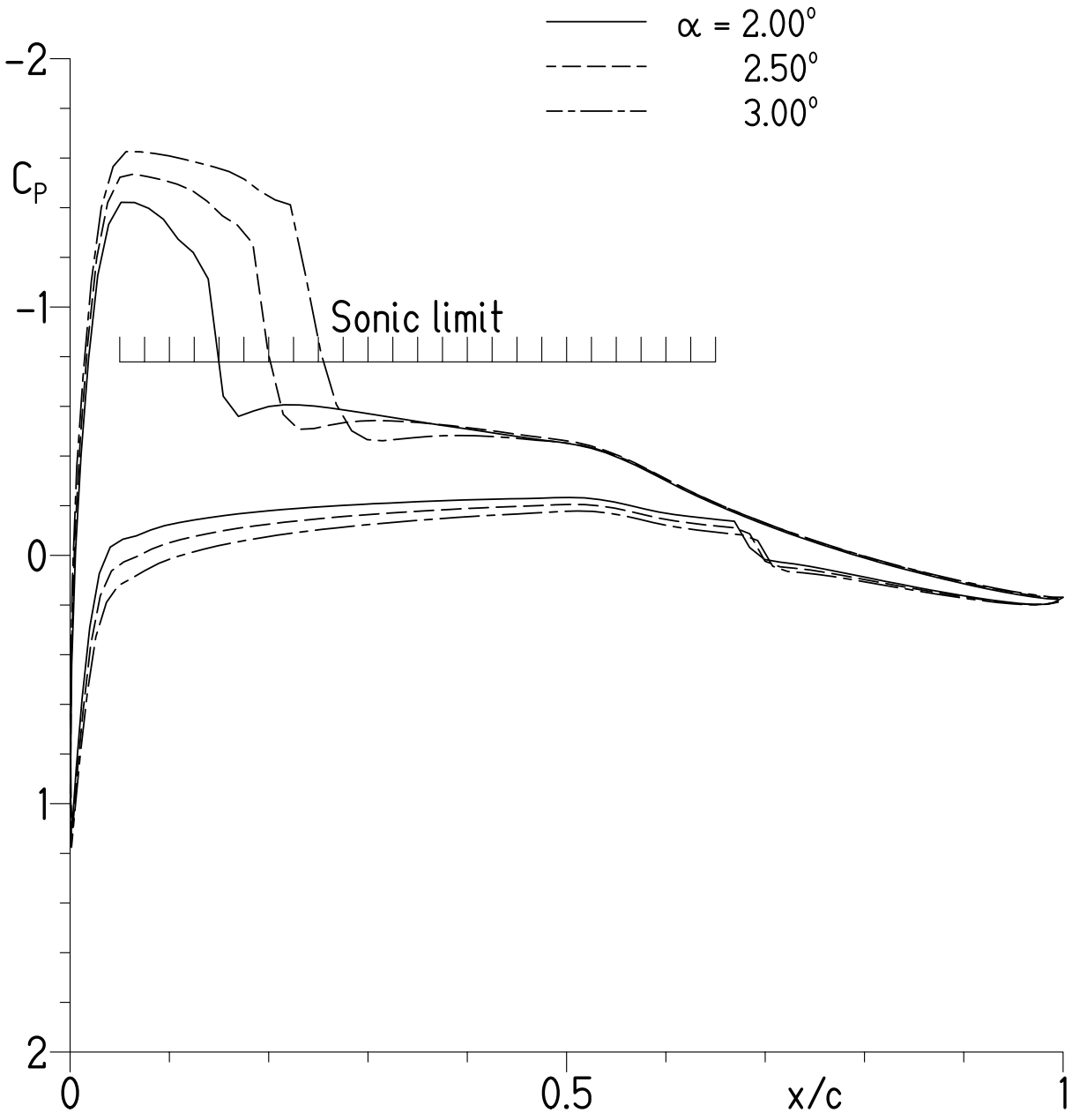

(b) α = 2.00°, 2.50°, and 3.00°.

Figure 17.- Concluded.

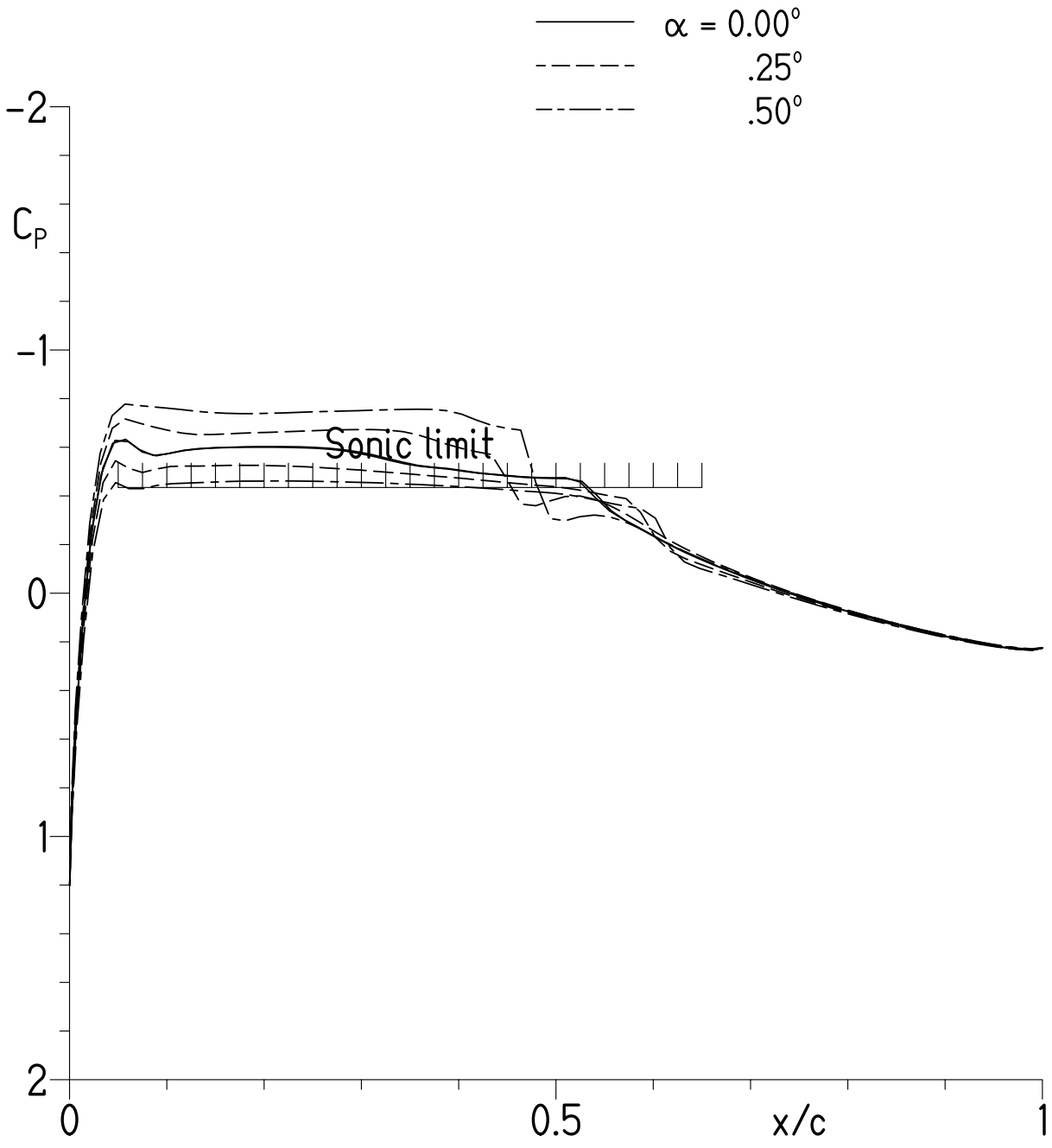

(a) $\alpha = 0.00°$, 0.25°, and 0.50°.

Figure 18.- Pressure distributions for S413 airfoil at $M = 0.80$ and $R = 2.61 \times 10^6$ with transition free.

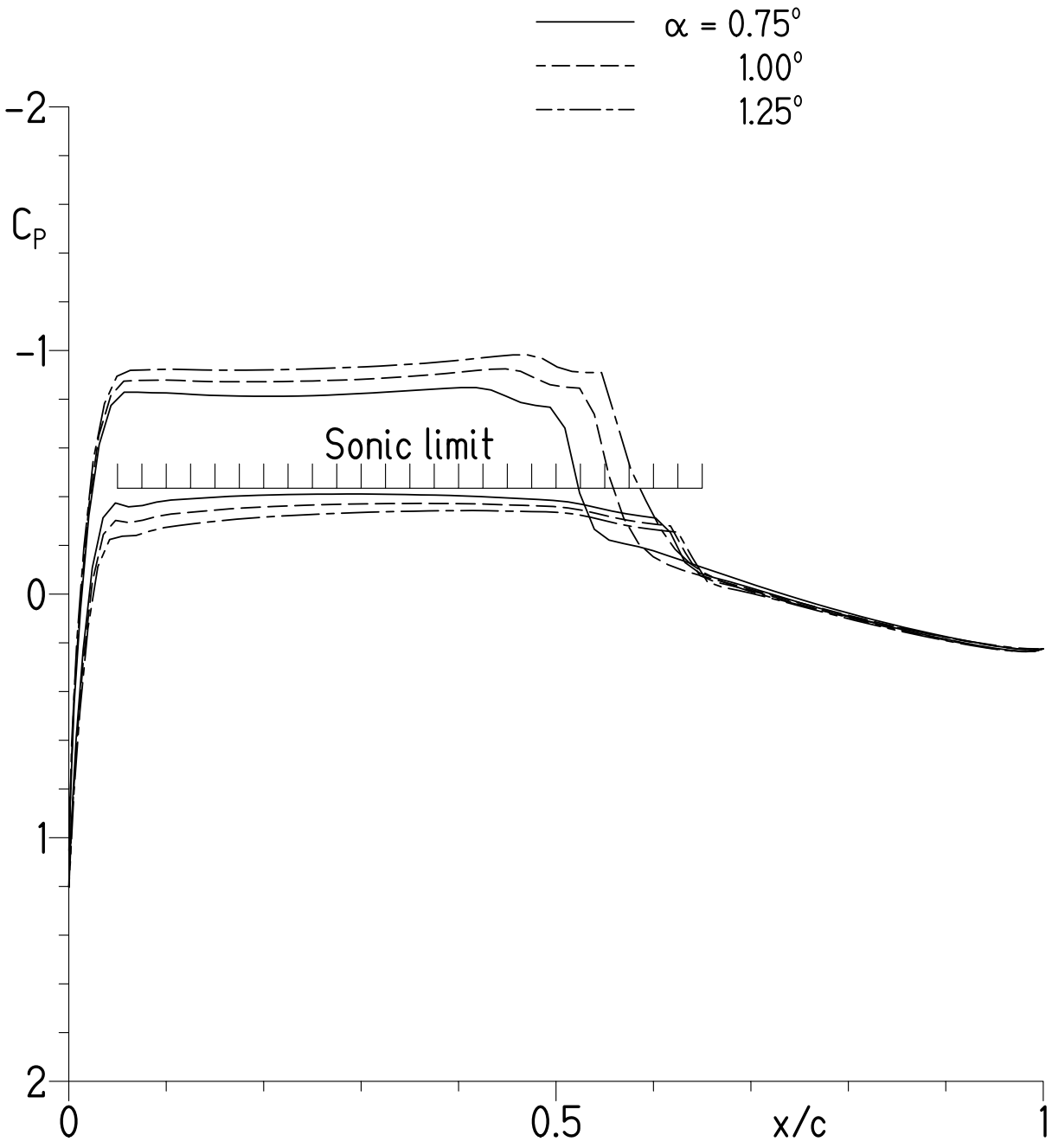

(b) $\alpha = 0.75°$, 1.00°, and 1.25°.

Figure 18.- Concluded.

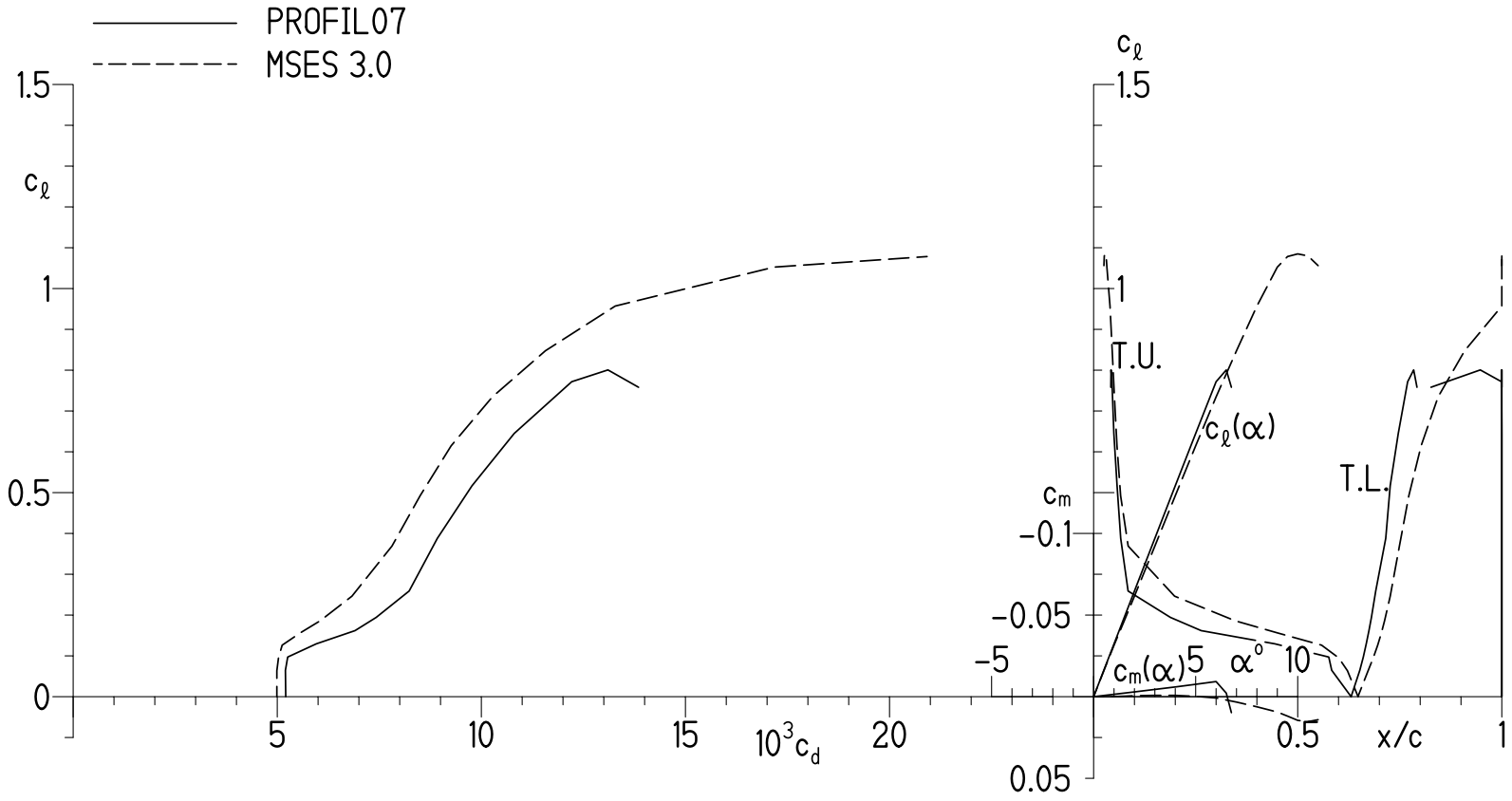

(a) M = 0.40 and R = 1.34×10^6.

Figure 19.- Section characteristics of S413 airfoil with transition free.

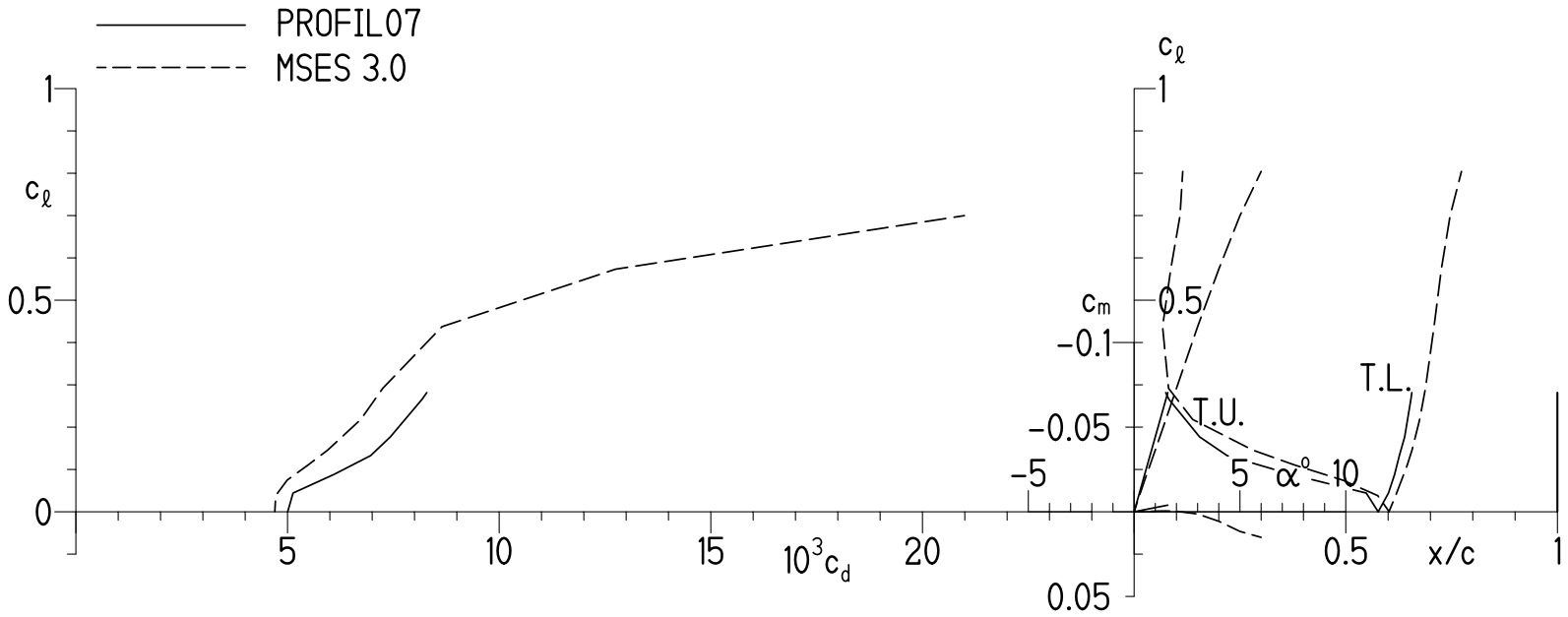

(b) M = 0.61 and R = 1.98×10^6.

Figure 19.- Continued.

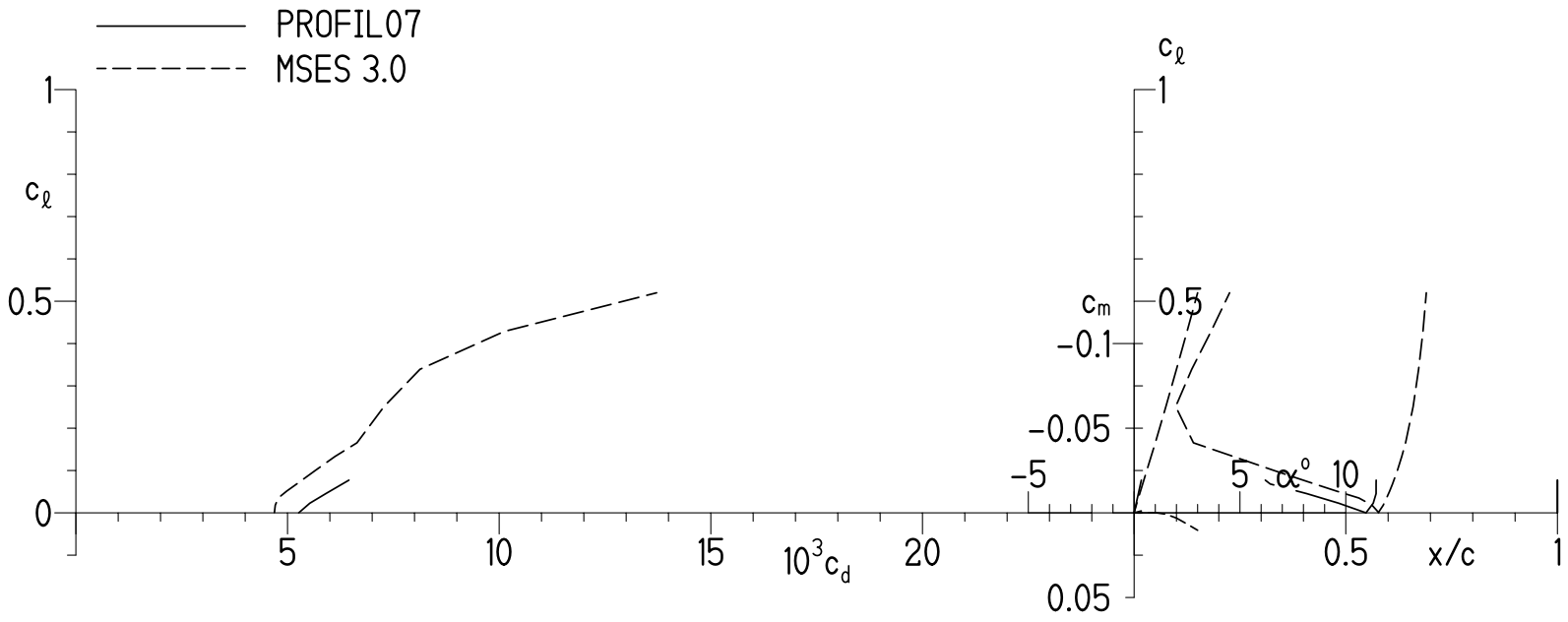

(c) $M = 0.70$ and $R = 2.28 \times 10^6$.

Figure 19.- Continued.

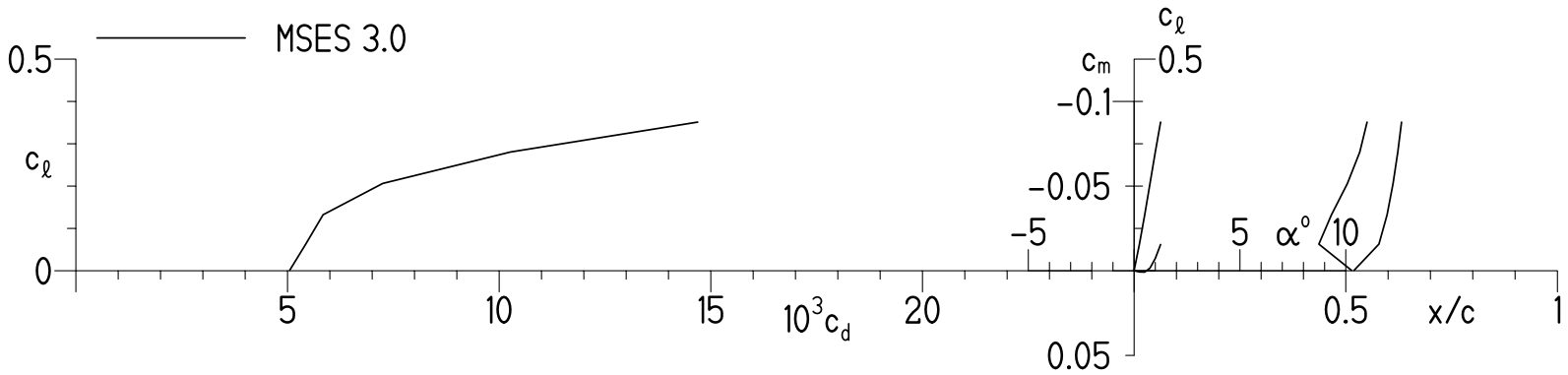

(d) M = 0.80 and R = 2.61×10^6.

Figure 19.- Concluded.

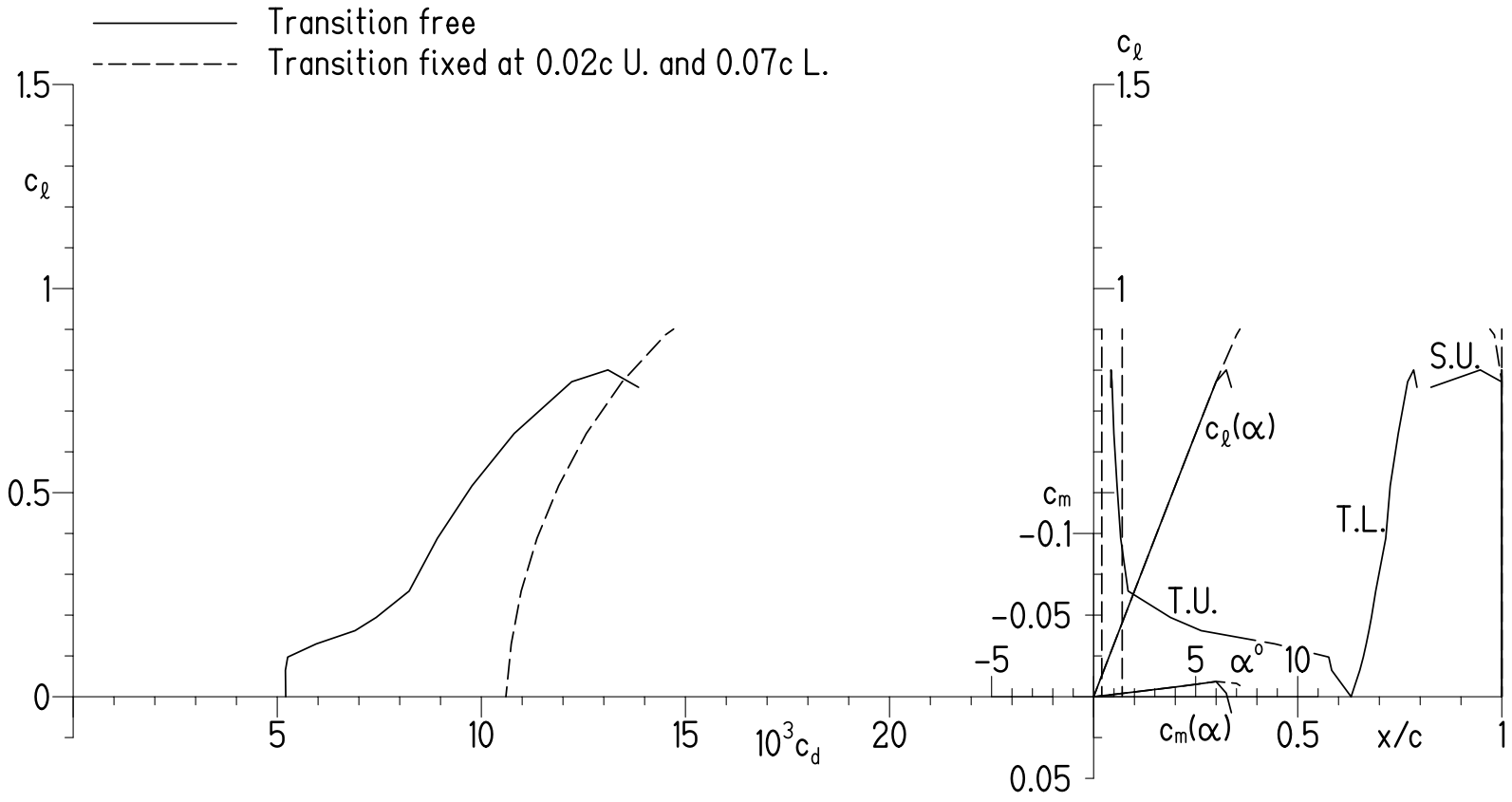

(a) $M = 0.40$ and $R = 1.34 \times 10^6$.

Figure 20.- Effect of fixing transition on section characteristics of S413 airfoil predicted using method of references 8 and 9.

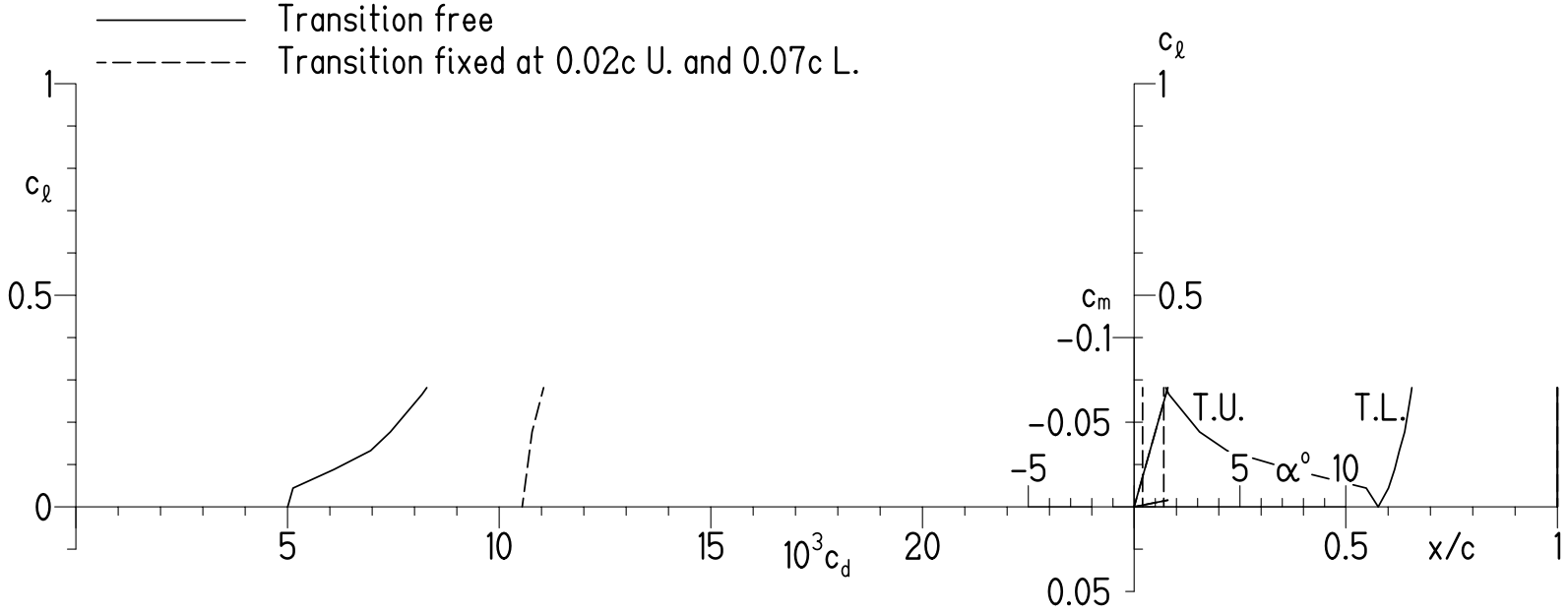

(b) M = 0.61 and R = 1.98×10^6.

Figure 20.- Continued.

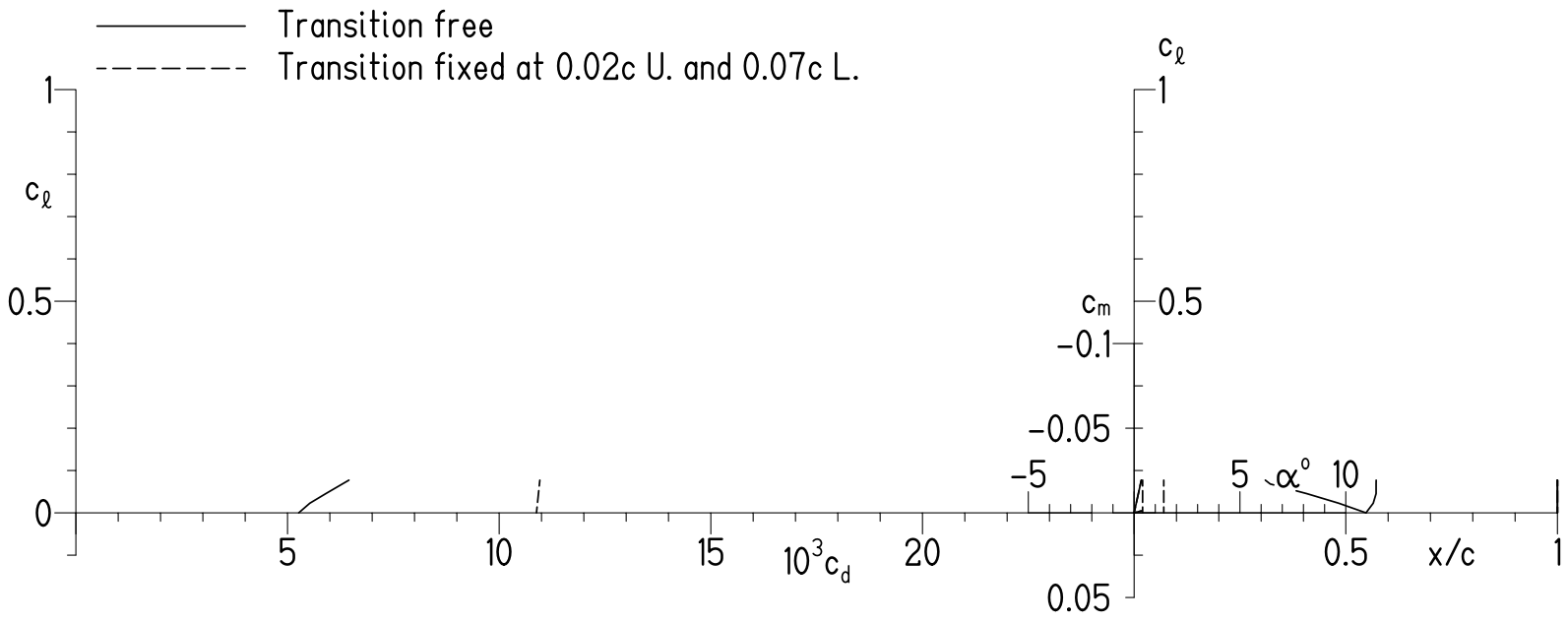

(c) M = 0.70 and R = 2.28×10^6.

Figure 20.- Concluded.

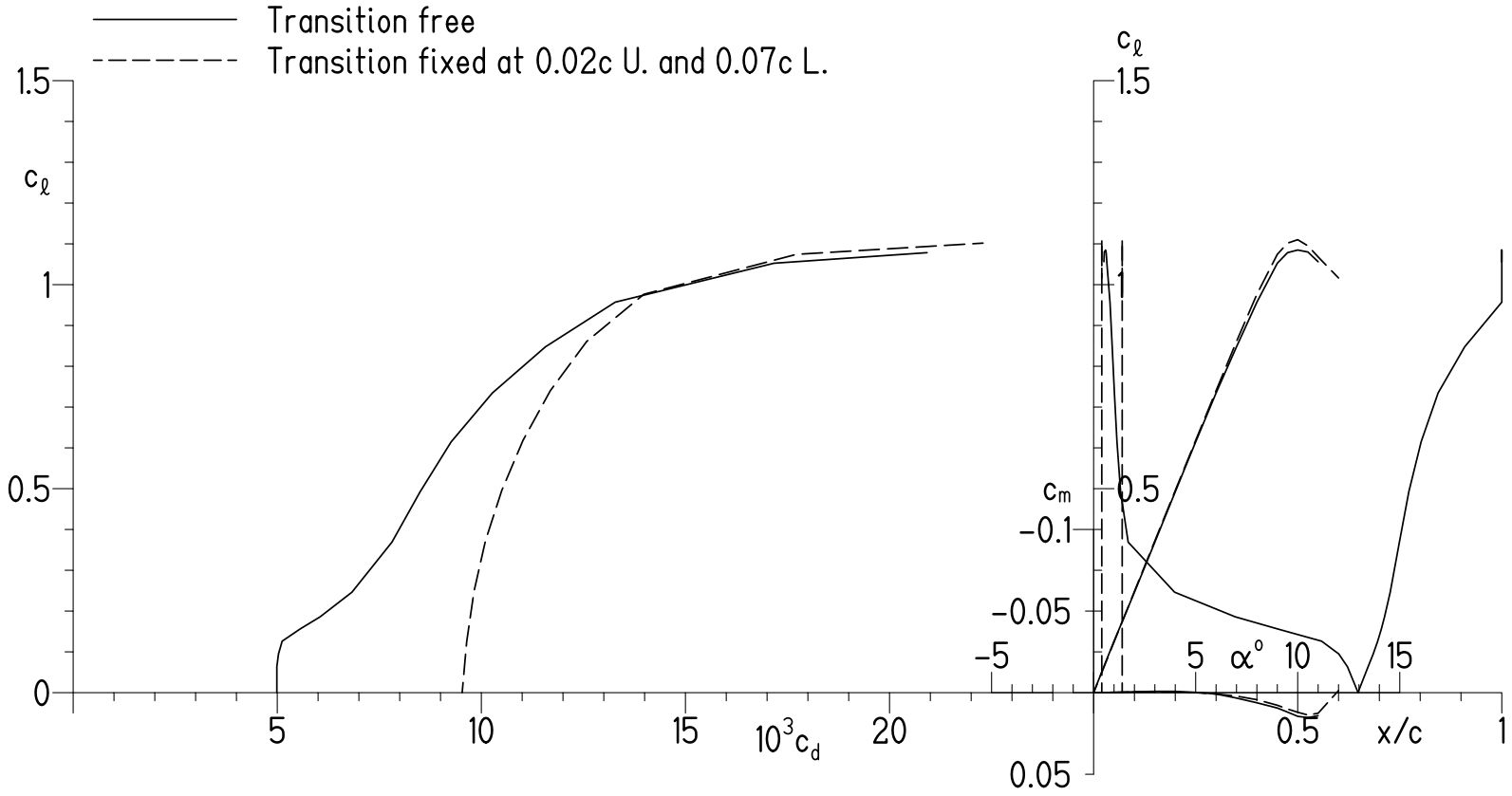

(a) M = 0.40 and R = 1.34×10^6.

Figure 21.- Effect of fixing transition on section characteristics of S413 airfoil predicted using method of reference 11.

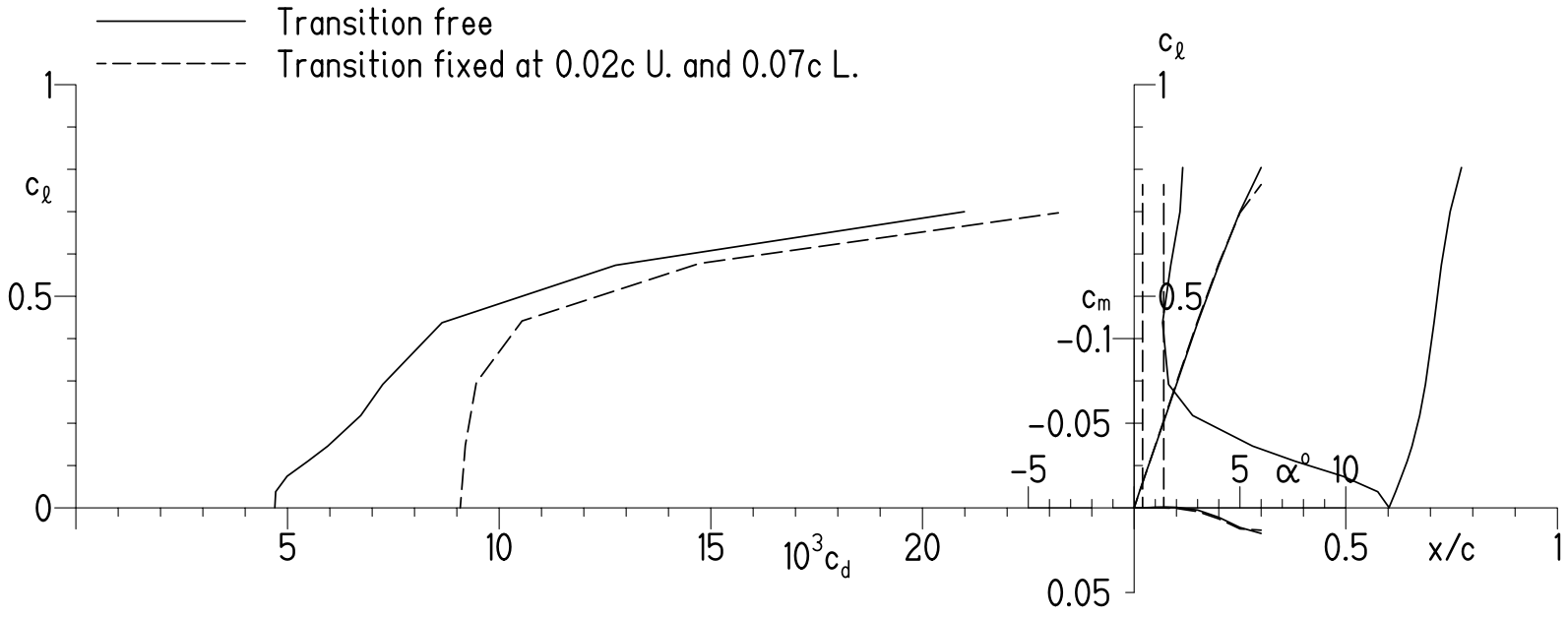

(b) M = 0.61 and R = 1.98×10^6.

Figure 21.- Continued.

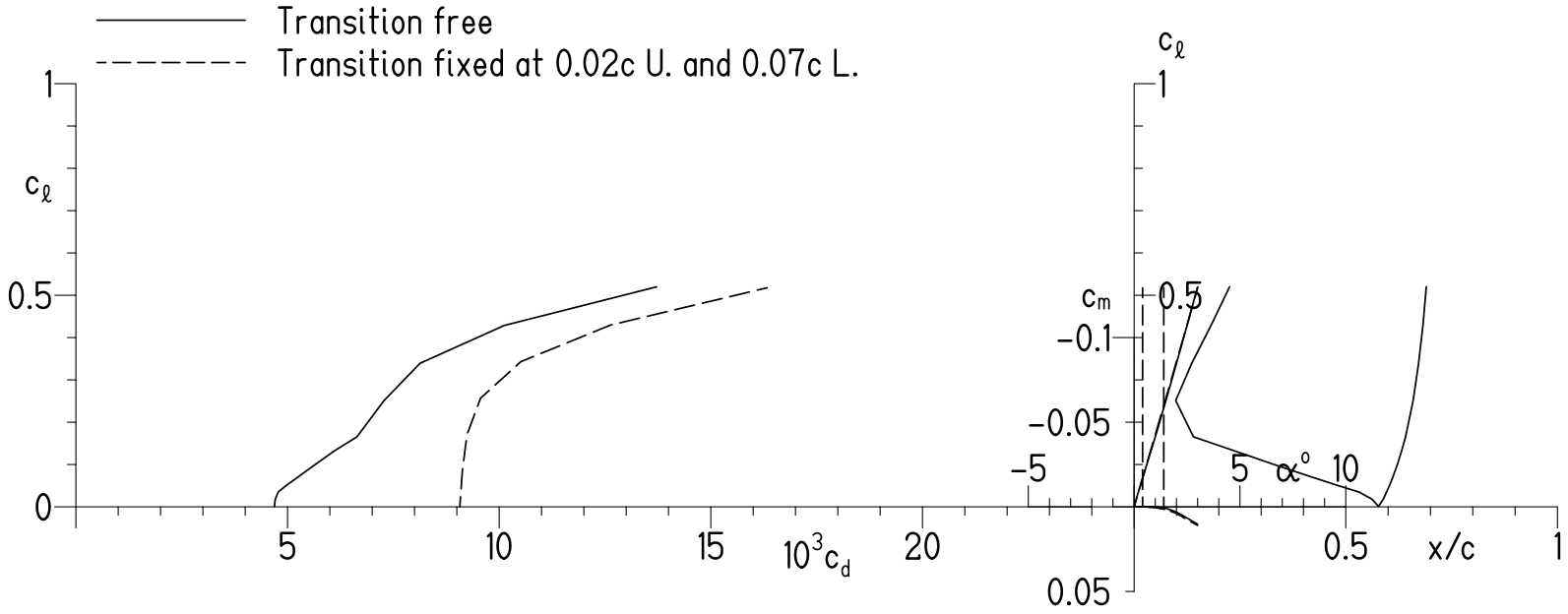

(c) M = 0.70 and R = 2.28×10^6.

Figure 21.- Continued.

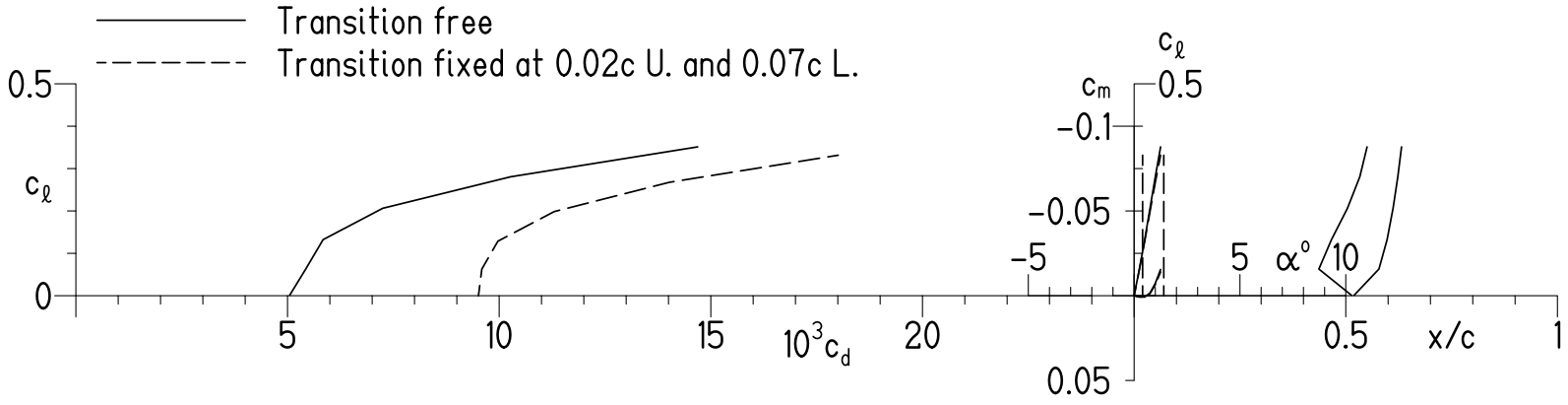

(d) $M = 0.80$ and $R = 2.61 \times 10^6$.

Figure 21.- Concluded.

REPORT DOCUMENTATION PAGE

Form Approved
OMB No. 0704-0188

1. REPORT DATE *(DD-MM-YYYY)*	2. REPORT TYPE	3. DATES COVERED *(From - To)*
xx-08-2010	FINAL REPORT	Sep 2007 - Jun 2010

4. TITLE AND SUBTITLE

The S411, S412, and S413 Airfoils

5a. CONTRACT NUMBER
W911W6-07-C-0047

5b. GRANT NUMBER

5c. PROGRAM ELEMENT NUMBER

6. AUTHOR(S)

Somers, Dan M.

5d. PROJECT NUMBER

5e. TASK NUMBER

5f. WORK UNIT NUMBER

7. PERFORMING ORGANIZATION NAME(S) AND ADDRESS(ES)

Airfoils, Incorporated
Attn: Dan M. Somers
122 Rose Drive
Port Matilda PA 16870-7535

8. PERFORMING ORGANIZATION REPORT NUMBER

SBIR Topic Number A06-006
Proposal Number A2-2972

9. SPONSORING / MONITORING AGENCY NAME(S) AND ADDRESS(ES)

US Army Aviation Research, Development and Engineering Command (RDECOM)
Aviation Applied Technology Directorate (AATD)
Fort Eustis VA 23604-5577

10. SPONSOR/MONITOR'S ACRONYM(S)

11. SPONSOR/MONITOR'S REPORT NUMBER(S)
RDECOM TR 10-D-110

12. DISTRIBUTION / AVAILABILITY STATEMENT

Approved for public release; distribution is unlimited.

13. SUPPLEMENTARY NOTES

UL Note: No proprietary / limited information may be included in the abstract.

14. ABSTRACT

A family of airfoils, the S411, S412, and S413, intended for rotorcraft applications has been designed and analyzed theoretically. The two primary objectives of high maximum lift, relatively insensitive to roughness, and low profile drag have been achieved. The constraint on the pitching moment of the primary airfoil, the S411, has been exceeded; those of the outboard and tip airfoils, the S412 and S413, respectively, have been satisfied. The constraints on the airfoil thicknesses have been satisfied. The primary airfoil incorporates a 5-percent-chord tab.

15. SUBJECT TERMS

Airfoils, rotorcraft, laminar flow

16. SECURITY CLASSIFICATION OF:			17. LIMITATION OF ABSTRACT	18. NUMBER OF PAGES	19a. NAME OF RESPONSIBLE PERSON
a. REPORT	b. ABSTRACT	c. THIS PAGE			Dan M. Somers
unclassified	unclassified	unclassified	UU	79	19b. TELEPHONE NUMBER *(include area code)* (814) 357-0500